Projecting the Hydrological and Geochemical Evolution of a Constructed Fen Watershed in the Athabasca Oil Sands Region, Alberta, Canada

by

Owen Francis Sutton

A thesis
presented to the University of Waterloo
in fulfillment of the
thesis requirement for the degree of
Doctor of Philosophy
in
Geography

Waterloo, Ontario, Canada, 2021

Examining Committee Membership

The following individuals served on the Examining Committee for this thesis. The decision of the Examining Committee is by majority vote.

External Examiner	Dr. Andrew Reeve Professor, University of Maine
Supervisor	Dr. Jonathan Price Professor, University of Waterloo
Internal Member	Dr. Richard Petrone Professor, University of Waterloo
Internal-external Member	Dr. David Rudolph Professor, University of Waterloo
Other Member(s)	Dr. James Craig Associate Professor, University of Waterloo

Author's Declaration

I hereby declare that this thesis consists entirely of material I authored or co-authored: see Statement of Contributions included in the thesis. This is a true copy of the thesis, including any required final revisions, as accepted by my examiners.

I understand that my thesis may be made electronically available to the public.

Statement of Contributions

This thesis has been structured in accordance with the manuscript option. Chapters two and three have been published, while Chapters four and five are in preparation and will be submitted for review; consequently, should the manuscripts be accepted for publication they may differ from what is presented in this thesis due to comments and feedback following peer-review.

Owen Sutton designed and conducted the modelling and data analysis presented herein, as well as writing the first draft of all chapters. Dr. Jonathan Price was the thesis advisor, and therefore had an instrumental role in the planning of all research presented in the following chapters. Owen Sutton and Dr. Price devised the methodological approach in collaboration. Furthermore, editorial comments and revisions from Dr. Price aided in the analysis and interpretation of data and improved the quality of the manuscripts. Eric Kessel and Dr. Behrad Gharedaghloo are co-authors on Chapter 4, both of whom contributed expertise in the preparation – and aided in the execution of – field and laboratory experiments, in addition to providing valuable editorial feedback.

Chapter two is published as:

Sutton, O. F., & Price, J. S. (2020). Soil moisture dynamics modelling of a reclaimed upland in the early post-construction period. *Science of the Total Environment*, *718*, 134628.

Owen Sutton was the primary author of this manuscript and performed the modelling, data analysis, and writing of the manuscript. Dr. Jonathan Price provided valuable feedback and comments regarding the interpretation of model results, as well as editorial revisions. Comments received from industrial partners were considered and largely incorporated, however they were minor and involved clarifications associated with the operational procedures and recommendations of cover soil prescriptions.

Chapter three is published as:

Sutton, O. F., & Price, J. S. (2020). Modelling the hydrologic effects of vegetation growth on the long-term trajectory of a reclamation watershed. *Science of the Total Environment*, *734*, 139323.

Owen Sutton performed the modelling, data analysis and writing of the first draft. Dr. Price, as second author, made valuable suggestions on data analysis and writing that improved the manuscript. Comments received from industrial funders were considered and, where appropriate, the manuscript

was amended. However, these comments were minor and improved the descriptions associated with operational procedures and recommendations of cover soil prescriptions.

Chapter four is prepared as:

Sutton, O. F., Kessel, E. D., Gharedaghloo, B., & Price, J. S. Characterizing the hydraulic and transport properties of a constructed coarse tailings sand aquifer.

Owen Sutton was the primary author of this manuscript and performed the majority of field work, data collection, data analysis, and writing of the manuscript. Eric Kessel aided in the installation of the monitoring network in the field, helped design and perform the laboratory experiments, and provided editorial feedback. Dr. Behrad Gharedaghloo advised on the experimental design and data analysis of the field and laboratory experiments, as well as providing editorial revisions to the manuscript. Dr. Jonathan Price provided valuable feedback and comments regarding the interpretation of results, as well as editorial revisions. The manuscript has not yet been submitted for review by industrial partners.

Chapter five is prepared as:

Sutton, O. F., & Price, J. S. Projecting the hydrochemical trajectory of a constructed fen watershed: implications for long-term wetland function

Owen Sutton performed the modelling, data analysis and writing of the first draft. Dr. Jonathan Price provided valuable feedback and comments regarding the interpretation of model results, as well as editorial revisions. The manuscript has not yet been submitted for review by industrial partners.

By signing below, I indicate that I am in agreement with the evaluation of the roles and contributions of the various authors expressed above.

J. Price E. Kessel B. Gharedaghloo

Abstract

Ongoing commercial bitumen surface mining operations have fundamentally altered large areas of the natural landscape in the Athabasca Oil Sands Region (AOSR), Alberta, Canada. The pre-disturbance boreal landscape comprised a mosaic of upland forest and wetland ecosystems that exhibited complex surface and subsurface hydrologic connectivity. The majority of these wetlands are fen peatlands, which are carbon accumulating ecosystems that receive ground and surface water, and perform an important water storage function within the boreal landscape. Returning fen peatland functions that are representative of the pre-disturbance state has become a matter of increasing public interest, and has been adopted into the regulatory framework administered by the Alberta government. Due to the intensity of the disturbance, returning the land to pre-disturbance function requires reclamation, which entails a complete reengineering of surface and subsurface topography, and reestablishment of hydrologic connectivity. Prompted by the prevalence of fens on the undisturbed landscape, this regulatory framework has recently mandated the trial of fen peatland reclamation at the pilot-scale to assess the viability of including these constructed ecosystems in mine closure planning. It was hypothesized that the creation of a surrogate fen that exhibited many of the same functional traits as a natural system could be accomplished by providing a reasonable approximation of the hydrogeologic setting of peatlands characteristic to the region. This principle guided the conceptual design of the Nikanotee Fen Watershed, one of the pioneering experimental watersheds built on the post-mined landscape. The design of this pilot project incorporated an upland aquifer capable of supplying the downgradient peatland with a consistent source of water, which was assumed to be a prerequisite for initiating wetland function given the prevailing regional climate. Pronounced interseasonal and interannual variability in precipitation, which on an average annual basis is less than potential evapotranspiration, can often cause moisture limited conditions that must be managed in the reclaimed landscape. Construction of the site was completed in January 2013, and used a combination of salvaged, process-affected and engineered materials. Residual concentrations of Na^+ and other solutes imparted to the coarse tailings sand aquifer material during the bitumen extraction process, introduced the potential for rooting zone salinization that could negatively impact fen vegetation. Initial assessments of the Nikanotee Fen Watershed demonstrated that in the early post-construction period the site was functioning in accordance with the design. However, meaningful changes in the function of the system will occur as the site matures due to soil evolution, vegetation development, and the progressive transport of solutes from the upland to the fen. The timeline that these processes will evolve

on preclude purely observational research and require the use of techniques that can project hydrologic behaviour into the future as the site matures. Generating information on the future efficacy of the Nikanotee Fen Watershed will be crucial to informing mine operators and reclamation planners of the viability of fen reclamation.

Assessing the probable trajectory of the upland and fen was accomplished using field data, laboratory experiments, and numerical modelling. The impact of the evolving upland in the short-term (due to soil weathering) and the long-term (due to vegetation development) was investigated with soil moisture dynamics modelling. Next, a thorough characterization of the hydraulic properties that influence the fate and transport of sodium from the tailings sand aquifer was conducted with a field-scale tracer test, and laboratory experiments. Finally, the likely developmental pathway of the fen was evaluated by integrating information from the previous research into a groundwater flow and solute transport model of the watershed. These studies have (1) illustrated the impact of weathering on the soil hydraulic properties and water balance fluxes of cover soils in the early post-construction period; (2) demonstrated the value of snowmelt for recharging groundwater in the reclaimed uplands and improved the understanding of the relationship between cover soil systems and vegetation growth; (3) identified the hydraulic and transport properties of coarse tailings sand – a material that will be ubiquitous on the closure landscape; and (4) provided a novel evaluation of the hydrochemical trajectory of a constructed peatland watershed with respect to water availability and sodium concentrations, which upheld the original conceptual design, and strongly suggested that the system will continue to support fen ecohydrological function. This research represents one of the first comprehensive attempts to illuminate the probable developmental pathway of a fen reclamation pilot project in a post-mined landscape. The Nikanotee Fen Watershed has accomplished many of its epistemic goals associated with the generation of research and operational knowledge, and ultimately, appears poised to replicate fen ecohydrological function into the future by successfully regulating the limited available moisture, and managing the salinity from process-affected materials.

Acknowledgements

The completion of my thesis represents the single most rewarding and engaging endeavour I have ever embarked upon. However, it was accomplished with the support of a fellowship of friends, family, and colleagues. First and foremost, I would like to extend my deepest gratitude and appreciation to my advisor, mentor, and friend Dr. Jonathan Price. Thank you for believing in me, thank you for teaching me. Your insight has immeasurably improved my research, your wisdom has helped me to become a better scientist, and your character has made this an experience which I enjoyed more than I could have possibly imagined. My life will be indelibly shaped by your tutelage.

None of this would have been possible without the support of Suncor Energy Inc., Imperial Oil Resources Ltd., Teck Resources Ltd., the Natural Sciences and Engineering Research Council, and the taxpayers of Canada. Your financial contributions allow people like me to do what we love. On many occasions Suncor Field Services, especially Jeremy Cameron, went above and beyond to ensure we collected our data. You have my sincere gratitude.

To my friends and colleagues in the Wetlands Hydrology Lab, your camaraderie and support made each and every day fun. Our friendly discourse around the lab (or Grad House) broadened my horizons and encouraged me to think critically about everything that I did. It will be sorely missed. In particular, I would like to thank Behrad Gharedaghloo, Eric Kessel, and James Sherwood, whose guidance helped me progress when I was adrift, and whose friendship helped make the past 5 years the best of my life.

To my past and present rock climbing partners, Collin, Tyler, Mel, Tijana, Marcus, Brandon, and Catherine you are the best. Climbing was my outlet and escape from the full-body experience that is grad school. Thank you for keeping me on an even keel. I cannot wait to get back on the wall with you.

I could not have completed my thesis without the love, support, and patience of my friends and family. To my wonderful friends, who I have shared drinks, campfires, canoes, and tents with I am so grateful for your companionship. Mom, Dad, Emma, and Sean I cannot describe how much I love you. You mean the world to me, and I am so fortunate to have you in my life. I simply would not be here without you.

Finally, I would like to recognize the Nikanotee Fen Watershed for holding me in rapt attention for the last 5 years. Proving time and again, life finds a way.

Dedication

To my wonderful parents: Josi Perotto & Peter Sutton. I am so grateful for your love and support. You inspire me to strive for good and great things every day.

Table of Contents

List of Figures

List of Tables

Chapter 1: Introduction

Surface mining of bitumen has disturbed hundreds of square kilometers of the boreal landscape in the Athabasca Oil Sands Region (AOSR) of Alberta, Canada (CAPP, 2018). The pre-disturbance landscape largely consisted of boreal forest and fen peatlands (Vitt et al., 1996), a type of carbon-accumulating wetland that receives minerotrophic ground and surface water. The intensity of this disturbance fundamentally alters the surface and subsurface ecohydrological processes to the extent that returning the landscape to resemble the pre-disturbance state requires the complete reconstruction of landforms and reestablishment of the hydrologic connectivity that existed between landforms. Instigated by regulatory obligations to return the land to an equivalent capability and guided by conceptual interpretations of water movement within the undisturbed landscape, two pilot projects were designed and built to explore the feasibility of fen peatland reclamation. The principal goal of these projects was to facilitate research and the development of operational knowledge that will aid in fen reclamation on a scale suitable for inclusion into mine closure planning. Furthermore, it was hoped that this conceptual design, and its first experimental implementation on a portion of the post-mined landscape, would possess many of the characteristics of undisturbed systems. Of particular importance was maintaining a high and stable water table, thus providing the conditions to support regionally-abundant fen vegetation species, and net carbon accumulation (Pollard et al., 2012).

Several challenges must be addressed in pursuit of peatland reclamation, chiefly, the relatively dry regional climate and limited material availability, which are compounded by the lack of prior experience with fen construction. The climate of the AOSR is characterized by distinct interseasonal and interannual variability in water availability, and potential evapotranspiration exceeding precipitation, on an average annual basis (Devito et al., 2005). Concerns over limited moisture conditions in the constructed wetlands led to the adoption of various design strategies intended to promote saturated conditions in the fens of the pilot projects. At one of these pilot projects, the Nikanotee Fen Watershed, an upland aquifer was included in the design to ensure a source of groundwater could supplement the fen during dry periods. Such an aquifer required a material that possessed the appropriate hydraulic and geotechnical characteristics to act as a water conveyance feature. Ultimately, coarse tailings sand, a byproduct of the bitumen extraction process, was selected as the most suitable material. While coarse tailings sand is anticipated to be a readily abundant material, which will also need to be reintegrated into the post-mined landscape, it contains residual concentrations of sodium, calcium, and sulfate due to the oil sands process. Therefore, its inclusion into the design of the system introduced the prospect of solute transport by groundwater leading to elevated salinity

in the fen. Since the level of salinity typically found in oil sands process-affected water has been shown to negatively impact the growth and productivity of fen vegetation (Pouliot et al., 2013; Rezanezhad et al., 2012), the use of tailings sand in the upland aquifer could inhibit the development of certain targeted plant species. In particular, mosses, which are desirable due to their natural abundance in undisturbed peatlands across the region (Chee and Vitt, 1989) and high carbon accumulation potential (Graf and Rochefort, 2009; Turetsky, 2003), typically exhibit low tolerance to saline conditions (Boerner and Forman, 1975).

While natural wetland function reflects complex and interconnected ecological, biogeochemical, and hydrometeorological processes, it was the hydrology that was interpreted as the foundational component that must be reproduced in constructed systems (Price et al., 2010). As the linchpin of wetland function (Mitsch and Wilson, 1996), it was hypothesized that instituting similar hydrological conditions in a salvaged peat deposit would initiate the emergence of other wetland functionality (Nwaishi et al., 2015). Though natural peatland development occurs over many millennia (Clymo, 1983), it was hoped that maintaining these hydrologic conditions in this setting would expedite the return to functionality equivalent to pre-disturbance ecosystems in a matter of decades (Ketcheson et al., 2016).

Although the role of the upland in the Nikanotee Fen Watershed is to supply groundwater to the peatland, the ambition is that these landforms will also be capable of supporting the growth of a forest similar in composition and density to the undisturbed landscape. Given the prevailing climate of the AOSR, achieving this requires a delicate balance between sufficient internal water storage to maintain plant growth and adequate recharge to the underlying aquifer to sustain consistent groundwater flow to the fen. Such a compromise must be replicated by reclamation planners with limited tools at their disposal, namely the type, layering, spatial arrangement, and thickness of soils. Yet upland design must conform to the limitations placed on soil availability, which realistically restricts options to the range of soils present prior to mine expansion. Creating an upland suitable to fulfill this role requires careful forethought on the needs of the fen, and the manner of interaction between upland and fen.

In constructed systems, the processes and properties governing the hydrological interaction between uplands and fens will evolve over a variety of timescales and could result in a system of greatly altered characteristics and function compared to the initial condition. Anticipating this trajectory requires the consideration of the dominant mechanisms that drive the progression of the system. Among the processes with the most profound consequences to the fen watershed trajectory are the evolution of upland hydraulic properties, vegetation succession, and the progressive downgradient transport of solutes from the tailings sand. Given the relatively recent implementation of these novel constructed fen designs, there is

little research to constrain expectations of future fen performance, and how these mutually-influencing processes may steer the development of the fen. Obtaining an indication of the probable trajectory of the Nikanotee Fen Watershed is necessary to identify issues associated with water quality and quantity that may hinder the development of the system; refine and optimize the design to address any deficiencies and improve the efficiency with which reclamation goals will be accomplished; and inform mine operators and regulatory bodies in a timely manner such that these systems may be included into closure landscape planning.

1.1 Objectives

The goal of this research is to assess the probable trajectory of the upland and peatland of the Nikanotee Fen Watershed from a hydrological and geochemical perspective, and based on this assessment, consider the implications of this trajectory on ecological development, and reflect on the salient characteristics of system design. The specific objectives necessary to accomplish this goal build upon one another and follow the journey of water through the system in space and time. Thus, the objectives of this research are to:

1) Illustrate the rapid evolution of soil hydraulic properties of the upland cover soil, assess the presence of spatial variability, and determine the point at which they reach equilibrium and the timeline associated with this stabilization;
2) Estimate the peak vegetation growth the upland is capable of supporting, and quantify the impact of this development on the water balance fluxes of the upland, particularly groundwater recharge;
3) Characterize the hydraulic properties of the coarse tailings sand that will have a dominant influence on the fate and transport of sodium from the aquifer; and
4) Use numerical modelling to project the future transport of sodium from the upland to the fen, evaluate the implications of elevated sodium on the ecological function of the fen, and reflect on the adequacy of the watershed design in the context of the original objectives for the site.

1.2 Organization of thesis

The thesis comprises six chapters that have been structured to conform to the manuscript option at the University of Waterloo. The introduction in Chapter 1 provides context for the thesis, the goal of the research and specific objectives. Each objective is addressed individually in sequence by the following four chapters.

Chapter 2 and 3 address the changes that will occur to the hydrologic behaviour of the upland, in the near-term due to freeze-thaw cycling and the long-term due to vegetation development. Chapter 4 is based on empirical field and laboratory data, which characterizes the hydraulic properties of tailings sand at a variety of scales. Finally, Chapter 5 explores the fate and transport of sodium within the watershed, with explicit consideration given to climatic variability, and placed within the context of the evolving nature of soils and vegetation at the site.

Following the conclusions in Chapter 6 are three appendices: Appendix A describes the methodology that was used to account for the winter processes of seasonal ground ice formation and snowpack accumulation and ablation; Appendix B contains a detailed account of the Monte Carlo simulation procedure; and Appendix C thoroughly discusses some of the purposeful decisions and inherent limitations of the modelling approach implemented in Chapter 5 that could contribute to model error.

Chapter 2: Soil moisture dynamics modelling of a reclaimed upland in the early post-construction period

2.1 Introduction

Extraction of oil sands through surface mining necessitates the removal of all overburden materials above the bitumen-bearing formation. In the Athabasca Oil Sands Region (AOSR) this overburden typically includes glacial material, saline-sodic shale, peat, and forest-floor soil. This disturbance alters the topography on a landscape-scale, and completely changes the partitioning and movement of water within the disturbed area and the connectivity to the surrounding landscape (Elshorbagy et al., 2005). Since these activities inevitably remove all surface features, including the boreal forest and fen peatland ecosystems that dominate the undisturbed landscape (Zoltai et al., 1988), reclamation of these systems and reestablishment of the associated hydrologic processes is mandated. Several constructed fen pilot projects have been built to test the feasibility of fen reclamation (Ketcheson et al., 2016). The objectives of these projects are to construct fen peatlands that will become self-sustaining ecosystems over time, develop research and operational knowledge in fen construction, and to test, refine, and optimize reclamation design to aid in implementation of fen reclamation on an industrial-scale (Daly et al., 2012; Pollard et al., 2012). In an attempt to meet these objectives, the Nikanotee Fen Watershed was constructed in 2012 on a post-mined portion of an oil sands lease (Daly et al., 2012). Optimizing the design of constructed peatland watersheds requires the prediction of current and future hydrologic performance, which will rely on the quantification of the dominant hydrologic fluxes.

The practice of forest reclamation following mine closure has been refined over a period of decades into an applied discipline that has generated guidelines intended to ensure the expectations of regulatory agencies are satisfied (Alberta Environment, 2010). These guidelines address the management of contamination, the revegetation of the disturbed landscape with communities that are representative of the local environment, and the application of specific soil prescriptions (CEMA, 2006). Mining activities generate waste materials that may contain residual levels of solutes that can adversely affect vegetation development. Therefore, contemporary mine reclamation often involves the use of cover soils that overlie contaminated material with the intention of hydraulically isolating the process-affected material from the surface, and the rooting zone of vegetation in particular (Kelln et al., 2008). These cover soils are typically sourced from either stockpiled or directly placed materials that are salvaged prior to the onset of mine operation or expansion. Due to constraints of local material availability or as a means of altering the soil

hydraulic properties of the cover, the soil is typically amended by salvaging the underlying mineral soil along with the upper organic horizons, in a process known as overstripping (Mackenzie & Naeth, 2007; Fung & Macyk, 2000). The hydrologic behaviour of covers can be further modified by varying the thickness (Huang et al., 2015) and layering of soils and waste material (Khire et al., 2000). In the AOSR the most common reclamation covers are peat-mineral mix (PMM) and over-stripped forest floor material known as LFH-mineral mix (Naeth et al., 2013), hereafter referred to as LFH. Since the role of cover soils in these conventional applications is primarily as a water storage feature, the minimization of moisture exchange between the cover and underlying substrate is considered advantageous (Meiers et al., 2011).

Recently, however, these cover soils have been integrated into the uplands of watersheds designed to support fen peatlands (Ketcheson et al., 2016). The purpose of cover soils used in these watersheds is to provide favourable conditions for vegetation growth while also allowing sufficient recharge to maintain groundwater flow to downgradient fens. This represents an increase in complexity, as covers used in these systems require hydrophysical properties that allow them to function as both water storage and water conveyance features.

The specific partitioning of water during the early post-construction period can have a profound influence on the trajectory of the system (Ketcheson et al., 2016). This partitioning is not only affected by the prevailing climatic conditions but also by the hydraulic behaviour of the construction materials, which experience rapid and marked change following placement (Meiers et al., 2011). The evolution of soil hydraulic properties is instigated and mediated by a variety of biotic and abiotic processes that systematically alter the physical structure of the soil and which operate on a variety of timescales. In the short-term, freeze-thaw cycles and wet-dry cycles can reduce bulk density, form larger pores, and increase saturated hydraulic conductivity (Benson et al., 1995; Meiers et al., 2011). Over longer time-scales root development due to vegetation growth and soil fauna can create macropores which have the potential to substantially increase the movement of soil moisture in wet conditions (Loch & Orange, 1997; Moreno-de-las Heras et al., 2009). Generally, this evolution is associated with increases in infiltration capacity, saturated hydraulic conductivity, saturated water content, a broader pore size distribution, and a lower air-entry pressure (Benson et al., 2007). The combined effects of these temporal changes can be quite pronounced in the initial post-construction period. After the first four years post-construction the saturated hydraulic conductivity of a reclamation cover soil can increase by at least an order of magnitude compared with the initial as-built properties (Meiers et al., 2011). Evidence from a variety of reclamation sites indicate that near-surface cover soils and overburden will tend to converge toward similar hydraulic characteristics

over time, regardless of the initial composition and compaction of the material (Benson et al., 2007). The point at which these properties reach equilibrium, the magnitude of the change, and the timeline on which stabilization occurs have profound implications on the hydrologic behaviour of cover systems. In the context of a constructed peatland watershed, determining the equilibrium hydraulic properties of the cover soil will be critical in evaluating the success of the upland design, quantifying the sensitivity of the system to deviations from targeted properties, and assessing its hydrologic trajectory.

Investigations of the soil moisture dynamics of peat-mineral mix and LFH cover soils have been undertaken at several sites in the AOSR (Naeth et al., 2011; Huang et al., 2011; Huang et al., 2015). However, these studies occurred on sites where rapid soil evolution had ceased and therefore soil hydraulic properties would have stabilized. Kelln et al. (2007) discussed the importance of macropore development on increasing saturated hydraulic conductivity at a peat-mineral mix cover. Yet, this paper did not examine changes to the temporal evolution of other soil hydraulic properties. Furthermore, contemporary reclamation guidelines have advocated the use of LFH-mineral mix for upland reclamation initiatives due to the favourable hydraulic properties and source of native vegetation propagules (Naeth et al., 2013). Therefore, this warrants a study focusing specifically on characterizing the hydraulic properties and the time-dependent evolution of the LFH soil prescription, and how this evolution will alter the hydrologic performance of the upland.

Given the apparent importance of the early post-construction period in initiating and sustaining the desired ecohydrological function of constructed fens (Ketcheson et al., 2016) it is necessary to characterize the spatial and temporal evolution of LFH cover soils integrated into these watersheds. Therefore, the objectives of this study are to: (1) calibrate and validate a numerical model capable of simulating soil moisture dynamics in the upland of the Nikanotee Fen Watershed; (2) assess whether the hydrologic behaviour of the upland can be adequately represented using spatially homogeneous hydraulic properties; and (3) evaluate the implications of soil evolution on the hydrologic function of the upland in the early post-construction period.

2.2 Study site

The Nikanotee Fen Watershed was built on a post-mined portion of an oil sands lease approximately 25 km north of Fort McMurray, Alberta (56°55’59” N, 111°25’00” W), and comprises a fen peatland (2.2 ha), upland designed to direct groundwater to the fen (7.7 ha), and surrounding hillslopes (22.2 ha) (Figure 2-1). The design of the system was informed by numerical modelling that identified the appropriate geometry,

fen to upland ratio, material hydraulic properties, and layering to maintain a sufficient level of saturation in the fen, even under prolonged drought conditions (Price et al., 2010). The design incorporates an upland aquifer constructed from coarse tailings sand to supply groundwater to the fen (Daly et al., 2012). As a consequence of the bitumen extraction process, the tailings sand aquifer contains elevated pore-water concentrations of sodium, which are mobilized by groundwater flow (Kessel et al., 2018). In order to minimize deep percolation losses from the aquifer to the underlying subsurface an impermeable geosynthetic clay liner was placed under the fen and upland, thereby isolating the system from regional groundwater interaction and establishing a hydraulic gradient towards the fen. The aquifer was capped with approximately 30 cm of a sandy loam reclamation cover soil (LFH) as a vegetation growth substrate.

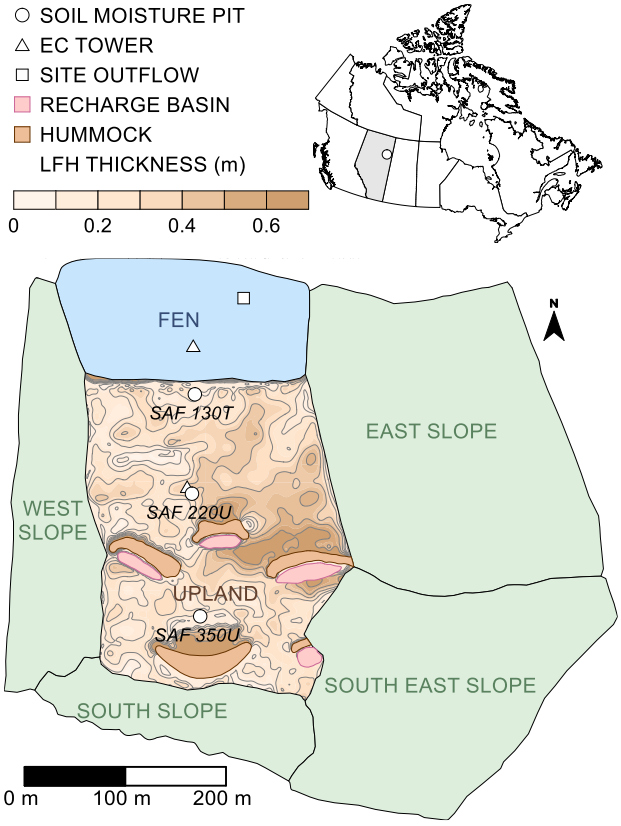

Figure 2-1. Study site map of Nikanotee Fen Watershed depicting the thickness of the LFH cover soil across the upland, meso-scale landforms (hummocks and recharge basins), and the upland soil moisture stations.

Immediately following construction, high-intensity precipitation events produced large volumes of surface overland flow in the upland, which directly entered the fen and subsequently flowed out of the system. This effectively bypassed the upland aquifer, and therefore did not contribute to groundwater recharge as

intended. To address this, two interventions were devised and implemented after the first field season in 2013. First, the upland was furrowed perpendicular to the slope to increase the surface detention capacity. Second, the LFH was scoured from the upslope side of large, raised landforms known as "hummocks" (Figure 2-1) to expose bare tailings sand, forming basins that were either adjacent to hillslope confluences or isolated from the surrounding landscape. The basins adjacent to hillslopes detained large volumes of surface runoff and disproportionately contributed to recharging the tailings sand aquifer (Kessel et al., 2019). Monitoring station nomenclature references the distance (m) from the berm at the north end of the fen (Figure 2-1), and are located in part of the site considered a transition zone (T), and more distal parts of the upland (U).

2.3 Methods

2.3.1 Field instrumentation

A meteorological station in the upland measured precipitation (Texas Instruments Canada Ltd. TR-525M tipping bucket rain gauge), net radiation (Kipp and Zonen NR-LITE2 net radiometer), air temperature and relative humidity (Rotronic HC2S3), ground heat flux (REBS HFT-3), wind speed and direction (R.M. Young 05103 Wind Monitor). Data collected from the meteorological station was used to derive potential evapotranspiration (PET) using the Penman method (Penman, 1948). An eddy covariance system at the upland meteorological station was used to estimate actual evapotranspiration (AET); details of the methodology can be found in Ketcheson et al. (2017). Continuous logging of volumetric moisture content occurred at three locations within the upland, SAF 130T, SAF 220U, and SAF 350U (see Figure 2-1), which were instrumented with 6 dielectric impedance reflectometry soil moisture probes (Stevens Hydra Probe II) nominally installed at -5, -10, -15, -30, -40, and -60 cm below ground surface. However, the actual depths of the probes varied by location (Figure 2-2). These probes recorded dielectric permittivity at hourly intervals, which was temperature and salinity corrected and converted to volumetric water content (θ) based on a calibration (Seyfried et al., 2005) specific to the material the probes were installed in.

2.3.2 Numerical modelling

The vertical soil water dynamics in the upland of the Nikanotee Fen Watershed was simulated with HYDRUS-1D, which solves Richard's equation for variably saturated water flow (Šimůnek et al., 2008). The model domain extended 0.7 m below ground surface, which is below the LFH-tailings sand interface and is lower than the evapotranspiration extinction depth. This was demonstrated by a sensitivity analysis which increased the depth of the model domain and revealed that the partitioning of water between recharge

and evaporation was negligibly altered. The lower boundary was a unit-gradient condition, representing a unidirectional movement of water across the boundary towards the water table (approximately 2-3 m below the model domain). Any soil moisture that passed across the lower boundary was assumed to eventually reach the water table, and consequently considered groundwater recharge. The upper atmospheric boundary condition allowed water to enter and leave the domain due to precipitation and surface evaporation, respectively. Due to the large proportion of bare ground and early successional stage of the vegetation on the upland during the modelled study period (2014, 2015, and 2017), root water uptake was ignored.

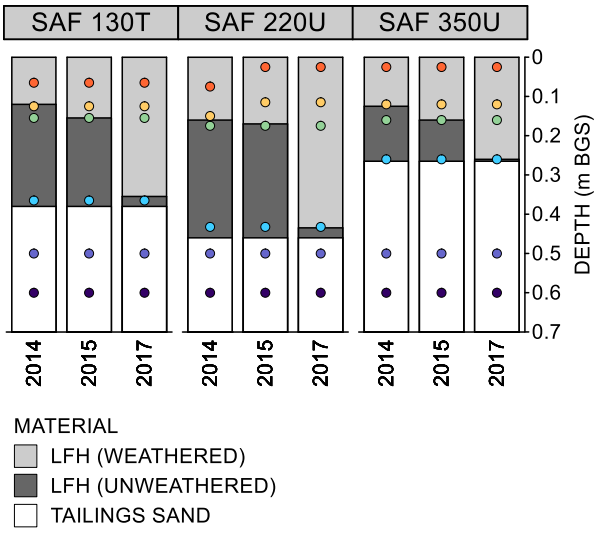

Figure 2-2. Model domains at the upland soil moisture stations. The inferred progressive deepening of the interface between weathered and unweathered LFH over time is illustrated. Also shown are the depths of the moisture probes (circle symbols) below ground surface.

Stratigraphic layers used in the model included weathered LFH, unweathered LFH, and tailings sand (only the upland is modelled in this study). Details of the hydrophysical properties of LFH and tailings sand can be found in Ketcheson (2015). The separation of LFH into two constituents (weathered and unweathered) was implemented in the numerical model to address the evolution of soil hydraulic properties and changes to the pore size distribution that occur following placement of the reclamation soil due to freeze-thaw cycling, and was necessary to achieve an adequate match with observed data. Initial parameterization of soil hydraulic properties was based on fitting the van Genuchten-Mualem equation (van Genuchten, 1980) to retention curve data:

$$\theta(\psi) = \begin{cases} \theta_r + \dfrac{\theta_s - \theta_r}{(1 + |\alpha\psi|^n)^m} & , \; h < 0 \\ \theta_s & , \; h \geq 0 \end{cases} \tag{1}$$

$$K(\theta) = \begin{cases} K_s\left(\frac{\theta-\theta_r}{\theta_s-\theta_r}\right)^L \left(1-\left(1-\left(\frac{\theta-\theta_r}{\theta_s-\theta_r}\right)^{\frac{1}{m}}\right)^m\right)^2, & h < 0 \\ K_s, & h \geq 0 \end{cases} \quad (2)$$

where h is pressure head, K_s is the saturated hydraulic conductivity, L is a parameter related to tortuosity and pore connectivity, θ_r is the residual saturation, θ_s is the saturated water content, α is a fitting parameter inversely related to the air-entry pressure, n is a fitting parameter that represents the shape of the pore size distribution, and m is equal to 1-1/n. Saturated water contents for tailings sand and LFH was specified based on the maximum volumetric water content observed over the study period. Residual water content for the LFH was prescribed to equal the minimum observed water content. The initial moisture distribution in the soil profile was specified from the measured soil moisture data immediately prior to the start of the simulation period.

2.3.3 Model calibration and validation

Manual calibration of soil hydraulic properties using trial-and-error adjustments of α, n, K_s, and L parameters was conducted for the growing season (May 17 – September 20) in 2014 at SAF 130T and 2017 at SAF 350U. Model validation at SAF 130T occurred for 2015 and 2017, while validation at SAF 350U occurred for 2015 and 2017. At the SAF 220U moisture profile, 2014, 2015, and 2017 were used for validation. Incomplete soil moisture and meteorological data in 2016 necessitated its removal from the analysis. The calibration and validation procedure led to the development of a single set of soil hydraulic properties for all locations, based on the assumption that the LFH and tailings sand exhibited negligible spatial heterogeneity; the validity of this assumption will be discussed below. The only modification to model structure during the validation procedure was the depth of the interface between weathered and unweathered LFH, which was decreased monotonically. This was done to account for the ongoing soil evolution and transient character of soil hydraulic properties in the LFH.

Due to the highly variable nature of soil moisture – particularly in close proximity to boundaries between different materials – simulated water content was spatially integrated over the sensing volume of the probes. The adequacy of the manual calibration procedure was assessed using visual inspection as well as several model performance metrics that compare observed and simulated soil moisture, including the mean absolute error (MAE), and modified Kling-Gupta efficiency (KGE; Kling et al., 2012):

$$KGE = 1 - \sqrt{(r-1)^2(\beta-1)^2(\gamma-1)^2} \quad (3)$$

$$r = \frac{cov_{s,o}}{\sigma_s \times \sigma_o}, \qquad \beta = \frac{\mu_s}{\mu_o}, \qquad \gamma = \frac{\sigma_s/\mu_s}{\sigma_o/\mu_o} \tag{4}$$

where r is the correlation coefficient between simulated and observed θ ($cov_{s,o}$ is the covariance between simulated and observed θ), β is a dimensionless measure for bias (μ_s and μ_o are the mean simulated and observed θ) and γ is a dimensionless measure for variability (σ_s and σ_s are the standard deviations of simulated and observed θ). The KGE varies between 1 and -∞, a KGE equal to unity indicates a perfect match between observed and simulated data. The criteria used to evaluate the adequacy of the manual calibration was an average MAE less than the accuracy of the probes (0.04 m^3 m^{-3}; Vaz et al., 2013) and a KGE greater than 0.3. This calibration procedure and criteria were only applied to the observation nodes in the LFH, and not the tailings sand, the rationale for which will be discussed in detail below. During calibration it was assumed that the soil hydraulic properties of the weathered LFH would have an air-entry pressure closer to zero, broader pore size distribution, and higher unsaturated hydraulic conductivity than the underlying unweathered LFH. The direction of these changes to soil hydraulic properties are consistent with those reported at other reclamation sites (Benson et al., 2007; Meiers et al., 2011).

2.3.4 Upland water balance estimation

Detailed surveys of stratigraphy taken during construction of the system allowed for the thickness of LFH across the upland to be determined with high spatial resolution (Figure 2-1). These measurements demonstrated that the as-built average thickness of the LFH cover soil deviated from the specified design thickness, and that there was substantial variability across the site, resulting in areas of thinner and thicker LFH than was intended. Cover soil thickness has been shown to alter the partitioning of soil moisture between evapotranspiration and deeper percolation, thereby exerting a control on the hydraulic function of a system (Huang et al., 2015). In order to represent the hydrologic behaviour of the upland as a whole, 14 model domains were developed that correspond to the different LFH thicknesses to capture the full range of variability found at the site (0 cm – 65 cm). Furthermore, given the progressive shift in soil hydraulic properties due to weathering that have occurred since the system was constructed, these model domains were modified to represent the changes to soil hydraulic properties in the LFH that occur on an annual basis, and will be referred to as the "actual" profiles. The cumulative fluxes of groundwater recharge and evapotranspiration across the whole upland were calculated for 2014, 2015, and 2017.

Since the interannual variability in climate confounds and obscures the influence of soil evolution on the water balance, additional model domains were developed with profiles comprising unweathered LFH and tailings sand, and weathered LFH and tailings sand (see Figure 2-10 for details). The former represents

the initial as-built condition, and the latter represents the equilibrium or steady-state condition that is reflective of the upland following the completion of soil weathering. These models were compared with the actual profiles and used to illustrate the impact of soil evolution on the partitioning of moisture between soil evaporation, groundwater recharge, and soil moisture storage in 2014, 2015, and 2017.

2.3.5 Uncertainty analysis

HYDRUS-1D includes a simple local-search optimization algorithm used for inverse parameter estimation (Šimůnek et al., 2012). However, due to concerns over the ability of the gradient-based Marquardt-Levenberg algorithm to find the global minimum and produce realistic confidence intervals, parameter uncertainty was assessed by performing pure random global search optimization. This global search optimization procedure was intended to characterize spatial heterogeneity and temporal evolution of hydraulic properties by independently calibrating each soil moisture dataset. While the global search optimization procedure produces realistic confidence intervals, it does not generate a specific optimal parameter set. Since all parameters within the confidence intervals generated by the global search must be assumed to be equally likely representations of the true parameter value, manual calibration was used to identify appropriate singular values to represent LFH and tailings sand soil hydraulic properties. For each individual year (2014, 2015, 2017) and location (SAF 130T, 220U, 350U) the global search algorithm was run 30,000 times, resulting in a total of 270,000 randomly generated parameter sets. The algorithm randomly generated van Genuchten-Mualem parameters (α, n, K_s, L) for the weathered and unweathered LFH. The parameter L, which represents the change in pore connectivity and tortuosity as the media desaturates, was constrained to be greater than 0. This constraint was imposed to ensure that L remained a physically-meaningful parameter, as values less than 0 indicate that relative connectivity increases as water content decreases (Peters et al., 2011).

The same evaluation criteria used for the manual calibration were applied to the global search optimization. Parameters which met the evaluation criteria (KGE > 0.3 and MAE <0.04) were used to identify the average value by determining the peak of the parameter probability density function. Since the underlying population probability distribution was unknown the confidence intervals could not be analytically calculated (Brunetti et al., 2017). Therefore, the generation of confidence intervals for the van Genuchten-Mualem parameters used bootstrap sampling (10,000 samples were taken) and the percentile technique (Archer et al., 1997).

2.4 Results

2.4.1 Observed soil moisture dynamics

Hydraulic behaviour of the cover soil at all profiles was similar, however more pronounced responses to precipitation events were observed at SAF 350U, which had the thinnest cover soil (Figures 2-3, 2-4, 2-5). Early season soil moisture was typically high in the LFH layer, with saturation maintained between 50-75% at all sites. Soil moisture in all profiles declined over the course of the growing season, although this change was most pronounced at SAF 350U - the monitoring location with the thinnest cover soil. Soil moisture in the LFH increased with depth at all monitoring locations, with the probes directly above the tailings sand interface generally maintaining water contents close to saturation (θ_s = 0.41) even during dry periods. Tailings sand exhibited markedly different hydraulic behaviour, often remaining invariant at field capacity for the entire season, with the exception of infrequent percolation events with rapid onset and recession. Furthermore, the tailings sand probes within the same profile often exhibited incongruent behaviour, despite the fact that they were separated by only 0.1 m.

The 2014 period received the most precipitation (223 mm) of the three years studied. The thicker covers (SAF 130T/220U) were capable of maintaining near-saturated conditions above the LFH-tailings sand interface throughout the study period. However, the thinner cover (SAF 350U) was incapable of holding soil moisture towards the end of the season and water content decreased below 20% (saturation less than 50%). The tailings sand probes at SAF 220U and 350U captured two pronounced percolation events. However, at the SAF 130T location the observed soil moisture did not vary throughout the 2014 season.

There was no change in soil moisture in the profile at any monitoring location between the end of the 2014 study period and the beginning of the 2015 period. In 2015, rainfall (185 mm) was concentrated in mid-June and late-August. The profiles with thicker cover soils (SAF 130T/220U) experienced little percolation into tailings sands. No response was evident in SAF 130T, and only 2 percolation events occurred in SAF 220U, corresponding to the previously mentioned wet periods. Furthermore, these thicker covers maintained higher and more stable soil moisture above the tailings sand interface compared to the thinner SAF 350U cover.

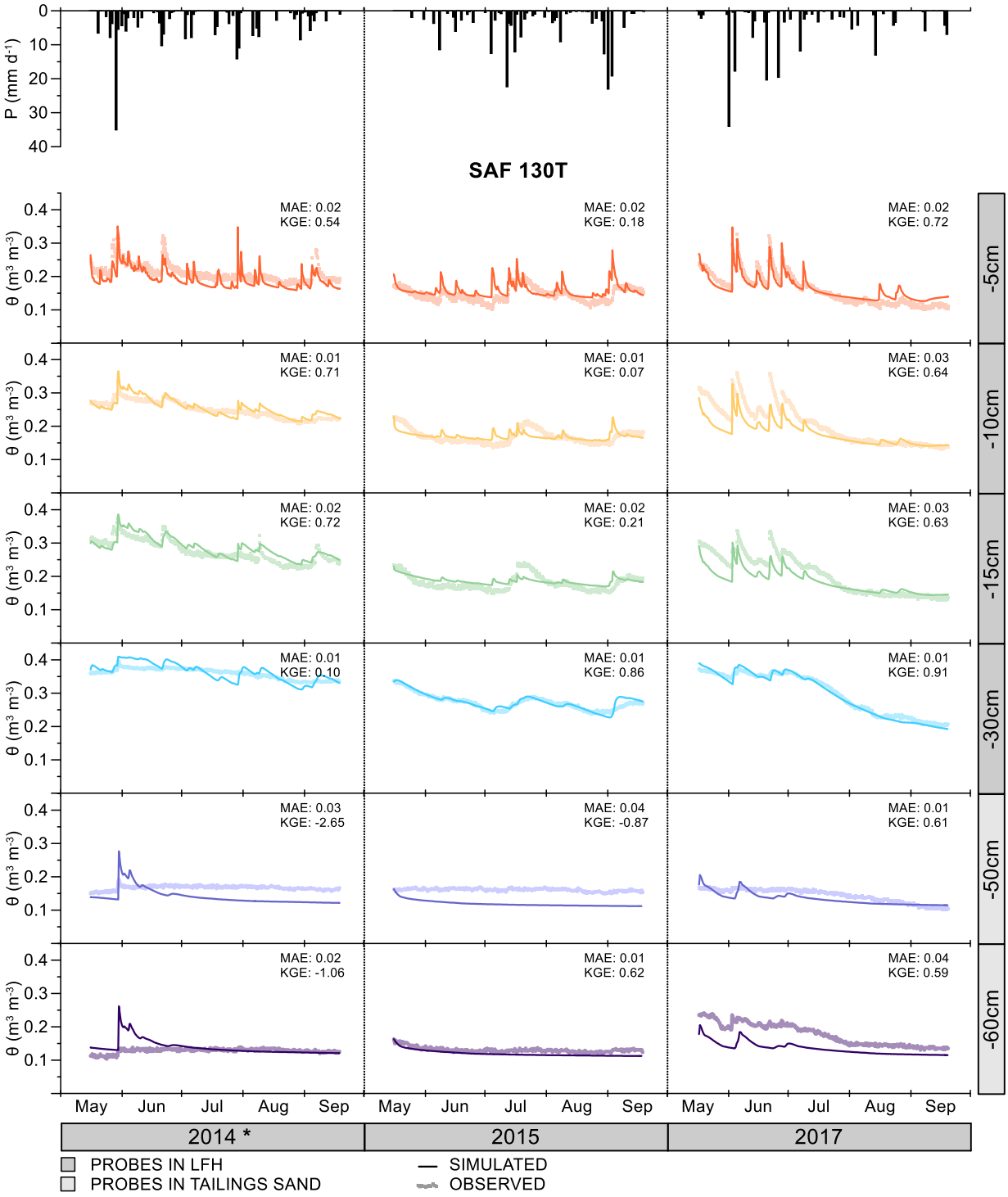

Figure 2-3. Daily precipitation and observed versus simulated soil moisture time series at SAF 130T. Calibration statistics (MAE and KGE) based on the manually calibrated soil hydraulic properties are shown for each individual soil moisture probe. * indicates that this study period was used for calibration.

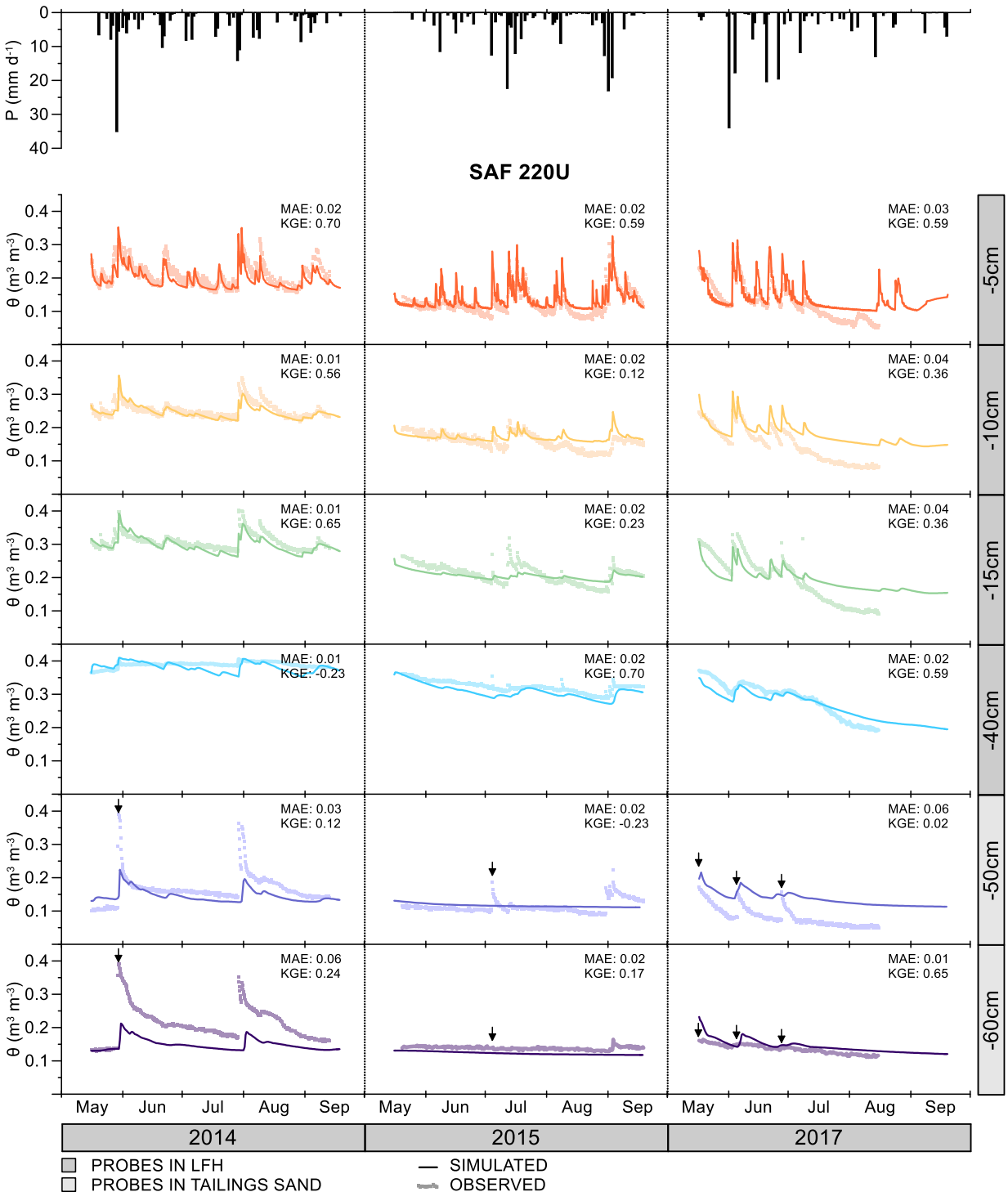

Figure 2-4. Daily precipitation and observed versus simulated soil moisture time series at SAF 220U. Calibration statistics (MAE and KGE) based on the manually calibrated soil hydraulic properties are shown for each individual soil moisture probe. Arrows indicate incongruities between the two probes situated in the tailings sand.

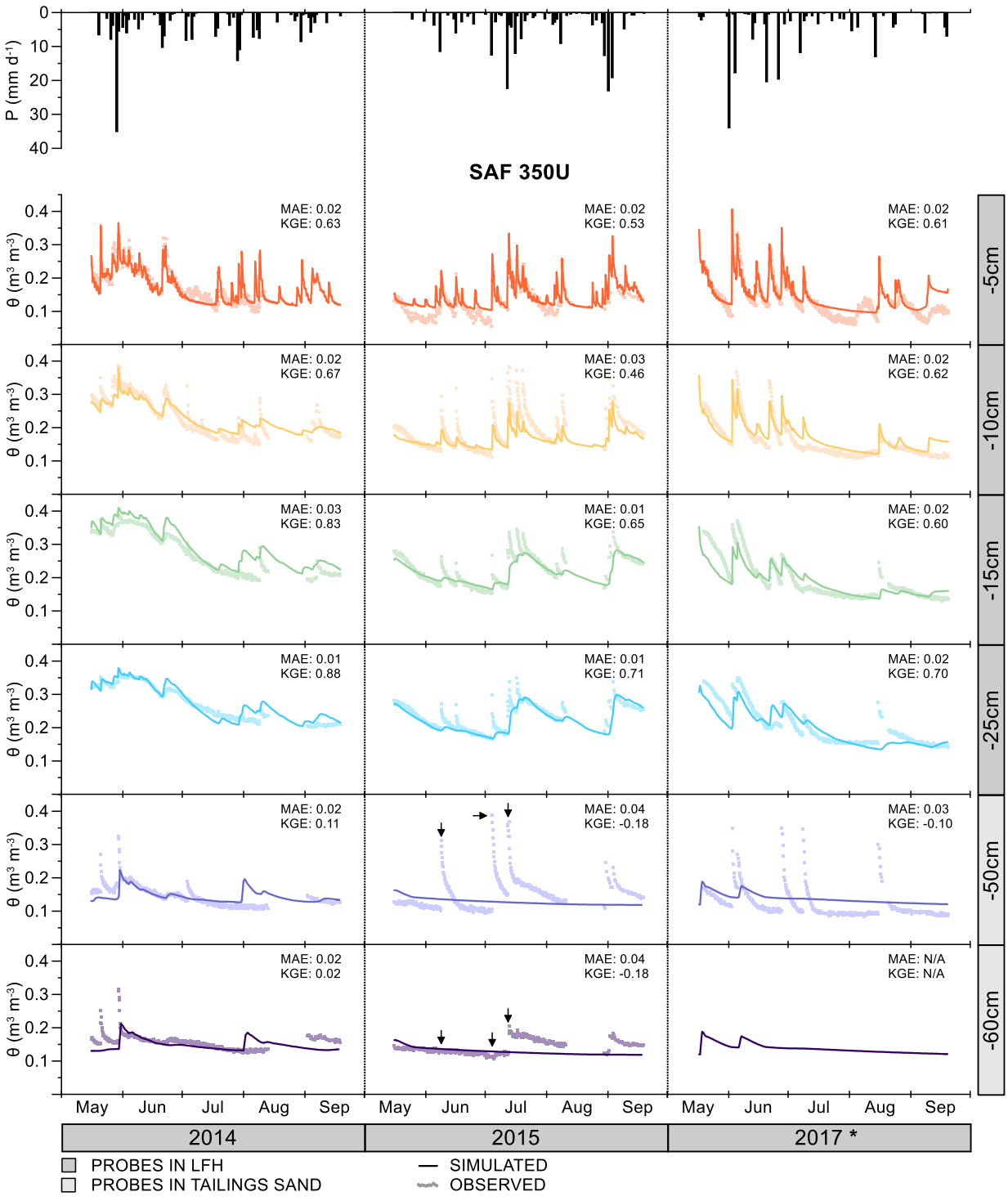

Figure 2-5. Daily precipitation, and observed versus simulated soil moisture time series at SAF 350U. Calibration statistics (MAE and KGE) based on the manually calibrated soil hydraulic properties are shown for each individual soil moisture probe. Arrows indicate incongruities between the two probes situated in the tailings sand. * indicates that this study period was used for calibration.

The 2017 study period had the least precipitation (176 mm) and the largest cumulative potential evapotranspiration (320 mm). The majority of precipitation arrived in May and June, followed by a prolonged dry period. As a consequence, soil moisture storage declined throughout the profile, even at monitoring locations with thicker cover soil. Several pronounced percolation events into the tailings sand were observed at SAF 350U, however soil moisture returned to field capacity within a matter of days.

2.4.2 Model performance and uncertainty analysis

All simulations relying on the manually calibrated hydraulic properties were generally capable of reproducing observed soil moisture dynamics in the LFH (Figures 2-3, 2-4, 2-5). The average MAE for probes located in the LFH at SAF 130T, 220U, and 350U was 0.016, 0.021, and 0.021, respectively – appreciably lower than the specified evaluation criteria associated with probe accuracy of 0.04. The average KGE for LFH at SAF 130T, 220U, and 350U was 0.52, 0.44, and 0.66, respectively. While the KGE indicates some deviation from observed soil moisture, the lower KGE values tended to be associated with probes that had little variation throughout the study period. Under these conditions the KGE can be heavily penalized due to a small difference between simulated and observed mean water content, which suggests a worse fit than what was actually achieved. In contrast to the LFH cover soil, the hydraulic behaviour of the tailings sand was poorly represented in most cases, with an average KGE of -0.07. In general, observed soil moisture movement through the tailings sand appeared to be dominated by several pronounced percolation events. However, the corresponding simulated soil moisture responses were either muted or entirely absent. This was not remedied by inverse or global search optimization – even when fitting soil moisture in the tailings sand was prescribed as the sole priority of the objective function.

Manual calibration of α, n, and Ks indicated a meaningful increase in α (from 1.4 to 5.8) and decrease in n (from 3.1 to 1.6) between the unweathered and weathered LFH. This corresponds to a decrease in the air-entry pressure consistent with the formation of larger pores, and a broadening of the pore size distribution. Saturated hydraulic conductivity also increased in the weathered LFH by one order of magnitude (from 0.002 to 0.02 m h^{-1}). The van-Genuchten parameter representing residual water content (θ_r) of weathered LFH was decreased to align with the lowest volumetric water content recorded by the soil moisture probes. The global search optimization confirmed that the model performance was not sensitive to the hydraulic tortuosity parameter L, as revealed by the uniform probability density function.

Table 2-1. Calibrated soil hydraulic properties.

Symbol	Soil hydraulic properties	Calibrated values ($p_{0.025} \leq \bar{X} \leq p_{0.975}$)[a]			Unit
		$LFH_{weathered}$	$LFH_{unweathered}$	Tailings sand	
θ_r	Residual water content	0.04	0.09	0.08	$m^3 m^{-3}$
θ_s	Saturated water content	0.41	0.41	0.41	$m^3 m^{-3}$
α	Van Genuchten-Mualem parameter related to inverse of air entry pressure	5.8 (5.28 ≤ 5.79 ≤ 6.32)	1.35 (1.2 ≤ 1.47 ≤ 1.82)	12.1	$1 m^{-1}$
n	Van Genuchten-Mualem parameter related to pore size distribution	1.56 (1.41 ≤ 1.49 ≤ 1.57)	3.08 (3.07 ≤ 3.29 ≤ 3.51)	2.2	-
K_s	Saturated hydraulic conductivity[b]	-1.70 (-1. 8 ≤ -1.69 ≤ -1.6)	-2.68 (-2.86 ≤ -2.72 ≤ -2.6)	-0.78	$m h^{-1}$
L	Van Genuchten-Mualem parameter related to tortuosity and connectivity[c]	0.24	0.01	2	-

[a] Manually calibrated soil hydraulic properties for the stratigraphic materials used in the model. In brackets are the average parameter and ±95% confidence intervals produced from the global search optimization. [b] Saturated hydraulic conductivity reported as log-transformed values. [c] Although L was included in the global search optimization, soil moisture dynamics were not sensitive to this parameter, thus the confidence intervals are not reported.

Of the 270,000 parameter sets generated by the global search optimization only 1,140 satisfied the evaluation criteria. These parameter sets were used to generate the bootstrap confidence intervals, which identified that all manually calibrated parameters were within the 95% confidence intervals of the independently calibrated global search optimization parameters (Table 2-1). Furthermore, the simulated evaporation, groundwater recharge, and change in storage across the upland determined using the single set of manually calibrated parameters were within the 95% confidence intervals of the global search estimates (Table 2-1). As demonstrated by the confidence intervals, the effect of soil heterogeneity resulted in a small deviation from the estimated mean upland AET and recharge by (on average) ±15 mm and ±8 mm, respectively. Throughout all years there was close agreement between measured AET, simulated AET using the manual calibration, and average simulated AET computed with global search optimization. The greatest discrepancy between simulated and measured AET occurred in 2017, whereby the cumulative measured AET was 20 mm higher than modelled.

Table 2-2. Cumulative annual totals of measured and simulated water balance components.

Symbol	Water balance components	Cumulative seasonal flux[a]			Unit
		2014	2015	2017	
P	Precipitation[b]	222.5	184.9	175.6	mm
PET	Potential evapotranspiration[b]	283.7	302.8	320.2	mm
AET	Actual evapotranspiration[b(c)[d]]	196.8 (203.1) [185.6 < 202.3 < 219.8]	168.5 (167.4) [154.8 < 166.6 < 188.0]	197.5 (177.8) [160.6 < 173.2 < 187.7]	mm
R	Groundwater recharge[c[d]]	49.2 [48.4 < 54.4 < 62.0]	14.5 [13.3 < 21.3 < 30.1]	41.9 [39.0 < 47.2 < 55.2]	mm
ΔS	Change in storage[c[d]]	-29.6 [-35.9 < -23.4 < -14.4]	2.7 [-6.0 < 6.8 < 12.5]	-43.4 [-43.1 < -36.1 < -30.5]	mm

[a] The cumulative measured and modelled annual fluxes represent the average across the whole upland for the May 16 - September 20 study periods. [b] Water budget component was measured. [c] Water budget component was simulated with manually calibrated values. [d] Simulated water budget component using the global search optimization ± 95% confidence intervals around the average.

2.4.3 Upland water balance

The simulated cumulative water balance for each year is shown in Table 2-2. The dominant hydrologic flux in most summer periods was precipitation, with the exception of 2017, where actual evaporation was slightly greater than P. As calculated by the model, simulated groundwater recharge across the upland in 2014, 2015, and 2017 was 49, 15, and 42 mm, respectively. Within the model, recharge resulted explicitly from rainfall and implicitly from stored snowmelt, the latter being represented through the specification of initial conditions at the start of each season's simulation. Despite the lower precipitation and higher potential evapotranspiration in 2017, high antecedent soil moisture attributed to infiltrated snowmelt resulted in substantially greater recharge than 2015.

2.4.4 Soil weathering and cover thickness

After accounting for interannual climatic variability, weathering of the LFH resulted in a greater quantity of soil moisture partitioned to groundwater recharge and a diminishing amount partitioned to evaporation (Figure 2-6). The impact of this evolution was pronounced during wet years such as 2014, where simulated evaporation was 41 mm greater, and groundwater recharge was 33 mm less, respectively, when comparing profiles comprising entirely weathered and unweathered LFH. Yet this effect was negligible during 2015, which was a particularly dry year in terms of both summer precipitation and low antecedent moisture from

limited snowmelt, where evaporation and recharge deviated by only 7 mm and 5 mm, respectively. Over time, the progressive evolution of the actual soil profile resulted in the hydraulic behaviour of the upland becoming increasingly similar to the equilibrium (weathered) condition.

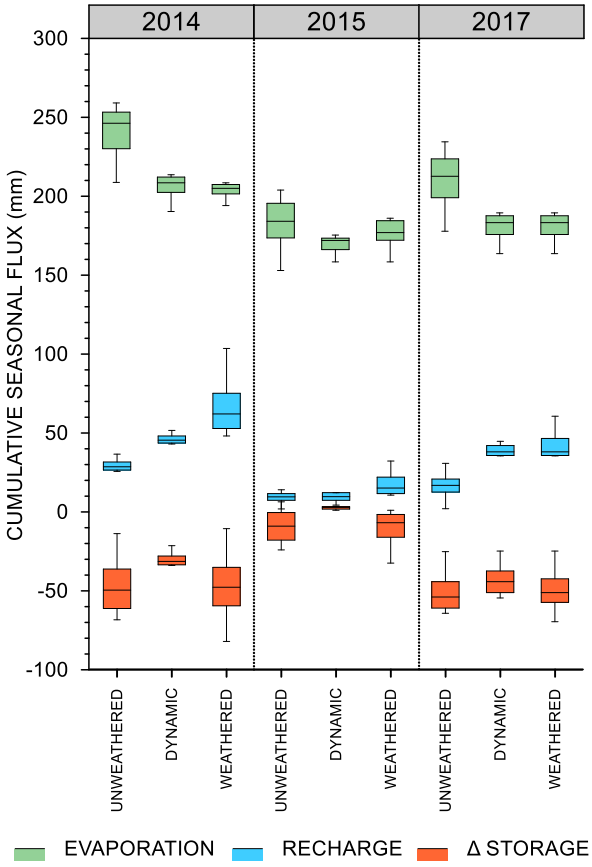

Figure 2-6. Box plots of the simulated soil water balance components using the actual model domains (which reflect the inferred partitioning of the cover soil between weathered and unweathered LFH), and the hypothetical scenarios where the cover soil consisted entirely of unweathered LFH and weathered LFH, representing the as-built and equilibrium conditions, respectively.

The relationship between recharge and cover soil thickness exhibited unexpected behaviour (Figure 2-7); specifically, recharge did not simply decrease monotonically with increased cover soil thickness. The minimum recharge of weathered LFH profiles occurred at intermediate cover soil thicknesses (~25-30 cm) and increased with both thinner and thicker covers. Cover soil thickness had a profound control on cumulative seasonal groundwater recharge in both wet and dry years, and resulted in a maximum deviation of 40 mm between 5 cm and 60 cm covers. This was particularly pronounced in the

scenario where profiles consisted entirely of weathered LFH, in which cumulative recharge varied by up to 63 mm when comparing 10 cm and 65 cm covers.

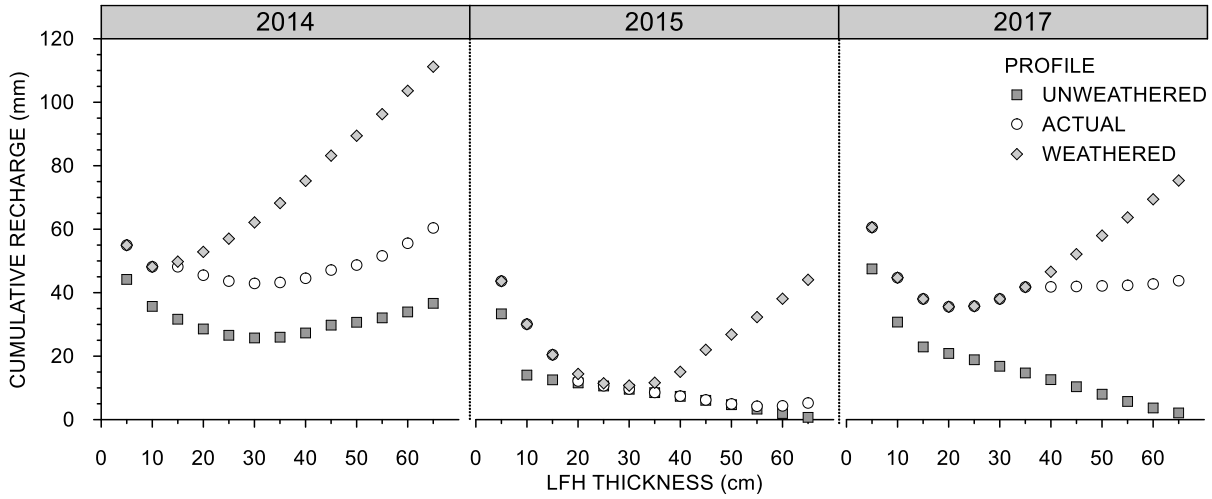

Figure 2-7. Relationship between cover soil thickness and groundwater recharge using the actual model domain, unweathered (as-built) LFH, and weathered (equilibrium) LFH domains.

2.5 Discussion

2.5.1 Soil moisture dynamics

In layered soil systems, where a fine-textured material overlies a coarse-textured material, a sharp change in soil hydraulic properties occurs along the interface. Continuity in pore-water pressure necessitates equal soil water potential at the interface between the two materials, however the contrast in hydraulic properties results in considerable differences in water content (Figure 2-8). Since the underlying coarse-grained material will maintain a comparatively lower water content for a given pressure, the relative permeability of this layer will be drastically reduced. This prevents appreciable downward movement of soil moisture across the inter-layer plane, as long as the pressure at the interface is below a threshold pressure associated with the marked increase in unsaturated hydraulic conductivity of the coarse layer, known as the effective water-entry pressure (ψ_{we}) (Hillel and Baker, 1988). Therefore, to allow for a meaningful percolation rate across the interface, the soil water pressure of the fine-grained material must exceed the water-entry pressure of the underlying coarse soil. It is through this capillary barrier mechanism that the overlying material and associated soil hydraulic properties regulates the release of water to the sublayer. The trend of increasing soil moisture with depth in the relatively fine-grained LFH and sharp contrast with the low soil moisture in the coarse-grained tailings sand demonstrates the presence of a capillary barrier. Similar

hydraulic behaviour attributed to capillary barriers was observed at a nearby reclamation site where LFH was placed over tailings sand (Naeth et al., 2011).

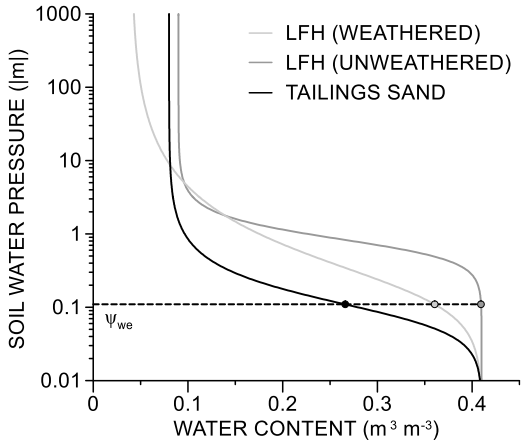

Figure 2-8. Soil water characteristic curves based on the manually calibrated soil hydraulic properties for tailings sand, unweathered LFH, and weathered LFH. Symbols represent the ψ_{we} inferred from measured soil moisture data.

The soil water pressure associated with the rapid increase in unsaturated hydraulic conductivity and therefore appreciable increase in percolation past the capillary barrier (ψ_{we}) can be approximated by identifying the observed soil moisture above the interface that corresponds to a percolation event in the tailings sand (Figure 2-8). The observed soil moisture data suggest that the water-entry pressure of the tailings sand is approximately -0.11 m. At this pore-water pressure the unweathered LFH must be tension-saturated before water will pass the interface and percolate through the tailings sand. At the estimated water-entry pressure of -0.11 m, the unsaturated hydraulic conductivity (K_{we}) of the tailings sand is greater than the K_s of the unweathered (as-built) LFH, which represents the maximum possible rate of water delivery to the interface. Due to the difference in hydraulic conductivity, the flow face must constrict and occupy only a fraction of the cross-sectional area of the porous media (Hillel and Baker, 1988; Baker and Hillel, 1990), resulting in flow breaking into unstable, isolated and elongated lobes known as fingers. Under idealized theoretical conditions, this means that prior to the weathering of LFH at the interface all percolation through the tailings sand must occur as finger flow. Tailings sand was found to be slightly hydrophobic when dry (Ketcheson, 2016), and the extensive and laterally continuous capillary barrier that occurs at the interface between LFH and tailings sand could inhibit the escape of entrapped air during infiltration causing increased air pressure, both of which can contribute to the propensity of a soil to develop unstable flow (Hillel and Baker, 1988). Preliminary dye tests conducted at the upland (G. Dubé, unpublished) confirm the existence of finger-like flow in the tailings sand. However, it is currently unclear if this pattern of percolation is a

consequence of small-scale heterogeneity in tailings sand hydraulic conductivity, the surface topography concentrating water beneath the furrowed surface of the upland, or genuine finger flow.

The presence of finger flow could account for the peculiar hydraulic behaviour of the observed tailings sand soil moisture. Specifically, observing a percolation event under these flow conditions requires the finger to intersect the sensing volume of the soil moisture probe. Evidently, percolation events were captured inconsistently by the monitoring network. This explanation is consistent with the discrepancy between measured and modelled soil moisture dynamics in the tailings sand, as Richard's equation is incapable of describing finger flow in a physically-based manner (Eliassi and Glass, 2001; Jury et al., 2003). This can explain why attempts to optimize the van Genuchten-Mualem parameters by matching observed tailings sand soil moisture were unsuccessful. Nevertheless, the van Genuchten-Mualem parameters of the tailings sand were clearly critical in the accurate representation of the capillary barrier and soil moisture dynamics of the LFH.

2.5.2 Model error and uncertainty

The global search optimization demonstrated that the manually calibrated values were within the 95% confidence intervals of the average parameter value. This supports the assertion that a single set of soil hydraulic properties can adequately represent the soil moisture dynamics of the entire upland and that the chosen manually calibrated parameters are appropriate. Moreover, this suggests that the LFH cover soil exhibits relatively low spatial heterogeneity of hydraulic properties. Whether this should be attributed to the characteristics of the source material, homogenization during placement of the cover, or the impact of weathering which results in soil hydraulic properties tending towards similar values (Benson et al., 2007) is uncertain. However, the fact that the unweathered (as-built) LFH soil hydraulic properties were validated at several locations across the upland (Figures 2-3, 2-4 and 2-5) and were capable of reproducing the observed soil moisture dynamics at these locations implies that the soil already exhibited low spatial variability in hydraulic properties immediately following placement. The modest impact of hydraulic property uncertainty on the upland water balance is a favourable indication of the reliability of the recharge estimates for the time period studied.

Confidence in both the model structure and manual calibration is further bolstered by the favourable comparisons with measured AET (Table 2-2). In 2014 and 2015 there was a +3% and -1% difference between measured and simulated AET, respectively. This suggests that the decision to exclude root water uptake from the model was a reasonable simplification due to the dominance of bare soil evaporation. The underestimation of simulated AET in 2017 could be caused by the increasingly prolific vegetation

development on the upland, which likely draws water from deeper in the LFH profile. While, the deviation of ~10% between observed and simulated AET is within the measurement error of the eddy covariance technique (Scott, 2010) it would not be reasonable to continue to exclude the influence of vegetation in future modelling work.

It should be noted that there is uncertainty associated with basic field measurements like precipitation and potential evapotranspiration, however, it is unlikely that these measurements represent large sources of error. Cumulative annual precipitation measured at the upland rain gauge deviated by less than 6% from a tipping bucket at the East Slope meteorological station. Further, potential evapotranspiration calculated independently using radiation data available from a nearby Environment Canada monitoring station resulted in a cumulative annual PET that differed on average by less than 9%.

2.5.3 Hydrologic function of the upland

An explicit goal of uplands integrated into constructed fen watersheds is to provide sufficient groundwater inflow to offset the cumulative seasonal moisture deficit in the adjacent fen. Cumulative annual AET from the fen averaged 324 mm between 2014 and 2017, which after accounting for precipitation, amounted to a ~8,600 m^3 deficit. Offsetting this deficit requires an annual recharge rate of 41 mm across the upland. Simulated upland recharge derived from precipitation resulted in an average of 35 mm y^{-1}, however including recharge contributions from surface overland flow (Kessel et al., 2019) this increases to 50 mm y^{-1}. This is evidence that the current configuration of the upland provides sufficient recharge, hence groundwater flow to the fen, to supplement the fen's large evaporative loss (Scarlett et al., 2017), at least during the early post-construction period. The average cover soil thickness of 30 cm was thus found to be appropriate; however, areas of both thinner and thicker LFH proved to be important in enhancing recharge, although for different reasons.

It was expected that increased cover soil thickness would have a declining monotonic relationship with groundwater recharge, due to the increased storage capacity of the LFH. While this was responsible for a decline in groundwater recharge in the range from thin (~5 cm) to intermediate (~30 cm) soil covers (Figure 2-7), at greater thicknesses (>35 cm) the capillary barrier was further from the surface, which isolated the 'pool' of near-saturated soil from moisture loss by soil evaporation, and resulted in increased groundwater recharge.

The recharge characteristics of the LFH cover soil influences the distribution and movement of solutes throughout the system. Kessel et al. (2018) illustrated the large-scale transport of sodium from the

upland to the fen and the associated processes of flushing and dilution in the tailings sand aquifer. In previous work, the observed flushing and dilution on the east side of the aquifer was solely attributed to the influence of the active recharge basin which received large volumes of surface overland flow from the hillslopes (Kessel et al., submitted). Here, the results indicated that spatial differences in cover soil thickness between the eastern and western upland (Figure 2-1) also contributed to greater recharge to the eastern portion of the tailings aquifer during wet years (Figure 2-9), and therefore was partly responsible for the increased sodium flushing.

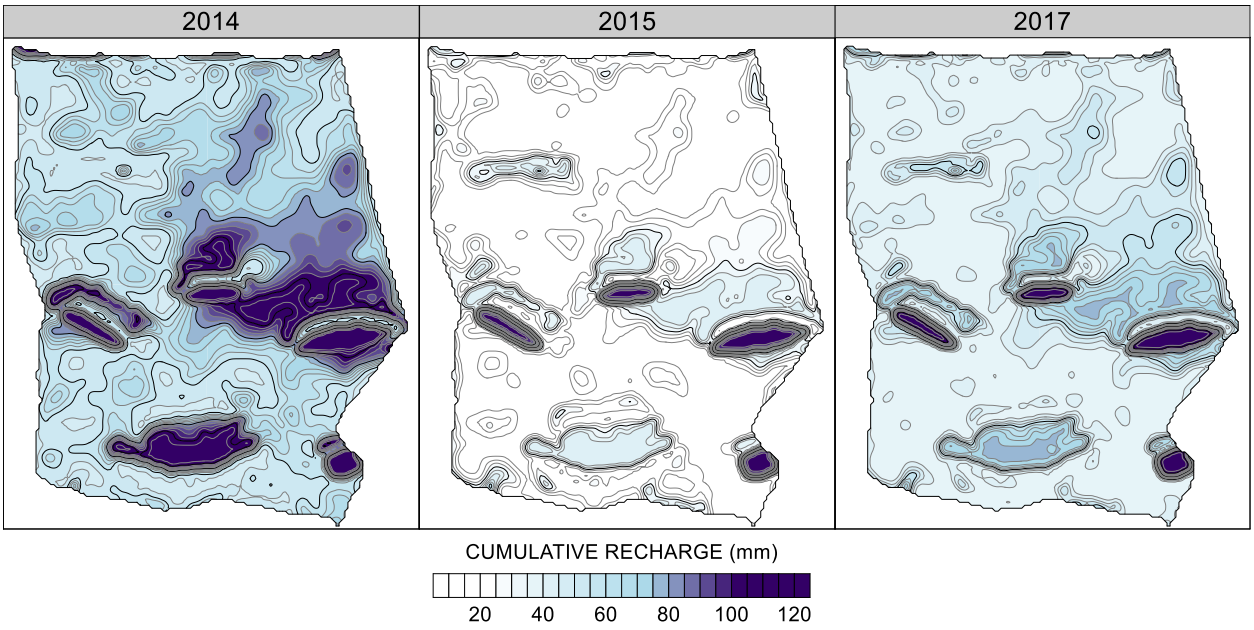

Figure 2-9. Spatial patterns of simulated groundwater recharge across the upland for 2014, 2015, and 2017 based on cover soil thickness.

2.5.4 Implications of soil evolution

The direction and magnitude of the changes in soil hydraulic properties are generally consistent with studies at other reclamation sites (Benson et al., 2007; Meiers et al., 2011). Although the effect of soil evolution on saturated hydraulic conductivity and the air-entry pressure were modest, they had a large impact on the hydraulic function of the cover soil. Soil evolution throughout the study period resulted in a 64% increase in simulated groundwater recharge compared to that simulated with unweathered (as-built) LFH. The simulations suggest that if soil evolution had finished prior to the study period (i.e., the cover was completely weathered or equilibrium LFH), it would have resulted in 30% more groundwater recharge. This highlights the importance of soil evolution in altering the partitioning of soil moisture and ensuring

the supply of groundwater to downgradient ecosystems. Furthermore, it suggests that inferring long-term hydrologic performance of a reclamation cover soil from as-built hydraulic properties can lead to significant deviations from the eventual performance.

Layered materials with a narrow pore-size distribution and a large disparity in air-entry pressure will have a more pronounced capillary barrier effect. Based on the calibrated soil hydraulic properties of weathered LFH, ongoing soil evolution will result in LFH with a higher air-entry pressure (closer to zero) and a broader pore-size distribution, both of which will result in a weaker capillary barrier. This is summarized by the lower moisture content associated with the water-entry pressure of the weathered LFH (Figure 2-8). As a result, the threshold for water-entry is exceeded more frequently and for a longer duration, which is the underlying cause for the greater groundwater recharge following soil evolution. Furthermore, since weathered LFH has a comparatively higher K_s compared to unweathered LFH, and a similar K_{we} to tailings sand, steady flow characterized by relatively uniform wetting fronts may become more common as a percolation mechanism. This potential shift from finger flow to diffuse flow has profound implications on the transport of solutes from the unsaturated zone of tailings sand aquifers and other process-affected materials.

Previous studies have demonstrated the importance of vegetation growth in changing the structure of the soil (Angers & Caron, 1998; Loch & Orange, 1997). However, the sparse and immature vegetation associated with the early successional stage of the upland during the study period suggest this may not have been the most important mechanism of soil evolution at the site. Consequently, freeze-thaw cycling may have been the primary factor in weathering the soil. Other studies that have examined the evolution of cover soil hydraulic properties have noted that the stabilization of these properties is associated with the number of freeze-thaw cycles that the profile has experienced. The progressive deepening of the interface between weathered and unweathered LFH observed in the soil profiles is attributed to the near-surface LFH experiencing more freeze-thaw cycles in any given year, due to brief temperature fluctuations around 0° C (see Figure A-1). By extension, the entire LFH profile experiences at least one annual freeze-thaw cycle, and therefore even deep LFH changes every year, albeit at a slower rate. Accordingly, a gradation of weathering exists, with no clear boundary necessarily present between weathered and unweathered LFH, as was represented in the model. While this was intentionally done to avoid over-parameterization, representing the evolution of the LFH in a realistic gradational manner may have improved the overall calibration of the model, and more accurately portrayed the progressive weakening of the capillary barrier.

The inferred average rate of soil weathering resulted in a deepening of the interface between weathered and unweathered LFH by approximately 11 cm per year. This apparent rate of weathering was intimately related to the climatic conditions observed at the site during the 2014-2017 study period. Specifically, the frequency and duration of temporary excursions above 0°C during the winter period influenced the number of freeze-thaw cycles that a particular portion of the subsurface experienced during a single year. The majority of the upland (>80%) had experienced the requisite number of freeze-thaw cycles for the entire LFH profile to reach equilibrium after 4 years. This is similar to soil evolution timelines at other reclamation sites, where stabilization of soil hydraulic properties occurred after the profile experienced 4-5 freeze-thaw cycles (Meiers et al., 2011; Benson et al., 2007).

2.5.5 Reclamation design

As vegetation establishes in the upland it is anticipated that plants will take advantage of the high soil moisture maintained by the capillary barrier by rooting directly above the LFH-tailings sand interface. As a consequence of root water uptake from this layer, soil water pressure would persist below the threshold (ψ_{we}) needed to overcome the capillary barrier, resulting in less frequent percolation events, particularly during the growing season. Root water uptake from this layer would also likely change the relationship between cover soil thickness and recharge, negating any increases in groundwater recharge yielded from thicker cover soils. Among the concerns regarding the construction of groundwater-fed peatlands such as this, is the length of time it takes to wet the aquifer and establish a hydraulic gradient towards the fen. Postponing planting for several years would lengthen the time following the completion of soil evolution but preceding the meaningful establishment of vegetation. These conditions would maximize the potential of the upland to partition soil moisture to groundwater recharge.

2.6 Conclusion

Contrasting hydraulic properties between the LFH cover soil and tailings sand caused the formation of a capillary barrier. This barrier regulated the release of water to the tailings sand and may have instigated unstable (finger) flow. The processes of soil evolution substantially changed the hydrologic behaviour of the cover soil by increasing saturated hydraulic conductivity by an order of magnitude, decreasing the air-entry pressure by a factor of 4, and decreasing the van Genuchten *n* parameter by a factor of 2. The altered soil hydraulic properties associated with the weathered LFH ultimately resulted in a greater proportion of soil moisture partitioned to groundwater recharge due to the weakened capillary barrier between the LFH cover soil and tailings sand. However, soil evolution will likely be of greatest relevance to the hydraulic

function of the upland in the few intervening years after the weathering is completed but prior to the development of dense vegetation, and during snowmelt. Following this, root water uptake will maintain the soil water pressure below the threshold necessary to exceed the capillary barrier – except during particularly large precipitation events or infiltration of detained snowmelt.

This work has identified temporally stable hydraulic properties for the LFH and tailings sand that are appropriate for use in predictive modelling; however, the processes currently considered by the model are inadequate to understand future groundwater recharge. Specifically, since the aforementioned growth and development of vegetation at the site is anticipated to substantially alter the partitioning of soil moisture between evaporation, transpiration, and groundwater recharge, future modelling work that is currently in progress will explicitly include root-water uptake.

While climate is the most important but most unpredictable determinant of recharge, cover soil thickness also had a profound influence on the partitioning of soil moisture. Although soil evolution had a considerable impact on altering the soil water budget, its dynamic effects on recharge are brief due to the rapid stabilization period. In contrast, the spatial variability of soil hydraulic properties was found to have an insignificant impact on the cumulative annual water budget fluxes. This was determined to be a consequence of the relatively homogeneous LFH cover soil. Ultimately, it will be cover soil thickness, climate and the patterns of vegetation that will be the enduring sources of spatial and temporal variability in groundwater recharge at the Nikanotee Fen Watershed.

2.7 Acknowledgements

Assistance from A. Green, E. Kessel, S. Ketcheson, J. Sherwood, and T. Weber in the field and laboratory is greatly appreciated. Funding from the following sources is gratefully acknowledged: Northern Scientific Training Program (NSTP), the Natural Sciences and Engineering Research Council (NSERC) Canadian Graduate Scholarship (NSERC-CGS) and Collaborative Research and Development Grant (NSERC-CRD; 418557-2011) titled “Evaluating the success of fen creation in the post oil sands landscape” with direct funding from Suncor Energy Inc., Shell Canada Ltd., Imperial Oil Resources Ltd, and Teck Resources Limited.

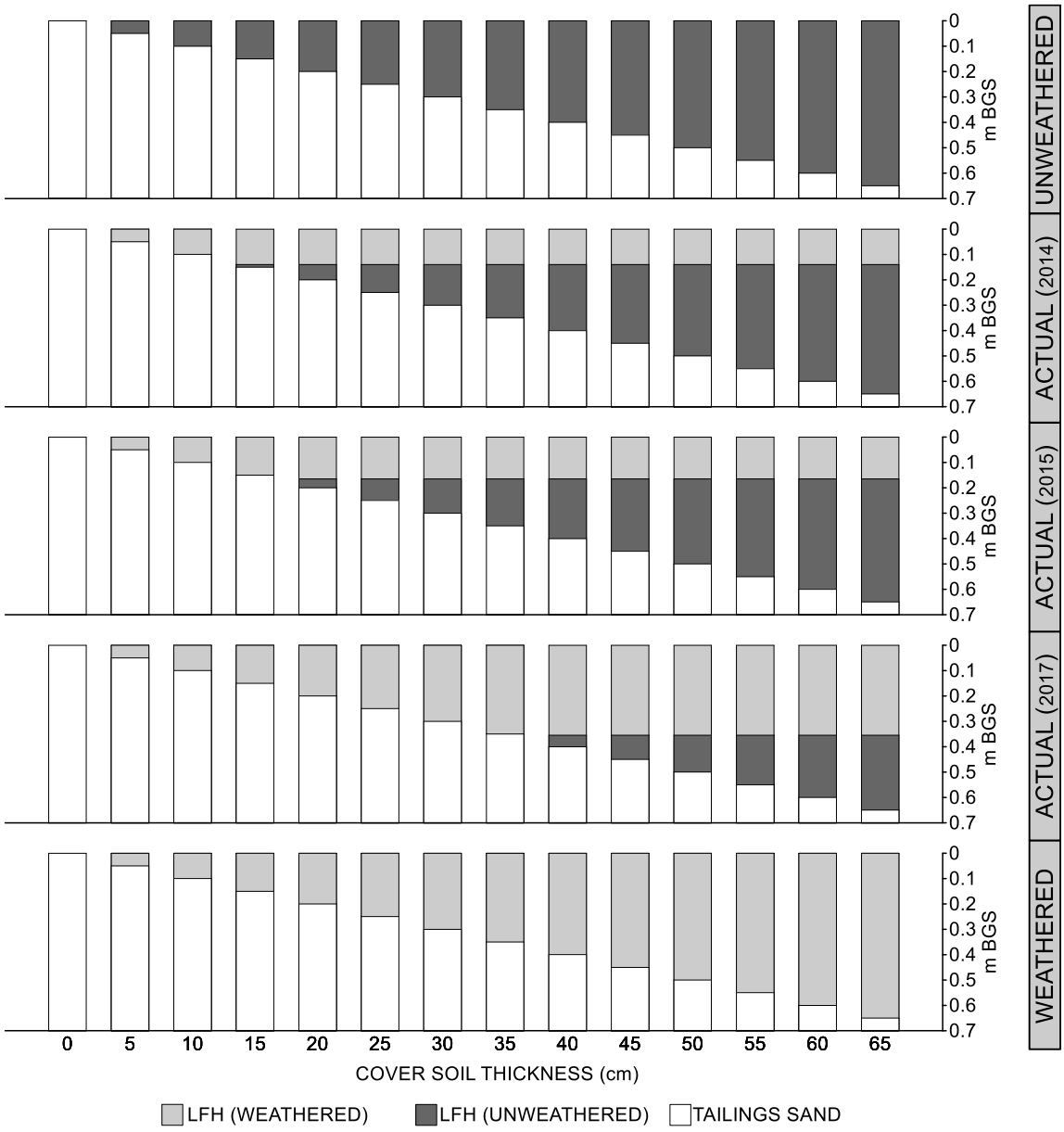

Figure 2-10. Illustration of the model domains used in the simulation of the upland water balance (actual) and comparison between the hypothetical entirely unweathered (as-built) LFH scenario and the entirely weathered (equilibrium) LFH scenario. The depth of the interface between weathered and unweathered LFH for the "actual" profiles represents the average depth at SAF 130T, 220U, and 350U for a given year.

Chapter 3: Modelling the hydrologic effects of vegetation growth on the long-term trajectory of a reclamation watershed

3.1 Introduction

The extraction of bitumen through surface mining of oil sands has disturbed over 900 km^2 in the Athabasca Oil Sands Region (AOSR) (CAPP, 2018). The oil-bearing formation underlies a portion of the Western Boreal Plain, a region characterized by boreal forest and wetlands, the majority of which are fen peatlands (Chee & Vitt, 1989). These landforms and ecosystems are completely removed during surface mining, which results in a landscape of greatly altered hydrologic characteristics (Johnson & Miyanishi, 2008) and one that lacks the ecosystem services of the pre-disturbance environment (Nwaishi et al., 2015). Returning the post-mined landscape in the AOSR to ecosystems of equivalent land capability has become both a matter of public interest and regulatory obligation for oil sands companies (Government of Alberta, 1993). Due to the severity of the disturbance, reclamation of this landscape requires the complete reconstruction of surface and subsurface hydrological processes. Since fen peatlands have been recognized as an important part of the pre-disturbance landscape (Vitt et al., 1996), assessing the feasibility of incorporating fens into mine closure planning has been deemed a priority. In response to this priority, the concept of fen reclamation is being explored at pilot projects within the AOSR, in which fens are integrated into larger watersheds designed to support and maintain wetland ecohydrological function. One such pilot project is the Nikanotee Fen Watershed (NFW), constructed in late 2012, which is the site of extensive research into the hydrological, ecological, biogeochemical, and micrometeorological processes that dictate system function.

Among the challenges in constructing wetlands in the Western Boreal Plain is the regional climate, which exhibits pronounced inter- and intra-annual variability. The regional climate is classified as subhumid, indicating that on an average annual basis cumulative potential evapotranspiration is greater than precipitation (Devito et al., 2005a; Petrone et al., 2007). Natural systems, therefore, operate on thin margins of moisture availability (Devito et al., 2012). This potential moisture limitation was identified as a major obstacle that needed to be addressed in reclamation planning, particularly within the context of constructing wetlands (Price et al., 2010). As a result, fen reclamation projects have included uplands capable of supplying groundwater to adjacent wetlands to supplement precipitation. The intent of this design is to encourage forest development in the uplands while simultaneously allowing for sufficient groundwater recharge to sustain ecohydrological function in the fen (Daly et al., 2012). Mine waste materials, such as

tailings sand, have been incorporated into these upland landforms due to their relative abundance and appropriate hydraulic properties, specifically their high permeability. However, the high hydraulic conductivity and poor moisture retention characteristics (Chapter 2) that allow these materials to act as suitable water conveyance features preclude their use as effective substrates to support vegetation (Fung & Macyk, 2000). Furthermore, these waste materials often contain residual solutes that are transported downgradient to the constructed wetlands by groundwater (Kessel et al., 2018; Biagi et al., 2019). Due to these adverse hydraulic and geochemical characteristics, upland features are typically capped with a cover soil, such as LFH-mineral mix (hereafter referred to as LFH) which is a salvaged forest floor soil that is amenable to upland vegetation growth (Naeth et al., 2013).

The relationship between the spatiotemporal patterns of soil moisture and vegetation development in the post-mined landscape of the AOSR has been explored by several researchers (Naeth et al., 2011; Huang et al., 2011; Huang et al., 2015). These investigations focused on reclamation cover systems that overlay mine waste materials such as saline-sodic shale. Under these conditions, minimizing moisture exchange between the cover system and mine waste is an explicit goal (Carey, 2008). Consequently, the standards by which cover soil performance is assessed have focused on the ability of the cover to supply sufficient moisture for plant transpiration (Huang et al, 2015). However, the reclamation design of constructed fen watersheds requires components to both store water for vegetation and facilitate groundwater recharge to supply downgradient wetland ecosystems. Therefore, the design of these uplands must achieve a compromise between adequate soil moisture storage to support forests and allowing for deeper percolation to underlying aquifers.

Initial assessments on how these constructed fen pilot projects are functioning are beginning to appear in the literature (Chapter 2; Ketcheson et al., 2017; Nicholls et al., 2016). While the ambition of these projects is that self-sustaining fen ecohydrological function will develop and stabilize over a period of decades, as opposed to the time-scales of millennia over which natural peatlands develop, the true trajectory is not yet known (Ketcheson et al., 2016). Prior to the establishment of vegetation, changes to the hydrologic behaviour and associated water balance fluxes of the NFW upland were investigated in Chapter 2, and attributed to the rapid, but brief, weathering of near-surface soil in the early post-construction period. In contrast, the growth and maturation of vegetation will be a comparatively gradual process. Understanding the point at which vegetation growth reaches equilibrium is critical to evaluating the efficacy of upland design, not only because these uplands are intended to have a similar species composition and density to an undisturbed forest, but also the development of vegetation has the potential

to greatly alter the partitioning of moisture into the components of the water budget. In particular, systematic variation in groundwater recharge received by the upland aquifer may have cascading impacts on the development of the fen, its plant community, and carbon accumulation potential.

Characterizing the spatial and temporal patterns of groundwater recharge generated by constructed uplands is a critical component to assessing the hydrologic trajectory of reclaimed systems, evaluating the viability of the current watershed design, and refining the design of future reclamation projects. Therefore, the primary objectives of this study are to: 1) estimate the maximum sustainable vegetation development in terms of leaf area index (LAI) that the upland could support as a function of cover soil thickness; 2) quantify the spatiotemporal patterns and statistical characteristics of upland groundwater recharge and 3) assess the implications of the current upland configuration on the hydrologic trajectory of the system and interpret the findings in order to develop design recommendations that will optimize the partitioning of water between soil moisture storage and groundwater recharge.

3.2 Study site

The Nikanotee Fen Watershed (Figure 3-1) was constructed on a formerly surface-mined area of an oil sands lease approximately 25 km north of Fort McMurray, Alberta (56°55’59” N, 111°25’00” W). The watershed consists of a fen peatland (2.2 ha), upland (7.7 ha), several reclaimed hillslopes (18.7 ha), and an undisturbed natural slope (2.8 ha). The system was designed to function in a simplified, but analogous manner to fen-upland systems in the undisturbed landscape of the Western Boreal Plain, where uplands supply groundwater to downgradient peatlands (Price et al., 2010; Ketcheson et al., 2016). Establishing groundwater flow from the upland to the fen required the construction of an upland aquifer, underlain by a sloped geosynthetic clay liner (GCL) that both instituted a hydraulic gradient towards the fen and limited deep percolation losses to the regional water table. Due to the constraints on material availability that are anticipated following mine closure, the upland aquifer was constructed using coarse tailings sand - a waste product of the bitumen extraction process. This process previously relied on the addition of sodium hydroxide (NaOH) to enhance bitumen recovery (Hepler and Smith., 1994), and along with naturally occurring sodium associated with the marine depositional environment of the overburden (Purdy et al., 2005), resulted in the tailings sand containing elevated concentrations of mobile sodium (Simhayov et al., 2017). Given the adverse geochemical conditions and unsuitable moisture retention characteristics of tailings sand, the upland was capped with an LFH soil prescription, which has been classified as a sandy loam or loam. Detailed textural descriptions of the construction materials can be found in Ketcheson (2015). Although the design specified a 20 cm layer of LFH across the upland, the as-built thickness deviated from

the targeted thickness, with an average and standard deviation of 31 cm and 15 cm, respectively. As a means of adding diversity to the landscape and enhancing infiltration to the aquifer, several raised landforms - referred to as hummocks - were constructed on the upland. Further modifications to the cover soil were made following construction to reduce the quantity of overland flow entering the fen. These modifications included furrowing the LFH perpendicular to slope and removing the LFH from the upslope side of the hummocks, thereby creating basins with exposed tailings sand at the surface. The created basins positioned at the foot of hillslopes received large volumes of surface overland flow, and therefore contributed a disproportionate amount of groundwater recharge to the fen in the early post-construction period (Kessel et al., submitted). In contrast, isolated basins with small upslope catchments were comparatively less effective contributors to groundwater recharge (Kessel et al., submitted). However, basins positioned adjacent to hillslopes filled with sediment entrained in the runoff, decreasing infiltration capacity and the total basin volume, while also increasing the storage potential of the near-surface unsaturated zone. These processes are anticipated to compromise the long-term efficacy of these features. Due to the positioning of the geosynthetic clay liner, surface overland flow from the hillslopes to the upland is the only hydrologic interaction between these landforms.

Previous research has indicated the presence of a capillary barrier between the relatively fine-grained LFH cover soil and the coarse-grained tailings sand (Chapter 2). This barrier has been shown to regulate the release of water from the cover soil to the underlying substrate. While the presence of the capillary barrier is anticipated to have a positive effect on the growth and productivity of vegetation, it diminishes the frequency of deep percolation events to the aquifer, thereby reducing groundwater recharge (Chapter 2). This effect was compounded by differences in cover soil thickness across the site, which, in combination with climatic variability, was the dominant control on the hydrologic behavior of the upland in the early post-construction period, as opposed to spatial variability in soil hydraulic properties (Chapter 2).

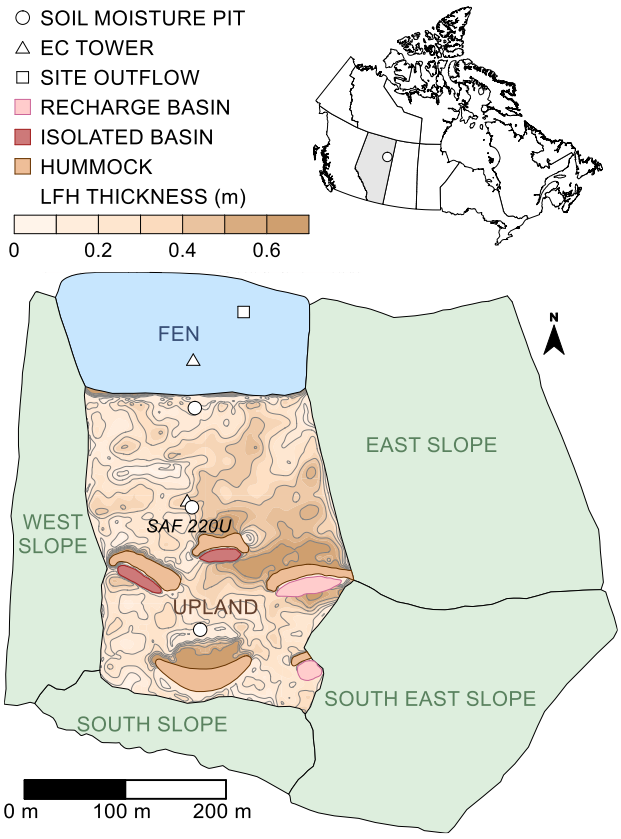

Figure 3-1. Study site map of Nikanotee Fen Watershed depicting the thickness of the LFH cover soil, locations of the upland soil moisture stations, eddy covariance / meteorological towers, and meso-scale landforms (hummocks and basins). Isolated basins do not receive surface overland flow from hillslopes or upgradient upland areas.

3.3 Methods

3.3.1 Model design

The numerical modelling software HYDRUS-1D (Šimunek et al., 2008) was used to simulate variably saturated soil water movement and root water uptake in the upland of NFW. The model domain was discretized with 0.5 cm node spacing, and extended 70 cm vertically into the subsurface. The bottom of the domain was chosen to be below both the maximum LFH cover soil thickness and the zero-flux plane - whereby all water below this point will percolate downwards to the water table. Since the water table remains meters below the model domain for the entire year, the lower boundary condition was set as a unit-gradient condition. The upper boundary condition was specified as an atmospheric boundary, which allows water to enter and leave the domain due to the processes of infiltration and evapotranspiration, respectively.

In order to account for the detention capacity of upland furrows, up to 0.1 m of ponding was permitted to accumulate at the surface before excess water was removed through overland flow.

Table 3-1. Model parameters and variable ranges.

Symbol	Parameter	Value/range	Unit	Source/calculation method
	Soil hydraulic properties			
θ_r	Residual water content	0.04[a] , 0.08[b]	$m^3\ m^{-3}$	From Chapter 2
θ_s	Saturated water content	0.41[ab]	$m^3\ m^{-3}$	From Chapter 2
α	Van Genuchten-Mualem parameter related to air-entry pressure	5.8[a] , 12.1[b]	$1\ m^{-1}$	From Chapter 2
n	Van Genuchten-Mualem parameter related to pore-size distribution	1.56[a] , 2.2[b]	-	From Chapter 2
L	Van Genuchten-Mualem parameter related to tortuosity	0.24[a] , 2[b]	-	From Chapter 2
K_s	Saturated hydraulic conductivity	0.02[a] , 0.167[b]	$m\ h^{-1}$	From Chapter 2
	Meteorological parameters			
P	Precipitation	-	mm	Measured (Environment Canada)
PET	Potential evapotranspiration	-	mm	Calculated using Penman[c]
PT	Potential transpiration	-	mm	Calculated using Eq. 2
PE	Potential soil evaporation	-	mm	Calculated using Eq. 3
I	Interception	-	mm	Calculated using Eq. 4
hCritA	Minimum allowable surface pressure head	-500	m	Estimated
	Vegetation parameters			
D_r	Maximum rooting depth	0.05 - 0.65	m	Specified to equal LFH thickness
a_i	Radiation extinction coefficient	0.76	-	From Aubin, et al (2000) for boreal forest jack pine and understory
LAI_{max}	Maximum annual leaf area index	0 - 4	$m\ m^{-1}$	Specified for different scenarios
SCF	Surface cover fraction	0.53 - 0.95	$m\ m^{-1}$	Calculated using Eq. 1
P_s	S-shaped parameter related to the slope of the transpiration reduction function	2.8	-	Fit to relationship between stomatal closure and soil water pressure
P_0	Soil water pressure that corresponds to the initiation of stomatal closure	-3.7	m	Calculated as average between aspen[d] and pine[e]
P_{50}	Soil water pressure corresponding to a 50% reduction in transpiration	-35.7	m	Calculated as average between aspen[d] and pine[e]
P_{100}	Approximate wilting point: pressure corresponding to complete stomatal closure and suspension of transpiration	-155	m	Calculated as average between aspen[d] and pine[e]
ω_c	Root water uptake compensation factor	0.5	-	Estimated
I_a	Interception constant	2	mm	Estimated

[a] Parameter for LFH. [b] Parameter for tailings sand. [c] Penman (1948). [d] Jarvis & Jarvis (1963). [e] Havranek & Benecke (1978).

In Chapter 2, the simulated the soil moisture dynamics in the near-surface of the NFW upland was simulated, and described the temporal evolution of LFH soil hydraulic properties during the early post-construction period. Capturing the hydrologic behavior of the cover soil in the model required the partitioning of the LFH layer into two constituents, an upper layer that experienced a greater degree of weathering, and a deeper layer with minimal weathering. Between 2014 and 2017 (1-4 years post-construction) the depth of the interface between these layers was inferred to move progressively deeper into the subsurface. For the purposes of this current manuscript it is assumed that this rapid evolution has ceased, and the soil hydraulic properties have stabilized. Therefore, the model domain consisted of two materials, weathered LFH and tailings sand. Separate model domains were constructed to represent the full range of LFH cover soil thickness. The thickness of the LFH was varied in 5 cm increments from 0 cm to 65 cm thick, resulting in 14 model domains. The van Genuchten-Mualem soil hydraulic property model was used to represent the relationship between volumetric water content (θ), soil water pressure (ψ), and unsaturated hydraulic conductivity (van Genuchten, 1980). The validated van Genuchten-Mualem parameters from Chapter 2 were used to parameterize the numerical model (Table 1) without further calibration or adjustment. Due to the low clay content of the coarse tailings sand (<1%) the effect of sodium on the hydraulic conductivity was excluded from the model.

3.3.2 Long-term simulations

Due to the short history of monitoring at the Nikanotee Fen Watershed, a 65-year meteorological dataset (1953-2017) from a nearby Environment Canada monitoring station was used to capture interannual climatic variability. The long-term climatic dataset was applied to simulations using every permutation of 14 cover soil thicknesses and 5 hypothetical vegetation development scenarios. The level of vegetation development was represented by the maximum annual leaf area index (LAI_{max}), and was specified as either 0 (unvegetated), 1, 2, 3, or 4. As a means of assessing the sensitivity of groundwater recharge and the maintenance of plant productivity to snowmelt, simulations were run including snowmelt and excluding snowmelt – in the latter scenario, water input into the model was solely provided by rainfall.

3.3.2.1 Simulation period

The duration of each annual simulation corresponded to the hydrologically active period, which commenced with the thawing of ground frost in the spring and freezing in the autumn. Freezing and thawing depth was calculated using the Stefan's equation (Jumikis, 1977). Snow that arrived during the frozen period accumulated but was subject to sublimation, which was calculated on an hourly basis using the

Kuz'min equation (Gelfan et al., 2004) and subtracted from the snowpack. The remaining snowpack snow water equivalent (SWE) was applied to the upper boundary of the model domain at the start of the simulation. Details of this procedure can be found in Appendix A. The implications of this assumption will be discussed below. For data management reasons, each year was simulated individually, this required applying the soil moisture distribution from the final time step of the previous year as the initial soil moisture profile for the subsequent simulation.

3.3.2.2 Potential evaporation and transpiration

Potential evapotranspiration (PET) was calculated using the Penman equation (Penman, 1948). PET was partitioned into potential transpiration (Tp) and potential soil evaporation (Ep) using the Beer-Lambert law, which describes the transmission and interception of solar radiation by the canopy (Ritchie, 1974):

$$SCF = 1 - e^{-a_i \cdot LAI} \tag{1}$$

$$T_p = PET \cdot SCF \tag{2}$$

$$E_p = PET(1 - SCF) \tag{3}$$

where a_i is the radiation extinction coefficient and represents the light attenuation by the canopy, and SCF is the surface cover fraction. Interception of rainfall by the canopy was calculated using the equation of Braden (1985):

$$I = I_a \cdot LAI \left(1 - \frac{1}{1 + \frac{SCF \cdot P}{I_a \cdot LAI}}\right) \tag{4}$$

where I is the interception, I_a is the interception constant representing the maximum rainfall interception per unit LAI, and P is precipitation.

The onset of leaf emergence and time until complete foliation was determined using a degree-day approach following ground thaw of the upper 30 cm of soil. As determined by Barr et al. (2004) for a boreal aspen forest, leaf emergence began after 69 degree-days and complete foliation occurred after 316 degree-days. Barr et al. (2004) found that senescence of aspen was controlled primarily by the decreased photoperiod in autumn, therefore the start and end of senescence was assumed to occur on the same dates every year (August 15 and September 15, respectively). The temporal LAI patterns used in the simulations are shown in Figure 3-2.

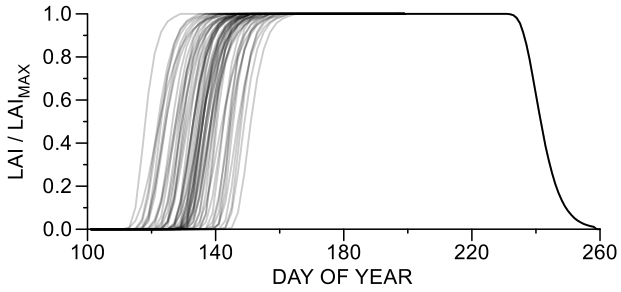

Figure 3-2. Seasonal patterns of leaf area index, describing leaf emergence, complete foliation, onset of senescence, and abscission. These patterns were based on the relationship between degree days and LAI found by Barr et al. (2004) for each of the 65 years in the long-term meteorological dataset.

3.3.2.3 Root water uptake

A uniform root distribution was specified in the LFH. It was assumed that roots did not penetrate the tailings sand due to the high sodium concentrations; this is corroborated by field observations. Actual transpiration (T_a), and therefore root water uptake, occurred at the potential level until a threshold soil water pressure was reached (P_0), which marked the initiation of stomatal closure and the onset of plant water stress (Figure 3-3). Subsequently, root water uptake was reduced according to the S-shaped function of van Genuchten (1987):

$$T_a = T_p \left(\frac{1}{1 + \left(\frac{\psi}{P_{50}} \right)^{P_s}} \right) \tag{5}$$

where P_{50} is the soil water pressure that corresponds to a 50% reduction in transpiration, and P_s is a parameter related to the slope of the transpiration reduction function. Although the function decreases asymptotically, it is approximately 0 at a soil water pressure of -155 m (P_{100}), which corresponds to complete stomatal closure and the wilting point of pine (Havranek & Benecke, 1978), and aspen (Jarvis & Jarvis, 1963), the dominant tree species on the upland. Simulating root water uptake using the S-shaped function of van Genuchten requires fewer parameters than the more widely used piece-wise Feddes function (Feddes et al., 1974) and in theory is a more physically-realistic representation of the reduction in transpiration due to low soil water potentials (Bradford & Hsiao, 1982; Schröder et al., 2014). Root water uptake compensation was considered, to allow for plant roots to continue to extract water at the potential rate, even if portions of the rooting zone had a pressure (ψ) less than the threshold for stomatal closure (Skaggs et al., 2006). This reflects the dynamic ability of vegetation to increase root water uptake from relatively moist soil to offset the loss from the stressed rooting zone (Jarvis, 2011).

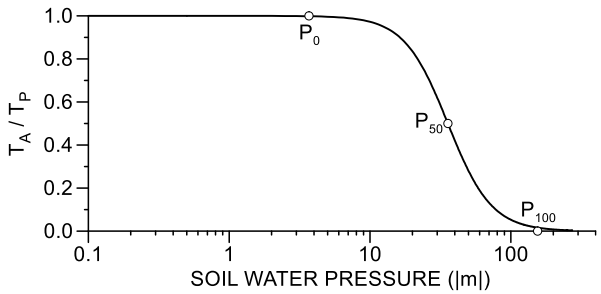

Figure 3-3. Transpiration reduction function based on the S-Shaped function of van Genuchten (1987). Where P_0 represents the soil water pressure that corresponds to the initiation of stomatal closure, P_{50} represents the soil water pressure corresponding to a 50% reduction in transpiration, and P_{100} represents complete stomatal closure and the cessation of transpiration.

3.3.2.4 Model validation

Validation of soil hydraulic properties and root water uptake parameters for the 2018 ice-free period was conducted at the SAF 220U soil moisture station, which was instrumented with a profile of 6 dielectric impedence reflectrometry soil moisture probes (Stevens Hydra Probe II). The SAF 220U soil moisture station was located in the center of the upland (see Figure 3-1) in an area with considerable vegetation development (LAI of 1). In previous work, rigorous model validation of soil hydraulic properties was conducted for 2014, 2015, and 2017 at several soil moisture stations in the upland; however, this model did not consider root water uptake (Chapter 2) since it represented the early post-construction period when vegetation was at an early successional stage. As an additional validation step, the simulated actual evapotranspiration (AET) was compared to an eddy-covariance system directly adjacent to the SAF 220U soil moisture station; details of the specific methodology for determining AET using eddy-covariance can be found in Ketcheson et al. (2017).

3.3.3 Maximum sustainable vegetation growth

In water-limited ecosystems, and over long periods of time, the spatial patterns of vegetation will reflect a community with characteristics that result in the minimization of water stress and maximization of water use (Rodriguez-Iturbe et al., 1999). The self-organized patterns of vegetation can therefore be determined by summarizing this tendency (Caylor et al., 2009). Using the spatiotemporal patterns of soil moisture generated from the long-term simulations, plant water stress (ξ) was calculated using the equation of Porporato et al. (2001) for every daily timestep:

$$\xi(t) = \begin{cases} 1 & s \leq s_w \\ \left[\dfrac{s^* - s(t)}{s^* - s_w}\right]^q & s_w < s \leq s^* \\ 0 & s > s^* \end{cases} \quad (6)$$

where s is the vertically-integrated saturation, s^* is the saturation associated with the onset of stress and assumed to correspond to the initiation of stomatal closure (corresponds to s at a pressure of P_0), s_w is the saturation at wilting point, and q is a parameter representing non-linearity in the relationship between soil moisture and plant water stress and specified to equal 4 to emphasize the greater physiological consequences associated with high levels of water stress, which may result in permanent or irreversible damage, as discussed by Rodriguez-Iturbe, et al. (1999). Scaling the average seasonal plant water stress by the average rate of root water uptake (T_a) during the growing season gives the stress-weighted root water uptake (ζ) equation of Caylor, et al (2009):

$$\zeta = \overline{T}_a \cdot (1 - \bar{\xi}) \quad (7)$$

The stress-weighted root water uptake integrates plant water use and water stress into an individual metric. Thus, when a plant experiences maximum stress ($s \leq s_w$, $\xi = 1$) the resultant ζ is zero, and when under minimal stress ($s > s^*$, $\xi = 0$) ζ will equal T_a. The maximum sustainable LAI was determined by identifying the maximum stress-weighted root water uptake associated with each cover soil thickness.

3.3.4 Statistical characterization of recharge

Detailed surveys taken during construction allowed for the delineation of LFH thickness across the upland with high spatial resolution. The spatial patterns of LFH were related to the maximum sustainable LAI based on the stress-weighted root water uptake relationship. Average and standard deviation groundwater recharge were calculated based on the maximum sustainable LAI and the LFH thickness across the upland.

3.3.5 Estimating needs of the fen

In order to assess the suitability of the upland design in regard to supplying sufficient groundwater to the downgradient fen peatland, the annual groundwater requirements of the fen were estimated and compared with cumulative annual upland recharge. This calculation represents a rough approximation of the assumed loss of aquifer storage required to offset any deficit sustained by the fen for a given year, or conversely the surplus of water that could contribute to aquifer storage or surface outflow. The fen was assumed to evaporate at the potential rate (AET equaled PET), receive the same rainfall as the upland, and require a

baseflow (measured as 0.138 L s^{-1}) out of the system for the entirety of the hydrologically active period. Therefore, the fen water budget for each year was calculated as:

$$\Delta S = P + GW_{in} - AET - SW_{out} \quad (8)$$

where ΔS is the change in storage, P is precipitation (including snowmelt), GW_{in} is groundwater discharge to the fen (assumed to equal upland groundwater recharge), AET is actual evapotranspiration, and SW_{out} is surface water outflow. Negative values indicate a water deficit that would manifest as either a decline in the water table or would be offset by contributions from aquifer storage, while positive values denote a surplus of water that would be partitioned toward excess surface outflow or replenishing aquifer storage.

3.4 Results

3.4.1 Model validation

The soil moisture dynamics at the SAF 220U soil moisture station were acceptably represented during the 2018 validation period (Figure 3-4). The average Kling-Gupta Efficiency (KGE; Kling et al., 2012) and mean absolute error (MAE) of the observations in the LFH cover soil was 0.66 and 0.023, respectively. Deviations between observed and simulated patterns of soil moisture in the tailings sand were similarly noted in Chapter 2, and attributed to wetting-front instability leading to the initiation of finger flow at the interface between the LFH cover soil and the tailings sand. During the peak growing season near-surface soil moisture decreased and approached residual saturation, primarily due to root water uptake. The discrepancy between simulated and measured actual evapotranspiration using the eddy covariance method for the 2018 growing season was 1 mm. Simulated and measured cumulative seasonal water fluxes for the 2018 validation period are shown in Table 3-2.

3.4.2 Simulated water balance

The average length of the hydrologically active period calculated using Stefan's equation was 183 days (Figure 3-5a). The average date of the spring thaw and fall freeze-up occurred on April 23 and October 23, respectively. During the winter period, an average of 120 mm of SWE was deposited by snowfall. Sublimation calculated using the Kuz'min equation resulted in an average loss of 38 mm SWE from the accumulated snowpack. The remaining 82 mm SWE was partitioned to snowmelt (Figure 3-5b). Throughout the 65-year simulation period, cumulative annual rainfall averaged 306 mm and potential evapotranspiration averaged 470 mm y^{-1}.

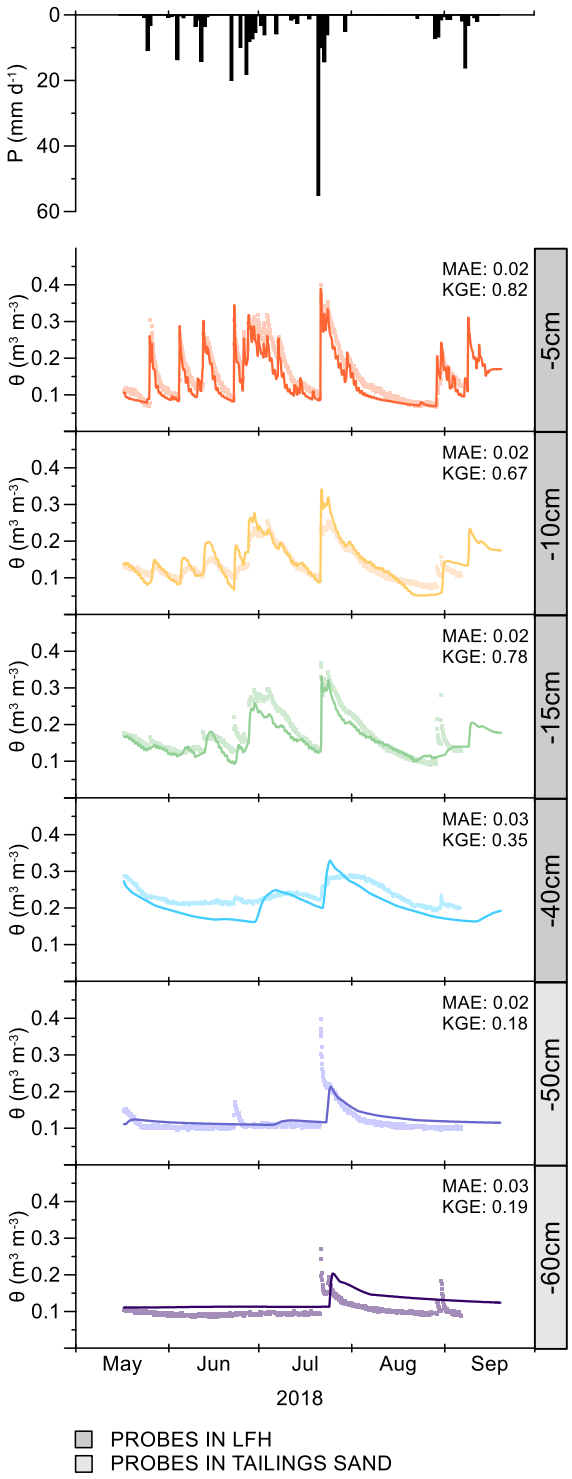

Figure 3-4. Daily precipitation and observed versus simulated soil moisture time series at the SAF 220U soil moisture station located in the center of the upland. Model fit summary statistics (MAE and KGE) are shown for each soil moisture probe. Thin solid lines represent the simulated soil moisture, pale dots represent observed soil moisture.

Table 3-2. Measured and simulated cumulative seasonal water fluxes and stores for the model validation period (May 16-September 20).

Symbol	Water balance components	Cumulative annual flux and stores (mm)
P	Precipitation[a]	280
PET	Potential evapotranspiration[a]	339
AET	Actual evapotranspiration[a (b)]	257 (258)
R	Groundwater recharge[b]	27
ΔS	Change in storage[b]	+16

The measured and modelled fluxes represent the cumulative total for May 16-September 20, 2018 at the SAF 220U soil moisture station and the upland meteorological / eddy covariance station. [a] Water budget component was measured. [b] Water budget component was simulated.

Soil evaporation did not exhibit a strong relationship with cover soil thickness (Figure 3-6a), and displayed minor variation at cover thicknesses greater than 20 cm. The exception to this was the unvegetated scenario (LAI of 0), which did not have a monotonic increase in soil evaporation with cover soil thickness. Maximum evaporation under unvegetated conditions occurred at a cover thickness of 30 cm, and declined modestly as cover thickness increased. Soil evaporation at higher levels of vegetation development was smaller (Figure 3-6a), and corresponded to greater amounts of water lost via transpiration when vegetation was present (Figure 3-6b).

The model revealed a monotonically increasing relationship between cover soil thickness and root water uptake (Figure 3-6b). Root water uptake increased asymptotically towards the potential level, but only the vegetation scenario with an LAI of 1 was capable of approaching the potential root water uptake, albeit only with the thicker cover soils (>45 cm). Vegetation development scenarios with an LAI of 2, 3, and 4 resulted in similar partitioning of soil moisture to root water uptake. Greater simulated rainfall interception by the canopy at high LAI decreased plant available water, and was associated with slightly reduced root water uptake for LAI of 4.

Groundwater recharge decreased monotonically with increasing cover thickness when root water uptake was considered (Figure 3-6c). However, vegetation development greater than an LAI of 1 resulted in only a marginal reduction in groundwater recharge. Bare tailings sand, which lacks an overlying cover soil, and which was assumed to preclude vegetation development, resulted in the maximum groundwater recharge. On an average annual basis, bare tailings sand cumulatively partitioned 281 mm of soil moisture to groundwater recharge. Recharge under unvegetated conditions had an opposite pattern to bare soil evaporation, with a minimum at 30 cm soil cover thickness (Figure 3-6c), corresponding to the bare soil evaporation maximum (Figure 3-6a). The standard deviation of recharge for each cover soil thickness (not shown) indicated that the greatest interannual variability in total cumulative recharge volume occurred for bare tailings sand and thin cover soils. However, by contextualizing the standard deviation in relation to the average recharge (Figure 3-6d) it is apparent that bare tailings sand is the most consistent supplier of groundwater recharge. The inclusion of snowmelt in the simulation resulted in substantially greater annual recharge for all cover thicknesses and LAI scenarios, but had a negligible effect on soil evaporation and root water uptake.

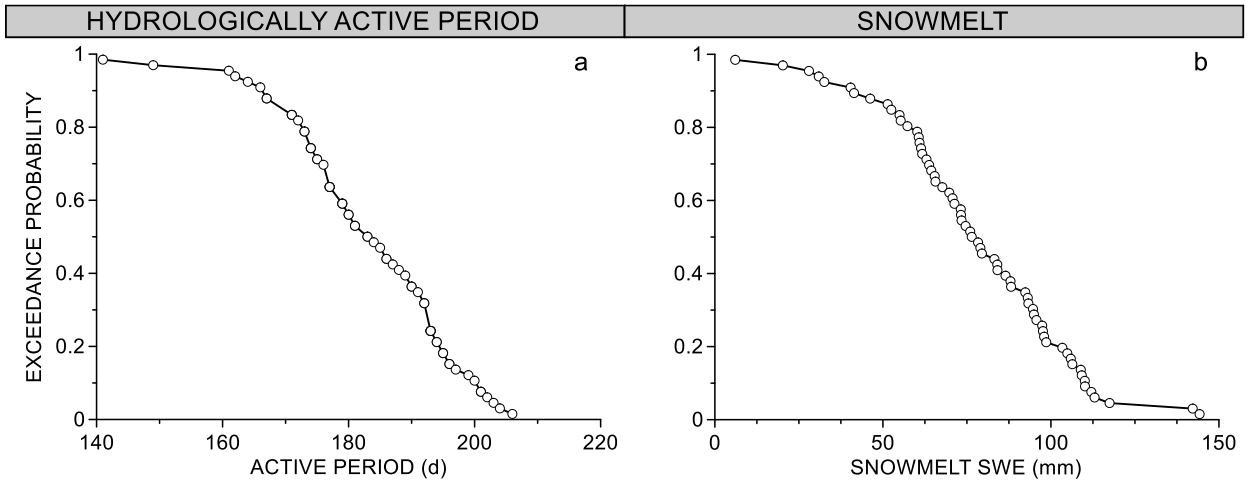

Figure 3-5. Exceedance probability curves for the length of the hydrologically active period (total number of thawed days) and snowmelt depth (as snow water equivalent) calculated annually for the 65-year meteorological record. The hydrologically active period was calculated using the Stefan equation, and the snowmelt was estimated using Environment Canada snow depth data minus sublimation calculated using the Kuz'min equation. See Appendix A for details.

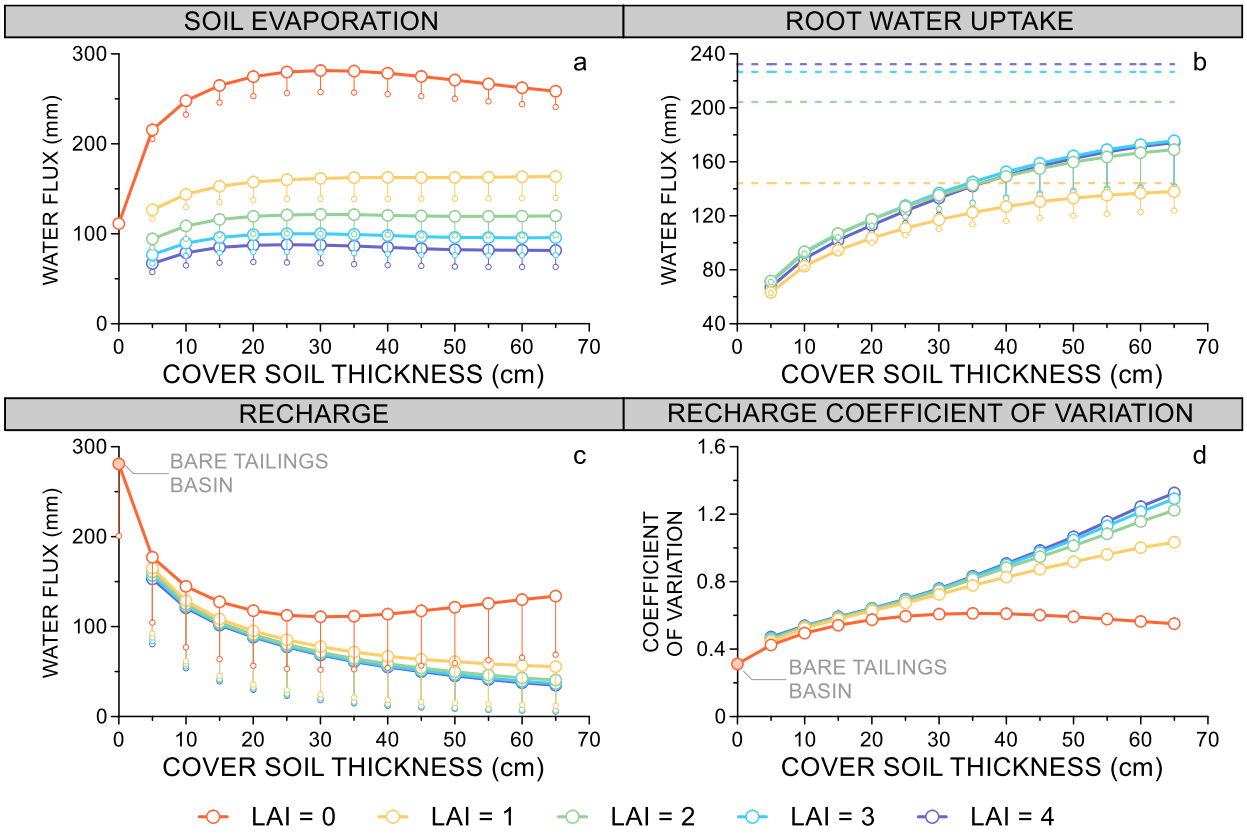

Figure 3-6. Simulated water balance fluxes of average soil evaporation (a), root water uptake (b), and groundwater recharge (c) for each cover soil thickness and vegetation development scenario. Vertical bars represent the average flux associated with the simulations that exclude snowmelt shown for a, b, and c. Dashed line represents potential root water uptake. The coefficient of variation (standard deviation normalized by the mean) for groundwater recharge is shown in panel (d).

3.4.3 Stress-weighted root water uptake

Generally, vegetation rooted in thicker cover soils experienced less static water stress in a given year (Figure 3-7). Among different vegetation scenarios, increasing LAI beyond 2 did not substantially increase the static water stress of thinner cover soils, as plants rooted in these thinner covers were already subject to very high levels of water stress. However, increasing LAI did result in higher levels of static water stress sustained by thicker cover soils. Ultimately, this led to a stress-weighted root water uptake that indicated that the maximum sustainable LAI for cover soils between 5-40 cm thick is 1, and 45-65 cm thick is 2 (Figure 3-8). No cover soil thickness simulated was capable of consistently maintaining LAI of 3 or 4.

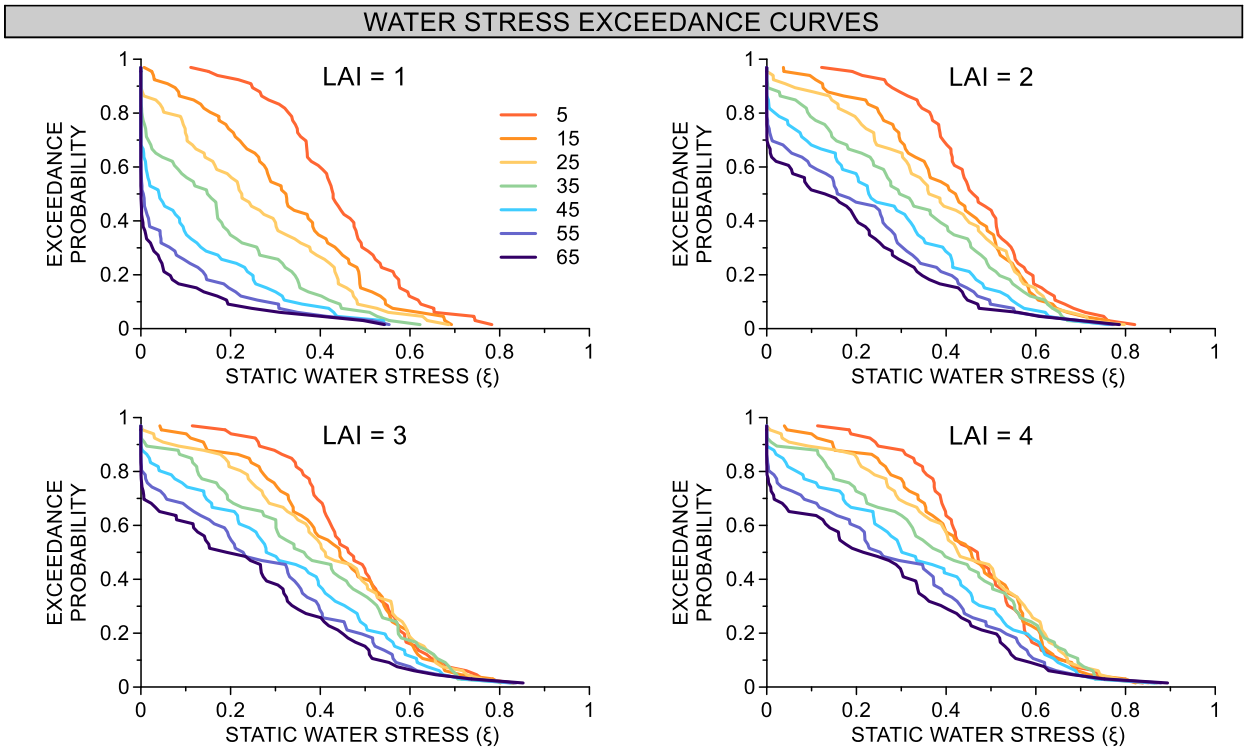

Figure 3-7. Exceedance probability curves of average annual static water stress for each cover soil thickness (5-65 cm) and vegetation development scenario (LAI).

3.4.4 Statistical characterization of recharge

The average maximum sustainable LAI of the upland was 1.2. Under these LAI conditions, and with explicit consideration given to the spatial variability in cover soil thickness, the average cumulative groundwater recharge across the upland was calculated to be 83 mm y^{-1}, with an interannual standard deviation of 58 mm. On an average annual basis groundwater recharge represented 20% of annual precipitation (snowmelt and rainfall). The maximum groundwater recharge was yielded by the central and western bare tailings sand basins, while the minimum recharge was generated by areas of the upland with 65 cm of LFH cover soil and a maximum sustainable LAI of 2.

3.5 Discussion

3.5.1 Hydrologic function

The spatial and temporal patterns of soil moisture movement within the upland were governed by the complex interactions between soil, vegetation, and atmospheric processes. The soil hydraulic properties of

the construction materials, their layering, and the level of vegetation development caused a consistent and systematic control on the partitioning of soil moisture, which induced spatial variability across the upland (Figure 3-9). Seasonal and interannual variations in snowmelt, rainfall, and potential evapotranspiration introduced temporal variability. Explicit representation of these sources of variability in soil moisture dynamics in space and time were important for characterizing the hydrologic behaviour of the upland.

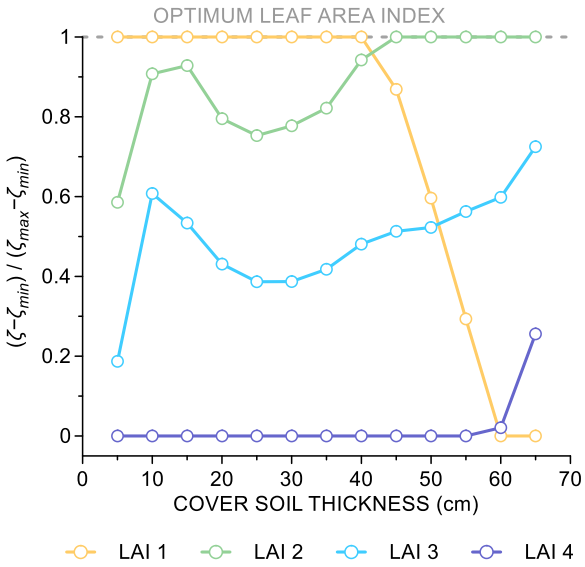

Figure 3-8. Normalized stress-weighted root water uptake for each cover thickness and LAI scenario. A normalized stress-weighted root water uptake of 1 indicates the maximum sustainable LAI for a given cover soil thickness. For any given optimal LAI, a lower LAI is not preferable since it is not fully exploiting available soil moisture, while higher LAI values result in an increase in water stress that outweighs the potential reward from additional water uptake.

One of the fundamental differences in hydraulic performance between the LFH cover soil and bare tailings sand basins is the absence of a capillary barrier when tailings sand is exposed at the surface. Capillary barriers prevent the passage of appreciable quantities of water across the interface until a threshold soil water pressure is exceeded in the overlying fine material (Khire et al., 2000). The presence of even a thin overlying layer of LFH markedly reduced the quantity of groundwater recharge due to the storage capacity of the cover soil (Figure 3-6c), lengthening the opportunity time for evapotranspiration to occur. During dry years, or years when the rainfall regime was characterized by frequent but small magnitude events, the threshold pressure at the interface was only exceeded during snowmelt (Figure 3-10). Rainfall events during these years could be completely held by the cover soil due to plant uptake maintaining the soil water pressure below the critical threshold for the entirety of the growing season. This effect was more pronounced with thicker cover soils, due to the larger storage capacity.

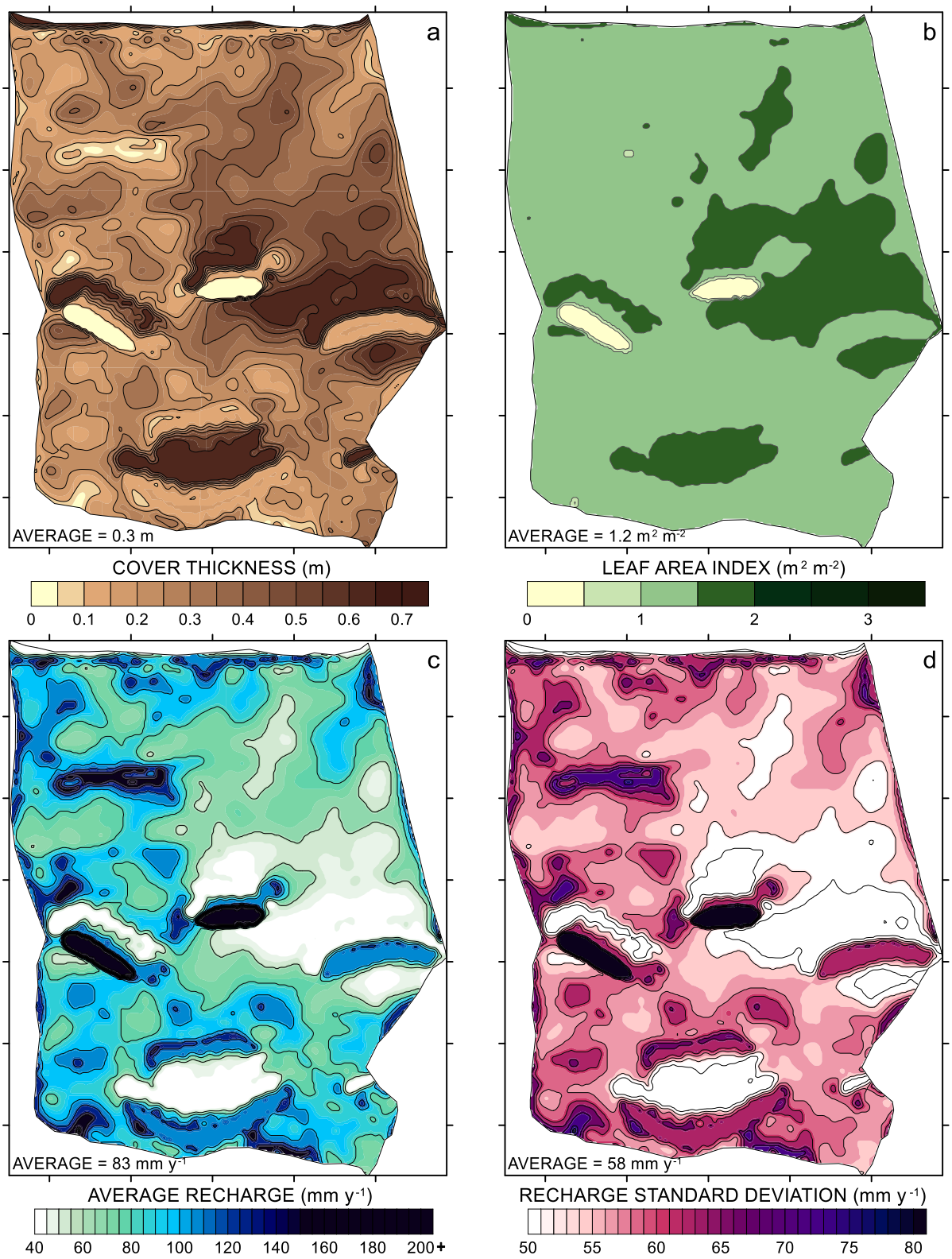

Figure 3-9. Spatial patterns of LFH thickness (a), maximum sustainable leaf area index (b), average groundwater recharge (c), and standard deviation of groundwater recharge (d) across the upland.

The non-monotonic relationship between soil evaporation and cover thickness was previously noted in Chapter 2 and attributed to the progressive isolation of the relatively moist layer directly overlying the capillary barrier (hence less evaporation loss) that occurs with unvegetated cover soils thicker than 30 cm. This phenomenon was responsible for the counter-intuitive increase in recharge that occurred as cover soil thickness increased beyond 30 cm. However, once root water uptake is considered, soil moisture in this relatively moist layer becomes accessible to vegetation; thus, the relationship between recharge and cover thickness reverts to a monotonic form.

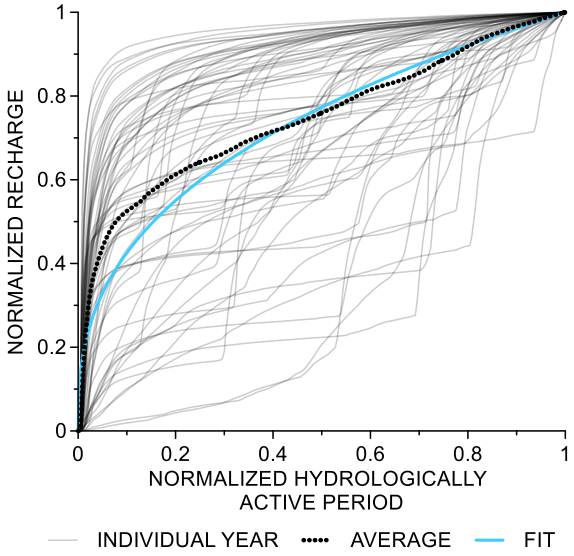

Figure 3-10. Temporal patterns of groundwater recharge integrated over the whole upland, for which both the cumulative annual volume and length of the hydrologically active period have been normalized to allow for comparisons between years. The average pattern of cumulative groundwater recharge can be closely approximated using a power function with the formula: $y = x^{0.371}$. Years above the average line indicate when recharge was dominated by snowmelt.

The identical soil moisture distribution in the profile between the snowmelt and rainfall-only models (Figure 3-11) immediately prior to freeze-up indicated that uplands disconnected from the water table experience little memory of past weather conditions. As a consequence, it is expected that snowmelt in this system will not contribute to interannual resilience to climatic stress for uplands following the development and maturation of vegetation. While the function of the upland aquifer is to provide downgradient ecosystems with a consistent supply of groundwater, thereby ameliorating the difference between wet and dry years, upland forests of similar design to the Nikanotee Fen Watershed have no such mechanism to enhance resilience. In fact, the characteristics of the layered cover soil system, particularly the hydrophysical properties and thickness of the LFH, resulted in snowmelt having a particularly short

residence time (Figure 3-11). The effect of the short residence time was illustrated by the negligible difference between the root water uptake of the models that include and exclude snowmelt (Figure 3-6b). Snowmelt did not greatly contribute to soil moisture storage during the peak growing season, since by the time complete foliation had occurred most of the stored snowmelt had either percolated past the capillary barrier or evaporated from the soil surface. Therefore, the water stress experienced by the upland vegetation was largely unaffected by the presence of snowmelt. In contrast, the simulations showed that snowmelt was a vital source of groundwater recharge, typically providing over 64% of cumulative annual recharge (despite snowmelt comprising – on average – only 28% of total annual precipitation). As a result, the timing of recharge was generally concentrated in the early portion of the hydrologically active period (Figure 3-10). In an average year, half of the total annual recharge was supplied within approximately the first month. The concentration of recharge in the early portion of the ice-free period is consistent with observations in the field by Ketcheson, et al. (2017), who identified that the largest water table rise occurred in the spring, following snowmelt. This temporal pattern has the potential to influence both the flushing of mobile solutes from the process-affected tailings sand, and the variation in hydraulic gradient throughout the growing season, which will affect the flux of water and solutes to the fen.

3.5.2 Nikanotee fen trajectory

The hydrologic performance of the upland, following the development of a climax vegetation community, is expected to be markedly different from the largely unvegetated early post-construction period, as shown by the difference in average hydrologic fluxes between the different vegetation development scenarios (Figure 3-6a, 3-6b, and 3-6c). However, while vegetation development is a slow process relative to the evolution of soil hydraulic properties that occurs over the first several years following reclamation (Chapter 2) the hydraulic behavior of the upland is expected to stabilize prior to the establishment of a climax vegetation community and the development of the maximum sustainable LAI. As demonstrated by comparing the water fluxes between different vegetation scenarios, the model indicates that once the upland approaches complete ground cover (LAI of 1), further vegetation development will cause diminishing changes to the partitioning of soil moisture between recharge and evapotranspiration (Figure 3-6b and 3-6c).

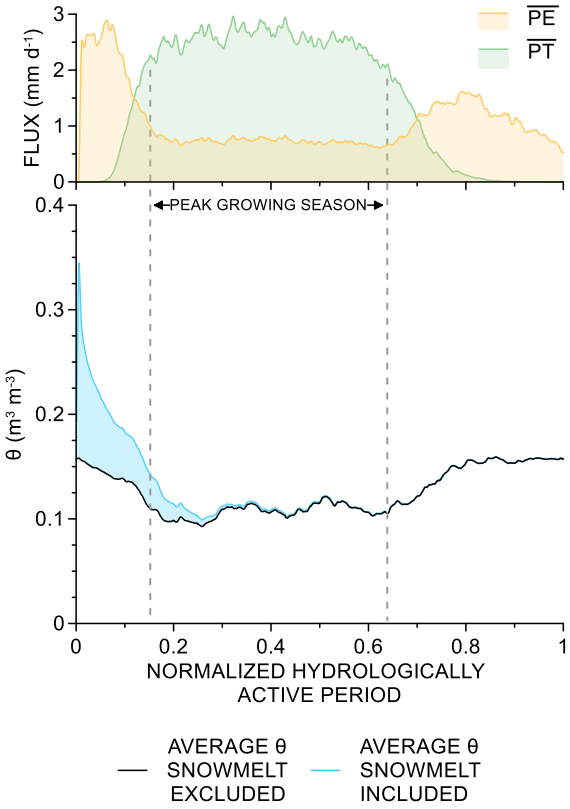

Figure 3-11. Temporal patterns of average daily potential soil evaporation (PE) and potential transpiration (PT), and comparison of average soil moisture (θ) integrated across the LFH cover soil for simulations that include and exclude snowmelt (values reported for D_{LFH} = 30 cm and LAI = 2). While the simulations converge over time until the soil moisture is identical, the majority of snowmelt is removed by soil evaporation and deep percolation prior to the onset of the peak growing season.

The long-term modelling suggests that the current upland configuration will continue to supply sufficient groundwater recharge to satisfy the needs of the fen (Figure 3-12). Specifically, groundwater flow from the upland will be capable of maintaining baseflow out of the system and offsetting evaporative losses in the fen, even following the development of a climax vegetation community. The upland to fen ratio of approximately 3:1 and spatial distribution of cover soil was found to be capable of supporting a maximum sustainable LAI of 1.2 and partitioning an average of 83 mm of soil moisture to groundwater recharge annually (Figure 3-9). Comparing the simulated maximum sustainable LAI and empirical measurements from a variety of boreal forest sites dominated by jack pine indicate that the upland will maintain a somewhat lower level of vegetation development than a natural forest, as stands older than 25 years had an average LAI of 2.5 (Vogel & Gower, 1998; Howard et al., 2004; Chasmer et al., 2008).

The simple fen water budget calculation (Figure 3-12) indicated that, cumulatively over the 65-year simulation period, rainfall and groundwater recharge from the upland would result in a substantial surplus of water (~193,000 m^3 or 42 mm y^{-1} standardized to upland area). This could be regarded as water that would be available to other downgradient ecosystems or waterbodies. Alternatively, this could be interpreted as rationale for decreasing the proportion of upland area relative to the fen, in an attempt to achieve a ratio that is more closely representative of the undisturbed landscape of the AOSR. However, given the uncertainty associated with projected climate change, particularly in regard to the spatiotemporal patterns and quantity of precipitation, maintaining a substantial water surplus can help mitigate any future systematic deviation from the long-term climatic record. Whether such a deviation has a more pronounced impact on rainfall or snowmelt would have different consequences for the trajectory of the system. Any departure from the long-term average of rainfall would have the greatest impact on plant available water, and therefore the maximum sustainable LAI. However, future changes to the amount of snowmelt would predominantly affect the partitioning of soil moisture to groundwater recharge (c.f. Figure 3-6b and 3-6c), and therefore have profound implications on the quantity of water that can be supplied from the upland aquifer to the downgradient fen. Yet, given the apparent magnitude of water surplus that the current upland design produces, the system could be expected to remain tolerant to relatively large shifts in future climate.

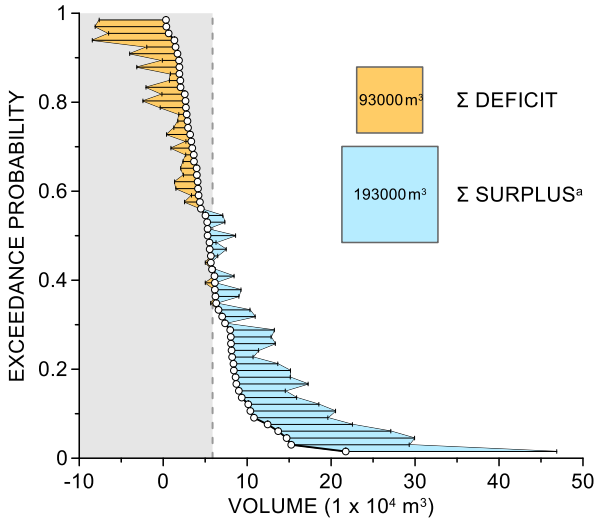

Figure 3-12. Exceedance probability of annual upland groundwater recharge reported as a volume (thousands of m^3). Dashed line represents the average upland recharge volume (5,880 m^3). Shaded areas show the water deficit (yellow) or surplus (blue) that results from calculating the fen water budget ($P + R - AET - SW_{OUT}$) for each year. Boxes visually depict the total volume of water over the 65-year record that accrues as a deficit, and the total volume of water that represents the water surplus. [a] after the cumulative deficit is offset, 99,500 m^3 could be partitioned to upland aquifer storage or surface water outflow.

3.5.3 Reclamation design

Although the original upland design intentionally specified the application of shallow thicknesses of LFH (~20 cm), simulations of these cover soils demonstrated their inability to sustain dense vegetation development (Figure 3-8) due to insufficient soil moisture storage and large losses of water to soil evaporation, leading to high static water stress (Figure 3-7). Yet, these cover thicknesses also limited percolation across the capillary barrier and therefore yielded relatively small quantities of groundwater recharge. Cover soil thicknesses that exceeded 45 cm were capable of supporting a higher maximum sustainable LAI (Figure 3-8), and the reduction in groundwater recharge compared to thinner cover soils was marginal (Figure 3-6c). Conversely, the model demonstrated the disproportionate effectiveness of bare tailings sand basins at partitioning soil moisture to groundwater recharge. This was a consequence of the high saturated hydraulic conductivity, steep soil water characteristic curve, and absence of a capillary barrier near the surface.

Research at the Nikanotee Fen Watershed has identified the importance of bare tailings basins placed adjacent to hillslope confluences, which are ideally positioned to detain surface overland flow, as preferential recharge features (Kessel et al., in review). Despite the small footprint of these basins on the upland they have been shown to supply a disproportionate amount of total upland groundwater recharge in the early post-construction period. However, these features are expected to have a limited period of effectiveness as a result of the soil evolution and vegetation development on the hillslopes, which will reduce the propensity for runoff generation (see Figure B-3), and due to the deposition of sediment entrained in the runoff, which both increases the water storage capacity of the unsaturated zone and reduces the total volume of the basin (Kessel et al., in review). In contrast, bare tailings sand basins that are isolated from slopes will not fill with sediment and are unlikely to develop vegetation due to the adverse hydraulic characteristics. Consequently, isolated tailings sand basins are expected to be enduring sources of groundwater recharge for reclamation watersheds.

By applying the concept of designing uplands to integrate two landforms of different character and purpose to the Nikanotee Upland, the same average annual recharge could be achieved (83 mm y^{-1}) by repartitioning the upland into bare tailings basins landforms, and areas where the thickness of the cover system is greater than 45 cm. Calculated algebraically, by dedicating 13% of the upland to isolated bare tailings basins, the remaining 87% of the upland could support a maximum sustainable LAI of 2. This design modification would result in an increase in average maximum sustainable upland LAI from 1.2 to 1.75, an increase of 46% compared with the current upland configuration. The benefits of this design

philosophy are further emphasized by a decrease in recharge variability for the proposed design since bare tailings sand has the lowest coefficient of variation (Figure 3-6d). Such a design strategy would allow the upland to support denser forest, while also providing more consistent groundwater flow to downgradient ecosystems. The disadvantage of this design is the requirement for a greater quantity (+29%) of cover soil. Given the scale of surface mining in the AOSR, and therefore the scale of reclamation, high quality cover soils may be a limiting resource and should be used parsimoniously. As a result, this represents a trade-off.

As indicated by the standard deviation in groundwater recharge (Figure 3-9d), the large interannual variability in recharge produced by the upland emphasizes the importance of incorporating aquifers with a large storage capacity and relatively slow discharge, where water stored during wet years will need to be dispensed sparingly to downgradient peatlands during subsequent dry periods. However, this brings into question the role of high permeability underdrain features, such as the petroleum coke underdrain used in the Nikanotee Fen that extended well into the upland (Ketcheson et al., 2017). The underdrain distributes hydraulic pressure from the upland aquifer beneath the fen, resulting in relatively uniform, predominantly vertical, discharge of groundwater into the fen. However, due to the high hydraulic conductivity of the material, it promotes drainage of the upland aquifer and could squander groundwater stored during wet years. Among the potential alternatives to this design would be to limit the lateral extent of the underdrain layer such that it did not project back into the upland aquifer.

Surface water discharge performs an additional function in reclaimed watersheds constructed using process-affected materials, specifically the removal of sodium from the system. Without discharge, sodium can accumulate and evapoconcentrate to a level several times the source concentration in the shallow subsurface of the fen (Simhayov et al., 2018). Due to the consistent need for surface water discharge, reclaimed fens likely require more groundwater recharge from adjacent uplands than in comparably sized undisturbed systems, at least until excess sodium has been flushed from the watershed. This requirement must be incorporated into the design of reclamation landscapes that use tailings sand and other process-affected materials.

3.5.4 Model error and uncertainty

There is a clear need to generate meaningful information about the trajectory of constructed watersheds on a timeline relevant to mine closure planning and regulatory decision-making. These time constraints preclude the possibility of simply observing the development of the system over the coming decades, and necessitates the use of models to aid in understanding the dominant hydrologic processes and how they may change as the system evolves. Unfortunately, this also prevents a genuine verification and validation of the

model estimates and contributes to uncertainty in the capabilities of the model as a tool for decision making in the design of reclamation watersheds.

Model validation for 2018 demonstrated the suitability of the soil hydraulic and root water uptake parameters, and previous investigations into the upland soil moisture dynamics included a rigorous evaluation of LFH and tailings sand hydraulic behaviour (Chapter 2). That work identified the relatively spatially homogeneous nature of hydraulic properties across the upland. The impact of any heterogeneities in soil properties is likely to be further minimized by the ongoing development of upland vegetation (Schluter et al., 2013). In spite of the favourable model performance when compared to field measurements, other aspects of the model design introduce uncertainty.

As demonstrated by the difference between the simulations that consider and exclude snowmelt (Figure 3-6), one of the greatest sources of uncertainty is associated with the assumption that all snowmelt infiltrates into the subsurface. This effectively represents a runoff ratio of zero, an assumption that was previously applied in earlier modelling studies of reclaimed uplands in the AOSR (Huang et al., 2013; Huang et al., 2015). However, more recently Huang et al. (2018) demonstrated an average runoff ratio of 0.3 for snowmelt runoff at a nearby comparatively steep (20% grade), unfurrowed slope with relatively high near-surface water content prior to freezing. The latter condition indicates a greater proportion of occluded ice-filled pores, thus limited infiltration capacity (Kurylyk & Watanabe, 2013). In contrast, the upland of the Nikanotee Fen Watershed has a relatively gentle slope (2% grade), cross-slope furrowed surface, and relatively low soil moisture content prior to freeze-up (Figure 3-11). This comparison would suggest that the upland of the NFW would tend to produce less runoff, and therefore the assumption that all snowmelt is partitioned to infiltration is reasonable.

Although we acknowledge the uncertainty associated with the estimates of maximum sustainable LAI, the model demonstrated that the hydrologic function of the system was relatively insensitive to vegetation scenarios once LAI exceeded unity. The lack of sensitivity in cumulative annual groundwater recharge under different vegetation development scenarios (Figure 3-6c) suggests that the estimates of average and standard deviation groundwater recharge are appropriate and robust. Irrespective of this uncertainty, this work has shown it is difficult for cover soils in the moisture limited environment of the AOSR to concurrently supply sufficient soil moisture to support and maintain vegetation productivity and generate large volumes of groundwater recharge. We therefore reiterate the design option of maintaining upland areas without a cover soil to maximize recharge and areas of thicker cover systems to minimize plant water stress. This approach would support the continued integrity of both the water storage and water

conveyance functions of uplands into the future. Given the current configuration of cover soils in the upland of the Nikanotee Fen Watershed, an estimated 45 cm of LFH is recommended to satisfy the water storage requirements of vegetation, however it is possible that similar hydraulic behaviour could be achieved with different combinations of materials, thicknesses, and layering. Given that the hydraulic behaviour of the upland cover system was largely controlled by the presence and strength of the capillary barrier effect, increasing the thickness of the cover system with a more abundant fine-grained material, such as glacial till, would allow for more efficient use of valuable high-quality cover soils.

3.6 Conclusion

This modelling work suggests that the current upland configuration will be capable of concurrently providing sufficient groundwater recharge to offset the deficit in the downgradient fen and supporting the growth of an upland forest. However, modifications to the upland design could allow for certain reclamation objectives to be achieved more efficiently. By purposely partitioning uplands to have areas of thick cover soil with a large available water holding capacity, and areas of isolated bare tailings sand to act as preferential recharge features, the same groundwater recharge could be supplied while supporting a larger maximum sustainable LAI. This design principle could be used to create watersheds that have an upland-to-fen ratio of ~50%, that is more closely representative of the undisturbed landscape of the AOSR (Vitt et al., 1996). However, by maintaining a large surplus of groundwater recharge – on which downgradient peatland ecosystems rely – these watersheds would effectively incorporate a margin of safety into the design. This margin of safety would not only mitigate the effects of future systematic deviations from historical climate but also implicitly buffer the error inherently associated with modelling work of this nature.

Since water in reclamation systems must be used efficiently and distributed parsimoniously to other elements on the landscape, it is expected that these ecosystems will operate on thin margins of moisture availability. As the difference between normal ecosystem function and altered or novel functionality has the potential to be decided by small amounts of water, it is critical that climate variability is considered in a stochastic manner. The statistical characteristics of groundwater recharge identified in this study will allow the interannual variability in climatic conditions to be fully realized in a complex groundwater flow and solute transport model. Such a model would allow the water balance of the fen to be explicitly simulated, and provide insight into the fate and transport of solutes that have the potential to negatively impact fen vegetation.

3.7 Acknowledgements

The authors would like to thank A. Green, E. Kessel, and J. Sherwood for their assistance in the field, data processing, and project management. Funding from the following sources is gratefully acknowledged: Northern Scientific Training Program (NSTP), the Natural Sciences and Engineering Research Council (NSERC) Canadian Graduate Scholarship (NSERC-CGS) and Collaborative Research and Development Grant (NSERC-CRD; 418557-2011) titled “Evaluating the success of fen creation in the post oil sands landscape” with field support and direct funding from Suncor Energy Inc., Imperial Oil Resources Ltd., Shell Canada Ltd., and Teck Resources Ltd.

Chapter 4: Characterizing the hydraulic and transport properties of a constructed coarse tailings sand aquifer

4.1 Introduction

Coarse tailings sand is generated as a waste product from the extraction and processing of bitumen in the Athabasca Oil Sands Region (AOSR) and has been used to construct reclamation systems on the post-mined landscape. However, little research has been conducted to characterize the hydraulic properties of coarse tailings sand, which will be vital to assess the transport of solutes within and from this material. On an average annual basis, 1.82×10^{11} kg of bitumen ore is processed from surface mining in the AOSR, of which coarse sand comprises approximately 60% (Mikula, 2012), forming the largest constituent of the oil sands waste stream (Majid et al., 1996). Furthermore, the volume of tailings materials produced by the bitumen extraction process exceeds the original pre-mined volume of oil sands by a factor of 1.4 (Mikula, 2012), which is anticipated to contribute to a reclaimed landscape with greater topographic variability than the pre-disturbance landscape (Rooney et al., 2012). In addition to elevated salinity in the connate porewater due to the marine depositional environment (Purdy et al., 2005), the processing of oil sands previously involved the addition of solutes to enhance separation and flocculation of the bitumen, primarily NaOH (Masliyah et al., 2004).While the majority of process-water is recycled through centrifugation or gravitational settling, a portion remains in the pore space of the tailings (Kasperski and Mikula, 2011), leaving residual quantities of salts and hydrocarbons in the pore-water (Simhayov et al., 2017). Despite the presence of high salt concentrations, tailings sand has been used as a construction material in embankments, slopes, and reclaimed systems due to its favourable hydraulic and geotechnical properties, and relative abundance on the mine landscape. Among these systems include two experimental watersheds, Sandhill Fen Watershed, and Nikanotee Fen Watershed, designed to test the viability of fen peatland reclamation. The Nikanotee Fen Watershed incorporates an upland tailings sand aquifer that supplies groundwater to the downgradient fen peatland. Recent studies demonstrate that residual sodium contained in the tailings sand has been transported by groundwater towards the fen peatland (Kessel et al., 2018), elevating salt concentrations in the rooting zone of the fen. This has the potential to negatively impact the establishment and growth of targeted vegetation species (Pouliot et al., 2013; Rezanezhad et al., 2012).

Along with hydraulic conductivity, one of the most important parameters used to characterize the transport of solutes through porous media is the dispersivity of the material, which accounts for unresolved velocity variations smaller than the scale of observation. While it has been shown that dispersivity tends to

exhibit a scale dependency (Gelhar et al., 1992) – increasing with volume of aquifer material sampled – it will theoretically reach a maximum value when the distribution of velocity variations is statistically stationary. This apparent scale-dependent relationship between dispersivity and the dimensions of the media through which groundwater flows, is generally interpreted as a consequence of the introduction of new heterogeneities that are encountered within the flow field over larger displacement distances, causing meaningful deviations to the distribution of porewater velocity (Dagan, 1987; Neuman et al., 1987).

Given the volume of coarse tailings material that will need to be included in reclamation design of the post-mined landscape, characterizing its hydraulic and transport properties is a priority. Several studies have investigated the hydrophysical properties of coarse tailings sand, including estimating or measuring the van Genuchten-Mualem parameters associated with soil water retention, and unsaturated hydraulic conductivity (Chapter 2; Ketcheson et al., 2017; Weber et al., 2019). However, these studies were conducted in a laboratory setting (as in the case of Weber et al., 2019) or based on small-scale field measurements. These scales have limited applicability when inferring the transport behaviour of solutes over distances relevant to landforms and watersheds.

Informing researchers and mine reclamation managers of the characteristics governing solute transport through coarse tailings materials will aid in the design of the reclamation landscape. Modelling the transport and fate of solutes issuing from process-affected coarse tailings sand will require an understanding of the transport characteristics of the porous media. Therefore, the goal of this study is to characterize the flow and transport properties of coarse tailings sand across a range of spatial scales.

4.2 Study site

The Nikanotee Fen Watershed (Figure 4-1), a 32 ha research site, constructed on a post-mined area of an oil sands lease approximately 25 km north of Fort McMurray, Alberta (56°55’59” N, 111°25’00” W). The watershed, which became operational in early 2013, consists of a fen peatland (2.2 ha), upland (7.7 ha), reclaimed hillslopes (18.7 ha), and an undisturbed natural slope (2.8 ha). The design of the system was informed by the conceptual understanding of undisturbed fen-upland systems in the AOSR, and hydrological modelling, which identified the requisite material properties and layering to maintain a relatively stable and high water table in the peatland (Price et al., 2010). Maintaining a high and stable water table required the inclusion of an upland aquifer to act as both a water storage and conveyance feature, which would supply the fen with groundwater, thereby offsetting evaporative losses. The aquifer was constructed with mechanically-placed coarse tailings sand and underlain by a low-permeability

geosynthetic clay liner (GCL) that established a hydraulic gradient towards the fen and minimized percolation losses to the regional groundwater flow system. The tailings sand aquifer was capped with a 30 cm layer of LFH-mineral mix – a common reclamation cover soil – to act as a substrate more amenable to vegetation growth. Several raised landforms – termed hummocks – were constructed across the upland. Upslope of these hummocks the LFH was excavated to expose the coarse tailings sand at the surface, creating basins that detained surface overland flow and enhanced groundwater recharge. Basins adjacent to the east and south-east slopes received the largest volumes of surface runoff, and supplied a disproportionate volume of total groundwater recharge to the upland aquifer (Kessel et al., submitted). As a consequence, the highest hydraulic gradients in the watershed were consistently located downslope of the east recharge basin and southeast corner.

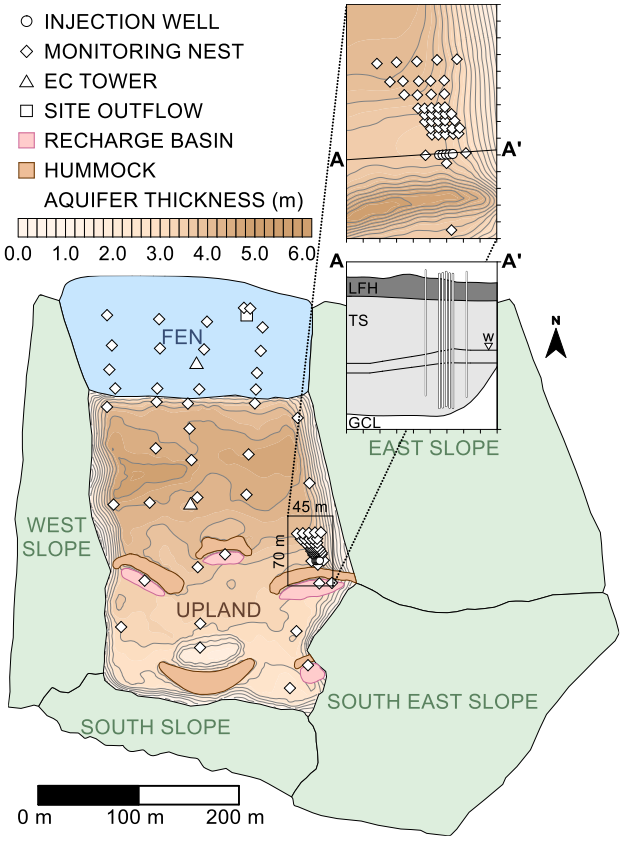

Figure 4-1. Study site map of the Nikanotee Fen Watershed, depicting the locations of monitoring nests, aquifer thickness, and the location of important site features. The inset map and cross-section show details of the monitoring network and injection wells installed specifically for the tracer test as well as the relevant materials in the vicinity of the tracer plume: LFH, TS (tailings sand), and the GCL (geosynthetic clay liner).

4.3 Methods

4.3.1 Column experiments

Three columns of coarse tailings sand, taken from the site in 2015, were reconstituted and packed in 10 cm diameter by ~35 cm tall tubes (specific core lengths were 0.32, 0.34, 0.37 m) to approximately the same bulk density as the field tailings sand (1.55 g cm^{-3}). Although the tailings sand cores were not collected in-situ, the reconstitution and packing of the columns represented a similar level of disturbance as the original placement in the site aquifer. The cores were packed in lifts of 1-2 cm, and were saturated from the bottom-up to reduce the potential for air-entrapment (Lewis & Sjostrom, 2010), and connected to a constant head apparatus to measure hydraulic conductivity (K) under a variety of hydraulic gradients. These hydraulic gradients included a value similar in magnitude to what is typically observed in the field within the vicinity of the east recharge basin (-0.05), and gradients that are closer to what may be established by a peristaltic pump (-0.15, -0.33). Subsequently, the columns were connected to a multichannel peristaltic pump, which had a volumetric flow rate of approximately 0.064 mL s^{-1}. The pumps were attached to a reservoir of deionized water and allowed to flush for several days (~10 pore volumes). The deionized water was then swapped for a reservoir of solute containing 1400 mg L^{-1} of Bromide (Br^-) tracer in the form of Lithium Bromide (LiBr) to characterize the solute breakthrough as it advanced through the column. Volumetric discharge (Q) from each core was measured throughout the experiment, and water samples were taken at regular time intervals. The analytical expression of Ogata and Banks (1961) was fit with a gradient-based optimization routine to the concentration breakthrough curves to estimate the dispersivity.

$$\frac{C}{C_0} = \frac{1}{2}\left[\operatorname{erfc}\left(\frac{l - \overline{v}t}{2\sqrt{D_l t}}\right) + e^{\left(\frac{\overline{v}l}{D_l}\right)} \operatorname{erfc}\left(\frac{l + \overline{v}t}{2\sqrt{D_l t}}\right)\right] \quad (1)$$

where C is the measured effluent concentration [ML^{-3}], C_0 is influent concentration [ML^{-3}], erfc is the complementary error function, l is the length of the column [L], $\overline{v}$ is the average linear pore-water velocity [LT^{-1}], t is the elapsed time [T], and D_l is the longitudinal hydrodynamic dispersion coefficient [L^2T^{-1}]. Average linear pore-water velocity was calculated with:

$$\overline{v} = \frac{Q}{A \cdot n_e} \quad (2)$$

where A is the cross-sectional area of the columns [L^2], and n_e is the effective porosity. Hydrodynamic dispersion was calculated by multiplying average linear pore-water velocity by the longitudinal dispersivity (α_L) [L]. The parameters n_e and α_L were fit during the calibration procedure.

Water samples were analyzed for Br^- concentration using an ion selective electrode (Thermo Scientific 9635BNWP bromide combination probe). Analysis followed recommended manufacturer procedure, which involved 5-point calibration from calibration standards that bounded the expected concentration range (1 mg L^{-1}, 10 mg L^{-1}, 100 mg L^{-1}, 1000 mg L^{-1}, 7990 mg L^{-1}). All samples and standards had a 2% solution of ionic strength adjuster added.

4.3.2 Single-well response tests

Between 2013-2019 hydraulic conductivity bail tests were conducted at groundwater monitoring nests installed across the fen and upland (see Figure 4-1). Monitoring nests in the upland typically consisted of a fully-slotted well and piezometers installed with a 0.2 m screened interval centred at 2.25 and 2.75 m below ground surface (bgs). Typically, only a single piezometer in each fen monitoring nest was screened in tailings sand at 2.75 m bgs. Single-well response tests were conducted annually in triplicate for most locations and a subset of the data (tests conducted between 2017-2019) was analyzed using the Dagan (1978) and Bouwer-Rice (1976) semi-analytical solutions. The majority of hydraulic conductivity tests were conducted manually, however the response of monitoring locations with particularly fast recovery was measured using a pressure transducer. Some monitoring locations were excluded if they were adjacent to the lateral boundary of the geosynthetic clay liner, if they were inferred to be screened across multiple aquifer materials, or were inferred to have clogged screens from peat smearing during installation. In total, the hydraulic conductivity measured at 57 wells and piezometers screened in tailings sand was included in the analysis.

4.3.3 Field-scale tracer test

A field-scale tracer test was conducted to characterize the large-scale hydraulic and transport properties of the tailings sand aquifer. The upland area chosen for the tracer test was approximately 20 m downslope of the east recharge basin, and selected because of the steep hydraulic gradients and access to (relatively) fresh water that collected in the basin. Five injection wells of 3.8 cm inner diameter (ID) were installed in a line perpendicular to the average groundwater flow direction with 1 m lateral spacing, to a depth of approximately 3.8 m bgs. This resulted in the injection wells being screened across nearly the entire saturated thickness of the tailings sand aquifer (Figure 4-1). Forty-two fully-slotted 0.64 cm ID observation wells were installed downgradient of the injection wells, and diverged with distance from the injection wells. This spacing pattern was intended to account for the transverse horizontal spreading of the plume due to both mechanical dispersion and transient groundwater flow conditions caused by infiltrated surface

water from the east slope and recharge basin. During installation, care had to be taken to avoid puncturing the GCL, therefore the monitoring wells were installed to a conservative depth of approximately 3.5m bgs. Boreholes were backfilled and compacted to approximately the same bulk density as the original material.

The experiment involved the injection of 1,500 L of tracer at a concentration of 1,400 mg L^{-1}, resulting in a total tracer mass of 2,100 g. Tracer was stored in two 1 m^3 containers, each with a continuously operating bilge pump to prevent stratification of the tracer solution. Tracer in the two containers was thoroughly mixed before being pumped into the 5 injection wells. To reduce the potential for a groundwater mound to form around the injection wells, thereby increasing the width of the plume perpendicular to the predominant groundwater flow direction, tracer was injected slowly over the course of approximately 36 hours. The test commenced on the afternoon of July 22, 2017 (injection ceased early July 24, 2017) and the tracer moved under ambient groundwater flow conditions for 1 week before the first sampling event on July 31, 2017 (day 7). Subsequently, water sampling was conducted on August 7 (day 14), August 14 (day 21), August 20 (day 27), September 15 (day 53), and September 21 (day 59). Prior to water sampling, monitoring wells were completely purged, which removed between 150-200 mL of water, allowed to recover, and then samples were collected in 60 mL HDPE bottles. Water samples were typically analyzed within several days of collection using a Br^- ion selective electrode, following the same methodology as the column experiments.

4.3.4 Spatial moment calculations

Spatial moments (Aris, 1956) of the spatially interpolated concentration distribution were used to analyze and characterize the transport of the Br^- tracer as it flowed under natural gradient conditions through the tailings sand aquifer. Since the tracer was injected over the entire saturated thickness of the aquifer, the moment analysis was only conduced with respect to the *x* and *y* spatial coordinates. The ij^{th} moment, $M_{ij}(t)$ of the two-dimensional concentration distribution is defined as:

$$M_{ij}(t) = \int_{-\infty}^{\infty}\int_{-\infty}^{\infty} nC(x,y,t)x^i y^j \, dx \, dy \tag{2}$$

where *n* is total porosity, and $C(x, y, t)$ is the vertically-integrated spatiotemporal concentration distribution. The zeroth ($M_{ij} = M_{00}$), first ($M_{ij} = M_{11}$), and second ($M_{ij} = M_{22}$) moments were used to calculate the tracer mass in solution, geographical location of the tracer centre of mass, and spread of the tracer about the centre of mass, respectively. The zeroth moment (mass in solution) is calculated as:

$$M_{00}(t) = \sum n \cdot A \cdot b \cdot C \tag{3}$$

where A is 25 cm^2, the area of the cell size of the interpolated concentration distribution, and b is the aquifer thickness. Given the assumption that the tracer concentrations were vertically uniform across the entire aquifer thickness, variations in the saturated thickness of the aquifer within the tracer plume, and over the duration of the experiment needed to be accounted for in the estimation of the tracer mass. Therefore, the saturated thickness of the aquifer was calculated independently for each sampling event. The location of the plume centre of mass perpendicular (X_c) and parallel (Y_c) to the velocity vector of the plume centre of mass is calculated as follows:

$$\begin{aligned} X_c &= M_{10}/M_{00} \\ Y_c &= M_{01}/M_{00} \end{aligned} \tag{4}$$

The spatial concentration distribution for each sampling event for which moments were calculated was transformed to local spatial coordinates and rotated to align the longitudinal axis of the spatial covariance tensor (σ_{yy}) with the velocity vector of the plume centre of mass. The rotation aligned the y-axis parallel to flow direction. The magnitude of the velocity vector (V) is calculated as the change in displacement of the plume centre of mass relative to time:

$$V = \left[\frac{\left(dX_c{}^2 + dY_c{}^2\right)^{0.5}}{dt}\right] \tag{5}$$

The angle (θ) of the velocity vector relative to geographic north is calculated as:

$$\theta = tan^{-1}\left(\frac{dX_c}{dY_c}\right) \tag{6}$$

The second moment (M_{22}), characterizing the spread of the solute about the centre of mass, can be used to calculate the two-dimensional covariance parallel and perpendicular to the movement of the centre of mass:

$$\begin{aligned} \sigma_{xx} &= \frac{M_{20}}{M_{00}} - X_c{}^2 \\ \sigma_{yy} &= \frac{M_{02}}{M_{00}} - Y_c{}^2 \end{aligned} \tag{7}$$

where σ_{xx} is the covariance perpendicular to the velocity vector, and σ_{yy} is the covariance parallel to the velocity vector. Assuming a negligible molecular diffusion coefficient, the estimates of covariance can be used to approximate the transverse (α_T) and longitudinal dispersivities (α_L) using Güven et al., 1984:

$$\begin{aligned} \alpha_T &= \frac{1}{2V}\frac{d}{dt}\sigma_{xx} \\ \alpha_L &= \frac{1}{2V}\frac{d}{dt}\sigma_{yy} \end{aligned} \tag{8}$$

4.4 Results

4.4.1 Laboratory column experiments

Hydraulic conductivities of the packed tailings sand columns ranged within an order of magnitude ($\overline{K}$ = 4.3 m d^{-1}), with minor variation under different hydraulic gradients. The average hydraulic conductivity across the three gradients was 6.1, 4.1, and 2.7 m d^{-1}, for core 1, 2, and 3, respectively. Once adjusted from laboratory (20°C) to field temperatures (8°C) to account for temperature dependence of fluid viscosity and density, these hydraulic conductivity measurements become 4.5, 3.0, and 2.0 m d^{-1} ($\overline{K}$ = 3.2 m d^{-1}). During saturation of the cores approximately 2 cm of consolidation occurred, resulting in bulk densities between 1.57-1.60 g cm^{-3}, within the range previously measured (Ketcheson, 2015).

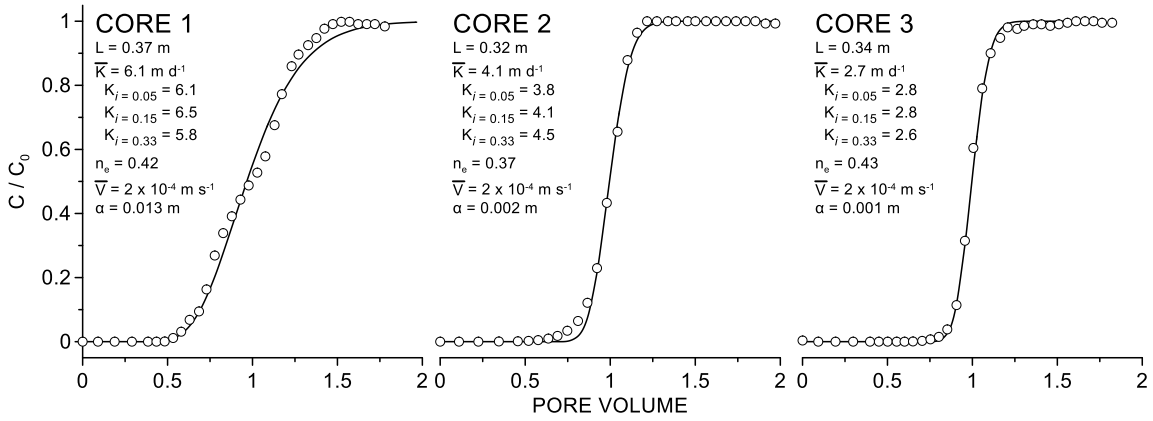

Figure 4-2. Br$^-$ breakthrough curves from the coarse tailings sand column experiments. Circles represent measured values, while the solid line is the calibrated Ogata-Banks (1961) analytical solution. Also shown are the dimensions (L), average hydraulic conductivity ($\overline{\boldsymbol{K}}$), measured hydraulic conductivity under a specific hydraulic gradient (K_i), calibrated effective porosity (n_e), average velocity ($\overline{\boldsymbol{V}}$), and calibrated dispersivity (α). The K values shown have not been temperature corrected.

The peristaltic pumps maintained a constant outflow of approximately 0.06 mL s^{-1} in each core throughout the duration of the breakthrough experiment. Calibration of Equation 1 resulted in n_e values of 0.42, 0.37, and 0.43, for core 1, 2, and 3, respectively. Core 2 and 3 demonstrated similar hydrodynamic dispersion (Figure 4-2), with an abrupt increase in outflow concentration after 0.8 pore-volumes. In contrast, core 1 exhibited a more gentle and steady increase in outflow concentration after 0.6 pore-volumes. This difference in transport behaviour is reflected in the calibrated α_L values, which were 1.3 x 10^{-2}, 1.5 x 10^{-3}, and 1.1 x 10^{-3} m, for cores 1, 2, and 3, respectively.

4.4.2 Single-well response tests

In-situ hydraulic conductivity measured in the field with bail tests varied between 0.58 and 29 m d^{-1}. The geometric mean hydraulic conductivity was 2.9 m d^{-1} (ln K = 1.1) with a ln K variance of 0.9. Although the histogram of ln K vaguely resembles a right-skewed Gaussian distribution (Figure 4-3), the log-transformed data did not satisfy the Shapiro-Wilk normality test (the hypothesis that the data conform to a normal distribution was rejected). It is conceivable that the right-skew in the ln K distribution is a consequence of certain monitoring well screens partially intersecting a layer of petroleum coke, a construction material with substantially higher hydraulic conductivity. However, efforts were made to exclude such locations from the analysis by comparing the screened interval with detailed stratigraphic information collected during site construction. It should be noted that hydraulic conductivity tests could not be performed on the observation wells installed for the purpose of monitoring the tracer experiment, as their quick recovery prevented manual measurement techniques, and the narrow internal diameter precluded the deployment of pressure transducers to record recovery.

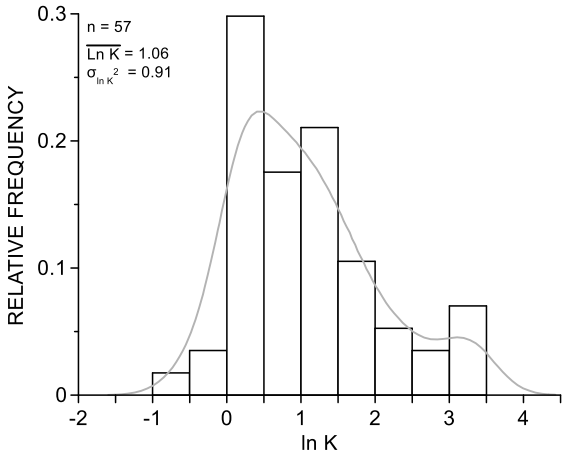

Figure 4-3. Histogram of log-transformed hydraulic conductivity (ln *K*) data measured using bail tests at the wells and piezometers screened in tailings sand across the site. Light grey line superimposed over the histogram is the kernel density estimate of ln *K*, converted from density to relative frequency.

4.4.3 Field-scale tracer test

The water table in the vicinity of the tracer test was influenced by its proximity to the east recharge basin, which periodically filled with surface runoff, during which a transient groundwater mound would develop beneath the basin. Prior to the experiment commencing, a series of runoff events resulted in a local water table rise. Over the course of the experiment the groundwater mound moved downgradient, and slowly dissipated, resulting in the average water table declining by approximately 30 cm, this was accompanied

by a modest decrease in the slope of the water table. The hydraulic gradient steadily decreased from -0.044 on day 21 to -0.034 on day 59. During the experimental period, 2.3 cm of rainfall was measured. However, based on soil moisture modelling in Chapter 2, this corresponded to less than 1 mm of groundwater recharge.

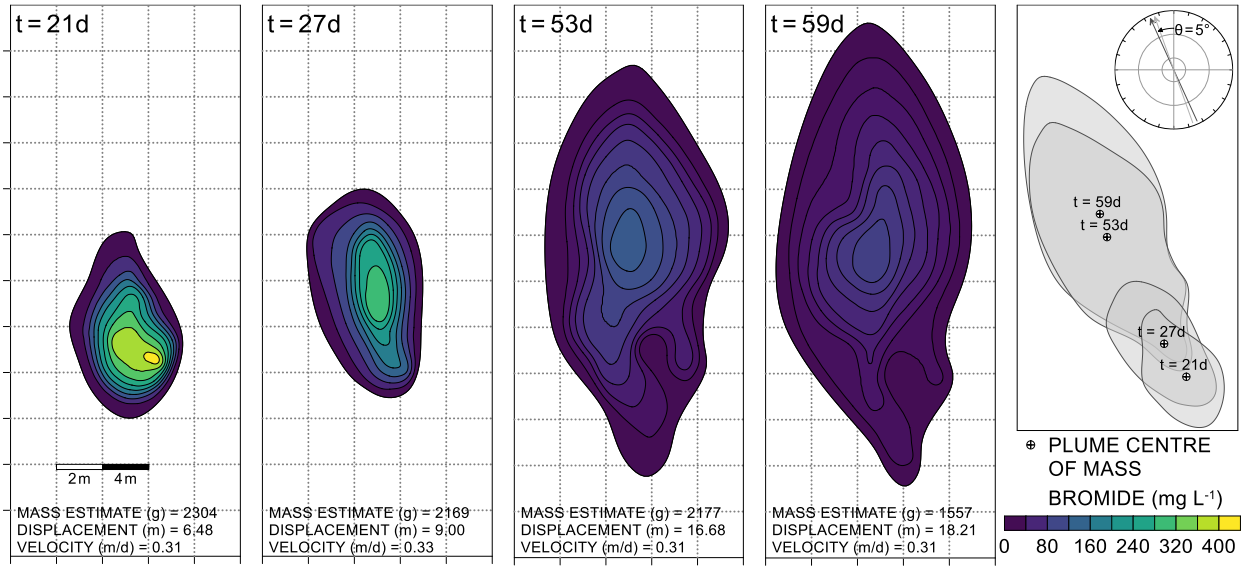

Figure 4-4. Contour plots of Br^- concentration from each sampling event (t = 21, 27, 53, 59 d), rotated and aligned with the average velocity vector of the plume centre of mass. The map on the right depicts the true position of each plume. The polar chart shows the discrepancy (5°) between the average velocity vector of the plume centre of mass (black) and the average slope aspect of the water table (light grey).

Six rounds of water sampling were conducted at the observation wells, however only the latter four sampling events (t = 21, 27, 53, 59 d) allowed for full delineation of the tracer plume. The small internal volume of the monitoring wells meant that purging and sampling removed less than 0.1% of the tracer mass. The dimensions of the plume on day 21 were 8 m x 5 m, and by day 59 had increased to 20 m x 9 m (Figure 4-4). By the end of the experiment the plume encompassed approximately 270 m^3 of aquifer material. The narrow plume dimensions on day 21 indicate that negligible groundwater mounding developed around the injection wells, which were positioned 1 m apart. Background Br^- concentrations at the observation wells prior to the experiment commencing were all non-detect (<0.7 mg L^{-1}). Average Br- concentrations for the day 21, 27, 53, and 59 sampling events were 165, 108, 43, and 21 mg L^{-1}, respectively. The plume did not exhibit any clear evidence of preferential flow pathways.

4.4.4 Analysis of spatial moments

The results of the spatial moment analysis are summarized in Table 1. The zeroth spatial moment, which provides an estimate of the total tracer mass in solution, is shown in Figure 4-5a. Bromide is considered a conservative or non-reactive tracer, and therefore deviations in estimated mass from the injected mass reflect inadequacies in the monitoring network and uncertainty associated with the analytical method. The mass in solution was generally approximated adequately by the zeroth moment, and varied between 74% and 110% of the known injected mass (2,100 g). The largest discrepancy in estimated mass on day 59 is likely a reflection of the plume moving to an area of lower sampling network density.

Table 4-1. Summary of spatial moments derived from Br^- tracer test.

Variable	Symbol	Sampling Event				
Sampling date		24/07/17	14/08/17	20/08/17	15/09/17	21/09/17
Elapsed time (d)	t	0	21	27	53	59
Cumulative displacement (m)	Δd	0.0	6.5	9.0	16.7	18.2
Temporal average plume centre of mass velocity (m d^{-1})	V	- -	0.31	0.33	0.31	0.31
Spatial average bromide concentration (mg L^{-1})	C	- -	164.9	107.6	42.9	21.1
Moment Analysis						
Estimated mass (g)	M_{00}	2,100	2,304	2,169	2,177	1,557
Transverse spatial covariance tensor (m^2)	σ^2_{xx}	- -	0.79	0.88	2.14	2.51
Longitudinal spatial covariance tensor (m^2)	σ^2_{yy}	- -	1.82	3.46	9.54	11.37
Transverse dispersion (m^2 d^{-1})	D_T	- -	- -	0.01	0.02	0.03
Longitudinal dispersion (m^2 d^{-1})	D_L	- -	- -	0.14	0.12	0.15
Transverse dispersivity (m)	α_T	- -	- -	0.02	0.08	0.10
Longitudinal dispersivity (m)	α_L	- -	- -	0.41	0.37	0.49

The first spatial moment, which estimates the spatial coordinates of the plume centre of mass, is shown in Figure 4-5b. The plume centre of mass moved at an average rate of 0.31 m d^{-1}, although varied between 0.26 m d^{-1} and 0.42 m d^{-1}, and travelled at a bearing of approximately N20°W (Figure 4-4). This deviated slightly from the average slope aspect of the water table within the boundaries of the plume (N25°W). At the conclusion of the experiment, the plume centre of mass had a maximum displacement of 18.2 m from the central injection well. Plume centre of mass velocity, as calculated by the first spatial

moment, can be used to derive an estimate of tailings sand hydraulic conductivity. Using the spatially-averaged hydraulic gradient within the boundaries of the plume, and a tailings sand porosity of 0.41

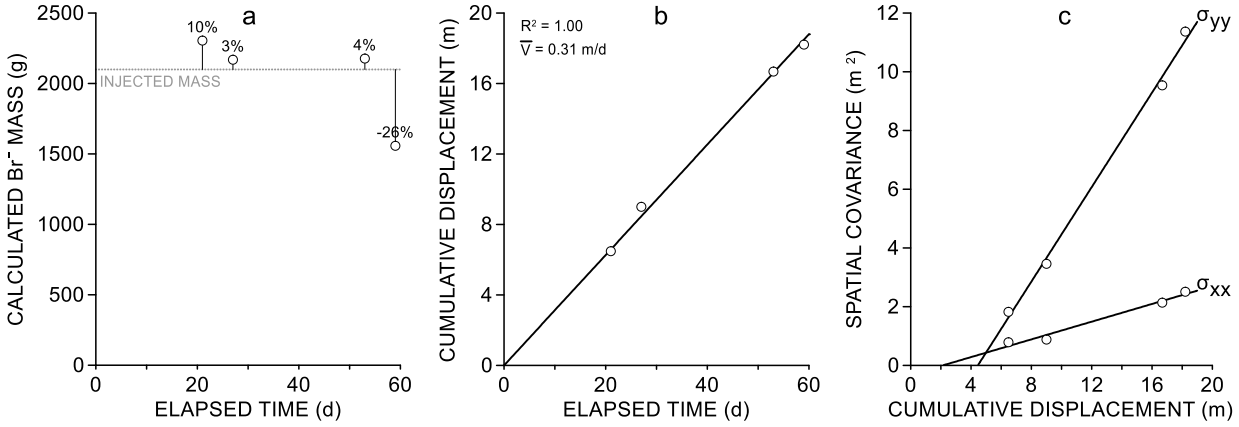

Figure 4-5. Estimated plume spatial moments: the zeroth moment (a) provides an estimate of the total tracer mass in solution; the first moment (b) estimates the displacement of the plume centre of mass, and the second moment (c) quantifies the spread of tracer about the plume centre of mass in the longitudinal (σ_{yy}) and transverse (σ_{xx}) directions, which are parallel and perpendicular to the velocity vector of the plume centre of mass, respectively.

(Chapter 2), the average hydraulic conductivity was 3.4 m d^{-1}, but when calculated for each individual sampling event, estimated K varied between 2.9 and 3.7 m d^{-1}.

The second spatial moment, or spatial covariance tensor, characterizes the concentration distribution about the centre of mass in directions parallel and perpendicular to the velocity vector (Figure 4-5c). The longitudinal and transverse horizontal spatial covariance tensors grew approximately linearly with displacement distance from the injection wells. These spatial covariance tensors corresponded to longitudinal dispersivities that remained approximately constant and varied between 0.37 m and 0.49 m, and transverse horizontal dispersivities that increased with displacement distance from 0.02 m to 0.10 m.

4.5 Discussion

Considerable attention within solute transport literature has been given to the issue of asymptotic conditions in field tracer experiments (Zech et al., 2015). Asymptotic dispersivity can be defined in practical terms as the dispersivity associated with sufficient travel through a porous media such that the probability distribution of pore-water velocity changes negligibly with further downgradient displacement. The transport can then be described as adhering to a Fickian regime, whereby the dispersive flux is proportional to the concentration gradient, and therefore fulfills a requirement of Equation 8. Once the asymptotic

dispersivity has been reached, dispersivity will not continue to grow unless a systematic deviation in geology is encountered. Evidence suggests that the plume needs to transit multiple (dozens of) correlation scale lengths of the aquifer to reach this state (Dagan, 1987). A correlation scale length is a property of the covariance structure of the aquifer hydraulic conductivity field. Put simply, it can be thought of as summarizing the decay in predictive power of a hydraulic conductivity measurement for estimating the hydraulic conductivity at successively larger separation distances (at what separation do two *K* measurements become uncorrelated?).

The approximately linear relationship between the longitudinal spatial covariance (σ_{yy}) and displacement of the plume centre of mass (Figure 4-5c) suggests, but does not definitively confirm, that the asymptotic longitudinal dispersivity was obtained during the field tracer experiment. This is consistent with expectations regarding the transport characteristics of the coarse tailings sand aquifer. Specifically, the segregation of particle sizes due to the industrial process from which tailings sand issues, and the mechanical placement of the sand during construction (using haul trucks, wiggle wagons and bulldozers). This was anticipated to result in an aquifer with a small variance in hydraulic conductivity, statistically stationary permeability, and a correlation structure of the hydraulic conductivity field with notably small spatial autocorrelation lengths, that lacked the stratigraphic features associated with natural deposition (e.g. lamination and stratification). Furthermore, the short distance associated with the development of the plume to this apparent asymptotic state (<9 m) is a similar indication of the minimally heterogeneous nature of the aquifer. However, this study was not complemented by a thorough characterization of aquifer permeability, which would allow for the identification of the correlation scale of tailings sand *K*. Therefore, evidence to support the adequacy of presumptions on statistical stationarity and small correlation scale of the hydraulic conductivity field is largely conjecture. However, by fitting the equation of Dagan (1984) to the estimated longitudinal spatial covariance tensor (σ_{yy}) derived from the tracer test, an approximation of the correlation scale can be identified. This equation takes the form:

$$\sigma_{yy}(t) = \sigma_{\ln K^2} \cdot {l_{\ln K}}^2 \left\{ 2\frac{t}{T} + \frac{3}{2} + 3\left[Ei\left(-\frac{t}{T}\right) - \ln\left(\frac{t}{T}\right) - \gamma \right] + 3\frac{e^{-t/T}\left[1+\frac{t}{T}\right]-1}{[t/T]^2} \right\} \qquad (9)$$

where $\sigma_{\ln K}^2$ is the variance of the natural logarithm (ln) of hydraulic conductivity, $l_{\ln K}$ is the correlation length of the ln *K* covariance function, *T* is a characteristic time equal to $l_{\ln K}$ / |*V*|, Ei is the exponential integral, and γ is the Euler-Mascheroni constant. This equation was used in a similar manner by Freyberg (1986) and Sudicky (1986), however this study had estimates of $l_{\ln K}$ to contextualize the results, which this present study lacks. Assuming a velocity of 0.31 m d^{-1} and ln K variance of 0.91, the calibrated value of

$l_{\ln K}$ that minimized the error between estimated and observed σ_{yy} was 0.36 m (Figure 4-6). Thus, providing some evidence to suggest that the correlation length of tailings sand hydraulic conductivity is quite small. In comparison to a natural sand aquifer that exhibited minimal heterogeneity in the hydraulic conductivity field ($\sigma_{\ln K}^2 = 0.24$), the correlation scale length ($l_{\ln K}$) identified using equation 9 was 2.7 m (Freyberg, 1986;

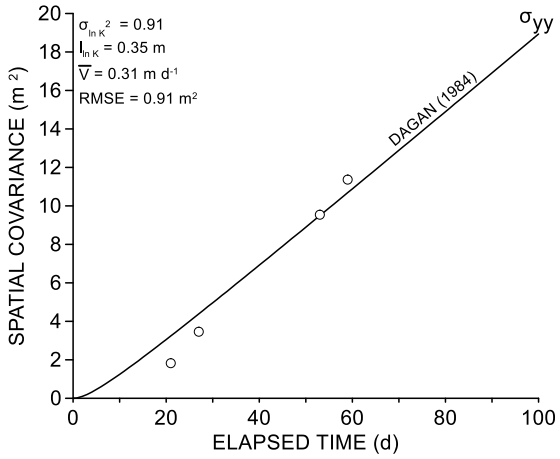

Figure 4-6. Estimated longitudinal spatial covariance tensor (σ_{yy}) calculated with spatial moments derived from the tracer test, and the calibrated theoretical curve of Dagan (1984). The formula used the ln *K* variance ($\sigma_{\ln K}^2$) measured with single-well response tests, the average velocity of the plume centre of mass ($\overline{\boldsymbol{V}}$), and the calibrated ln *K* correlation scale length ($l_{\ln K}$).

Sudicky, 1986). Assuming the correlation length of 0.36 m is representative of the length in the vicinity of the tracer test, the plume centre of mass will have transited over 50 correlation scale lengths at its maximum displacement of 18.2 m.

While it may be coincidental, this correlation length lies between the short tailings sand columns (0.32 and 0.34 m), which had dispersivities on the order of 1 x 10^{-3} m, and the longer column (0.37 m), which had a markedly larger dispersivity on the order of 1 x 10^{-2} m (Figure 2-2). However, determining if this reflects a meaningful threshold would require additional replicates of tailings columns in conjunction with a detailed characterization of aquifer hydraulic conductivity autocorrelation.

4.5.1 Contextualizing this study

Gelhar et al. (1992) performed a comprehensive review of field tracer tests, which involved the classification of dispersivities into a hierarchy of reliability. In brief, their criteria for high reliability experiments included: (1) test conducted under natural gradient / ambient groundwater flow conditions; (2) tracer input concentration, mass, and temporal distribution should be known; (3) the tracer should be

conservative / non-reactive; (4) monitoring of test should occur in three-dimensions, or two-dimensions if the tracer was injected across the entire saturated thickness of the aquifer; and (5) concentration data was analyzed using the method of spatial moments (Gelhar et al., 1992). Based on these criteria the tracer test conducted in the coarse tailings aquifer would be classified as high reliability. More recently, the work of Gelhar et al. (1992) was refined and updated by Zech et al. (2015), this tracer test remains consistent with their definition of a high reliability experiment. Comparing the field-estimated asymptotic longitudinal dispersivity (0.49 m) and associated scale (18.2 m) with the combined analysis of Gelhar et al. (1992) shows

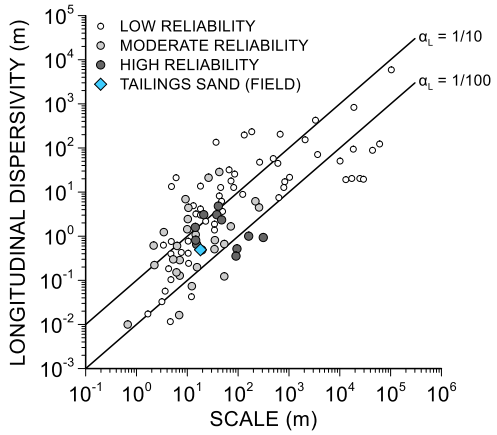

Figure 4-7. Estimated dispersivity for coarse tailings sand (0.49 m) placed in the context of other field tracer tests compiled by Gelhar et al. (1992).

the relatively short displacement distance and low-moderate longitudinal dispersivity of this experiment (Figure 4-7). The ratio of transverse dispersivity to longitudinal dispersivity of 1:5 is larger than the 1:10 ratio frequently assumed (when not directly measured), however as discussed in Zech et al. (2019) this is a convention without empirical or theoretical justification.

4.5.2 Implications for landscape-scale reclamation planning

The hydraulic conductivity of coarse tailings sand identified by the laboratory column experiments (3.2 m d^{-1}), single-well response tests (2.9 m d^{-1}) and field tracer test (3.4 m d^{-1}) is close to the targeted hydraulic conductivity (8.6 m d^{-1}) specified in the original theoretical aquifer design conducted by Price et al. (2010). A high aquifer conductivity was recognized as a necessary design feature to ensure a sufficient supply of groundwater to the fen. While it is advantageous that coarse tailings sand appears to have the appropriate hydraulic conductivity to perform the function of a water conveyance feature in the reclamation landscape, the presence of residual solutes requires characterization of transport properties to predict the timing and extent of solute redistribution. To that end, dispersive mixing will ameliorate the

considerable initial geochemical heterogeneity with further downgradient transport, resulting in a more spatially and temporally uniform input of salinity from a tailings sand aquifer to a wetland, or other downgradient receptor.

Whether the industrial processes that generate and segregate coarse tailings sand, and mechanically deposit the material for use in reclamation will result in aquifers with common transport properties is a matter that will require further investigation. While tailings sand in the AOSR has generally been shown to be a minimally heterogeneous material in a large, multi-scale evaluation of hydraulic conductivity conducted in the context of landscape reclamation (McKenna, 2002), there was spatial variability that manifest at a variety of scales. However, in spite of any differences in the physical characteristics of the parent material, the macroscopic structure (field-scale heterogeneities) of the hydraulic conductivity field will have a larger impact on field-scale dispersivity (macrodispersivity) (Dagan, 1987). At a reclamation site, this structure (or lack thereof) is expected to be predominantly influenced by the manner of its deposition – specifically, mechanically placed using heavy earth-moving equipment. Based on this assumption, it would be reasonable to anticipate other coarse tailings sand aquifers in the AOSR have asymptotic dispersivities of similar magnitude to this study. Incorporating a material with consistent hydraulic properties into reclamation design on the mine closure landscape has clear advantages, allowing practitioners to reliably predict hydrologic behaviour.

4.6 Conclusion

Hydraulic conductivity of coarse tailings sand was estimated and measured using a variety of techniques and across a range of spatial scales (from 2.9 x 10^{-3} m^3 to 2.7 x 10^2 m^3 of aquifer material sampled). This evaluation demonstrated close agreement between laboratory (3.2 m d^{-1}), in-situ field (2.9 m d^{-1}), and tracer test derived (3.4 m d^{-1}) values of average *K*. Yet, despite the grain size segregation that occurred as part of the tailings waste stream and the assumed homogenization that occurred due to mechanical placement, the coarse tailings sand exhibited a non-trivial spatial variability in hydraulic conductivity ($\sigma_{\ln K}^2 = 0.91$). Demonstrating, once again, the notoriously heterogeneous nature of field soils. Dispersivity values estimated from breakthrough in the coarse tailings sand cores, reflective of pore-scale mechanical dispersion, were expectedly small. The longitudinal and transverse dispersivity derived from the tracer test reached a maximum of 0.49 m, and 0.10 m, respectively after 59 days of transport and 18.2 m of displacement. The approximately linear growth of the longitudinal spatial covariance tensor suggested that the asymptotic value of dispersivity was obtained. By conducting further hydraulic conductivity measurements to obtain estimates of spatial autocorrelation, this claim could be more rigorously evaluated.

Given the anticipated expansion of coarse tailings sand landscapes in the post-mined AOSR, the detailed characterization of hydraulic and transport properties is warranted. This study will contribute to a small but growing – and increasingly necessary – body of literature on the transport of solutes through formerly-mined and reclaimed materials. In forthcoming work, the tailings sand dispersivity and large-scale effective hydraulic conductivity identified in this study will be used to parameterize a fate and transport model of solutes from the upland to peatland at the Nikanotee Fen Watershed (Chapter 5). Characterizing tailings sand hydraulic conductivity with a high degree of confidence will help to reduce the compensatory behaviour between hydraulic conductivity and groundwater recharge that could lead to nonuniqueness in the model.

4.7 Acknowledgements

The authors would like to thank J. Cameron, N. Popovic, J. Sherwood, C. van Beest, and the numerous undergraduate and master's students for their assistance in the field. We are also appreciative of the logistics and coordination provided by Suncor Field Services. Funding from the following sources is gratefully acknowledged: Northern Scientific Training Program (NSTP), the Natural Sciences and Engineering Research Council (NSERC) Canadian Graduate Scholarship (NSERC-GS) and Collaborative Research and Development Grant (NSERC-CRD; 418557-2011) titled "Evaluating the success of fen creation in the post oil sands landscape" with field support and direct funding from Suncor Energy Inc., Imperial Oil Resources Ltd., Shell Canada Ltd., and Teck Resources Ltd.

Chapter 5: Projecting the hydrochemical trajectory of a constructed fen watershed: implications for long-term wetland function

5.1 Introduction

The expansion of oil extraction activities in the Athabasca Oil Sands Region (AOSR) has resulted in landscape-scale disturbance of boreal forest and fen peatlands (Gosselin et al., 2010). Returning the land to resemble pre-disturbance ecosystems will require re-establishing the surface and subsurface ecohydrological processes and replicating the hydrologic connectivity of the natural landscape. To satisfy regulatory obligations and return the land to equivalent pre-disturbance capability, the investigation of peatland construction is required, with the intention that these ecosystems be incorporated into the mine-closure plans of oil sands companies. In response to this obligation, the Nikanotee Fen Watershed was built with the purpose of understanding how to construct fen peatlands that will become self-sustaining ecosystems over time, develop research and operational knowledge in fen construction, and test, refine, and optimize reclamation strategies and design to aid in implementation of fen reclamation on an industrial-scale (Daly et al., 2012). Due to a lack of prior experience in fen reclamation, it is unclear how this novel ecosystem will evolve hydrologically, ecologically, and geochemically. The anticipated timeline associated with this evolution necessitates the use of modelling to constrain expectations of system trajectory.

Constructing wetlands that can replicate the function of natural systems in the region presents several challenges related to water quantity and quality. The regional climate of the AOSR is characterized as sub-humid, with distinct inter- and intra-annual variability in cumulative annual precipitation (Petrone et al., 2007). Large variations in water availability within and between years necessitates design strategies that result in systems that are parsimonious with water use, have internal mechanisms for water storage and conservation, and are therefore resilient to climatic stress. This potential for limited water availability is one of the major obstacles in wetland reclamation that needs to be assessed at constructed fen projects. Furthermore, it is anticipated that reclaimed landforms will largely be constructed using overburden and processes-affected materials, due to the absence of readily available alternatives, and a need to reintegrate these materials back into the landscape. However, as a consequence of the bitumen extraction and upgrading processes, these materials have residual concentrations of solutes, including sodium (Na^{+}), calcium (Ca^{2+}), and sulfate ($SO4^{2-}$) (Kessel et al., 2018). Groundwater flow through these process-affected materials has been shown to transport solutes downgradient towards the wetlands, potentially impacting the ecological development of these nascent ecosystems (Kessel et al., 2018). To what degree the presence of these solutes

constitutes a threat to the success of constructed peatlands is currently unclear, however, salinization of the shallow subsurface in the wetlands has been shown to hinder the establishment of targeted vegetation species (Rezanezhad et al., 2012), as many wetland vegetation species exhibit low salinity tolerance (Glaeser et al., 2016).

The design philosophy of these experimental constructed fen pilot projects reflects the current conceptual understanding of water storage and movement within natural systems of the AOSR (Ketcheson et al., 2016). This inspired the inclusion of uplands that are hydraulically connected to the peatlands, which can supply groundwater to the downgradient ecosystem (Price et al., 2010). These uplands need to be capable of holding sufficient moisture to support the growth of upland forests, yet concurrently generate a surplus of water to groundwater recharge. Initial assessments conducted at the Nikanotee Fen Watershed confirm that the upland is functioning as intended (Ketcheson et al., 2017), and will likely continue to fulfill its role as a water storage and conveyance feature into the future (Chapter 2; 3).

Recent assessments of the Nikanotee Fen Watershed, and Sandhill Fen Watershed – a reclamation project with similar goals – have investigated the hydrology, geochemistry, micrometeorology, and ecology (Borkenhagen and Cooper, 2019; Biagi et al., 2019; Ketcheson et al., 2017; Vitt et al., 2016). These studies have illustrated that these novel ecosystems share many meaningful functional similarities with the natural systems that inspired their design. Yet, these reclaimed systems will continue to evolve over the coming decades, as vegetation matures, and solutes migrate from process-affected materials. Informing mine closure planning and regulatory decision making of the likely successional pathway is necessary to evaluate the feasibility of fen reclamation. Furthermore, understanding the influence of different design elements on the overall function of the system is critical to improving the resilience of these systems to climatic and geochemical stresses (Ketcheson et al., 2016). On both accounts, numerical modelling offers a promising technique.

To inform future reclamation design and decision-making, it is necessary to evaluate the trajectory of these systems and determine whether they will possess the appropriate characteristics to encourage long-term peat accumulation and support the growth of vegetation assemblages that reflect the undisturbed landscape. The timeline on which these systems are expected to evolve, and the present need for information on the likely long-term ecohydrological trajectory, make it impractical to merely observe the development of the system and thus requires the aid of modelling. Therefore, the objectives of this study are to: 1) calibrate and validate a numerical model capable of simulating groundwater flow and solute transport at the Nikanotee Fen Watershed; 2) use the model to investigate the timeline associated with sodium export,

including the probable peak and longevity of elevated sodium concentrations in the shallow subsurface of the fen; and 3) evaluate the probable trajectory of the system in the context of water quality and water quantity, and the broader implications of this trajectory on reclamation design.

5.2 Study site

The Nikanotee Fen Watershed was constructed on a formerly mined area of an oil sands lease approximately 25 km north of Fort McMurray, Alberta (56°55'59" N, 111°25'00" W), and comprises a fen peatland (2.2 ha), upland aquifer that stores and directs groundwater to the fen (7.7 ha), and surrounding reclaimed and undisturbed hillslopes (22.2 ha) (Figure 5-1). Construction of the watershed was completed in January 2013, and closely adhered to the conceptual design of Price et al. (2010), which estimated the appropriate morphology, fen-to-upland ratio, material hydraulic properties and layering to consistently maintain a sufficient level of saturation in the fen. The design incorporated an upland aquifer constructed from mechanically-placed coarse tailings sand to supply groundwater to the fen (Daly et al., 2012). The upland aquifer was capped with approximately 30 cm of a common reclamation soil prescription known as LFH-mineral mix (hereafter referred to as LFH) to provide a substrate amenable to vegetation growth. As a means of enhancing infiltration and reducing surface overland flow to the fen, the upland LFH was furrowed perpendicular to slope and basins were excavated on the upslope side of large, raised landforms termed "hummocks". These interventions markedly increased the surface detention capacity. Basins positioned adjacent to hillslope confluences detained large quantities of runoff and were disproportionately effective at recharging the upland aquifer in the early post-construction period (Kessel et al., submitted). Underlying the fen and upland aquifer is a low-permeability geosynthetic clay liner (GCL), which was placed to reduce percolation losses from the watershed to the regional groundwater flow system, and establish a hydraulic gradient towards the fen. Surface water is discharged through a water level control structure in the northeastern corner of the fen. When the water table was below the surface, discharge occurs at an approximately constant seepage rate. However, during periods when the water table rises above ground surface, flow can occur over a weir and through a drain.

As a consequence of historical bitumen extraction processes and the marine depositional environment, the coarse tailings sand that forms the upland aquifer contains high pore-water concentrations of sodium, which are mobilized by groundwater flow towards the fen (Kessel et al., 2018). To reduce the potential for rooting zone salinization in the upland, the ground surface and geosynthetic clay liner were sloped to 2% and 3%, respectively. This maintained a sufficiently deep water table in the upland, which consistently fluctuated below the rooting zone of upland vegetation. Concerns over direct movement of

process-affected water across the transition zone to the fen surface led to the inclusion of a highly permeable underdrain (constructed with petroleum coke), which due to the contrasting hydraulic conductivity of the tailings sand, directed water and solutes underneath the fen and upwards through the peat. This was intended to fully exploit the large adsorptive capacity of the peat (Rezanezhad et al., 2012) and delay the arrival of solutes at the fen surface (Daly et al., 2012). Peat from a nearby donor site was directly placed as a ~1.8 m thick layer overlying the petroleum coke, however the natural physical structure of the donor peat was altered by the excavation, transportation, and placement by heavy equipment during construction (Nwaishi et al., 2015). Notably, this process removed the former acrotelm from the donor peat. Following site construction, the fen was planted with species representative of undisturbed fens in the region, most notably, *Carex aquatilis*, *Juncus balticus*, and a variety of bryophytes via the moss layer transfer technique (Borkenhagen and Cooper, 2019).

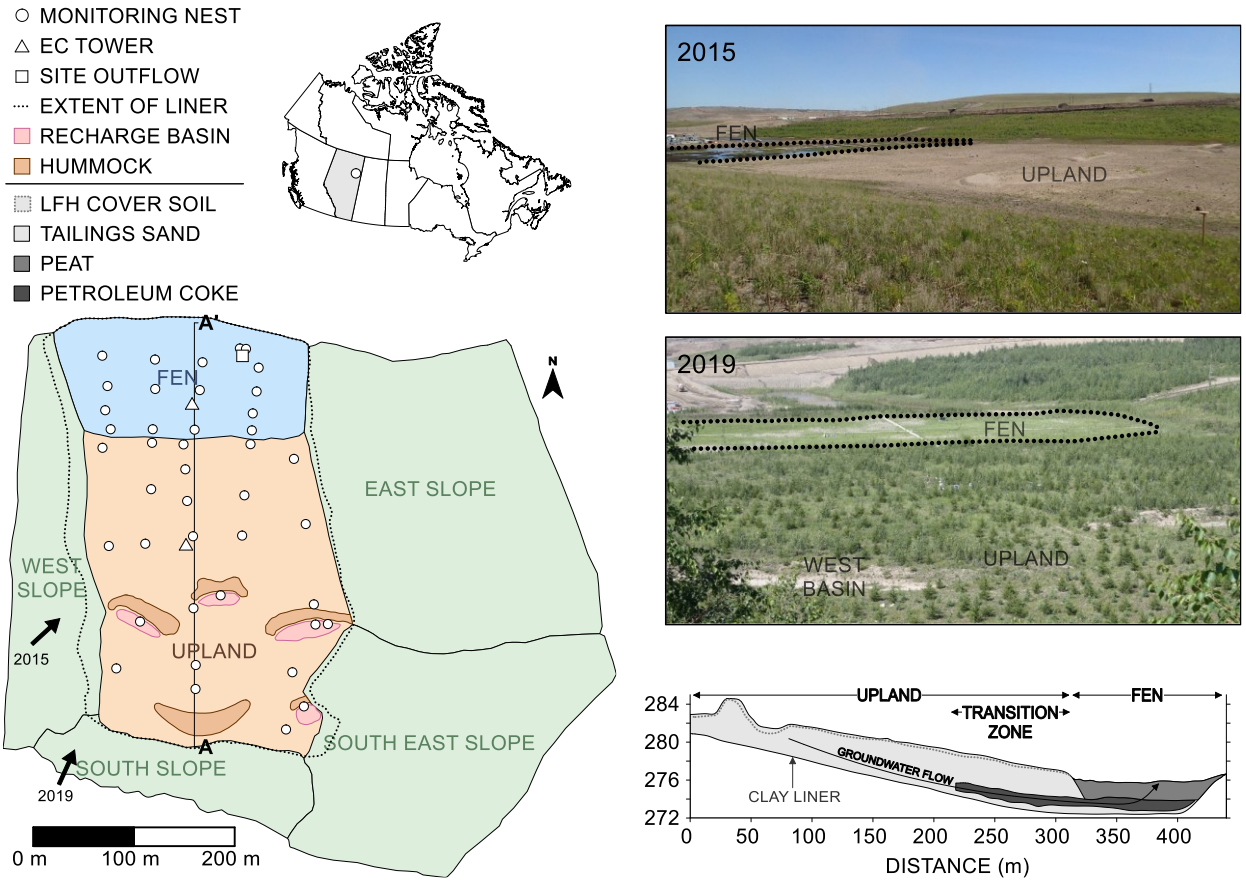

Figure 5-1. Study site map of the Nikanotee Fen Watershed, depicting the locations of groundwater monitoring nests and EC stations. The stratigraphic cross-section along the central transect of the system illustrates the layering of materials and dominant groundwater flow direction. Also shown are photographs taken in 2015 (from west slope) and 2019 (from south slope), illustrating upland vegetation development.

5.3 Methods

5.3.1 Field instrumentation

Meteorological stations located in the fen and upland measured precipitation (Texas Instruments Canada Ltd. TR-525M tipping bucket rain gauge), net radiation (Kipp and Zonen NR-LITE2 net radiometer), air temperature and relative humidity (Rotronic HC2S3), ground heat flux (REBS HFT-3), wind speed and direction (R.M. Young 05103 Wind Monitor). Data collected from the meteorological stations was used to derive potential evapotranspiration (PET) using the Penman method (Penman, 1948). Eddy covariance (EC) systems at the fen and upland meteorological stations were used to estimate actual evapotranspiration (AET); a detailed description of the methodology can be found in Ketcheson, et al. (2017).

Hydraulic head was monitored with a network of wells and piezometers installed in 15 nests in the fen, 9 nests in the transition zone, and 17 nests in the upland. Fen monitoring nests consisted of a fully-slotted well installed to a depth of 1.5 m below ground surface (bgs), and five piezometers with a slotted length of 0.2 m installed to 0.5, 0.9, 1.5, 2.25, and 2.75 m bgs. Upland and transition zone monitoring nests had a well installed to approximately 2.5 m bgs, and piezometers installed to 2.25 and 2.75 m bgs. Logging pressure transducers (Schlumberger Mini-Diver) and capacitance water level recorders (Odyssey Dataflow Systems) recorded hydraulic head in 10 monitoring locations in the upland, 3 locations in the transition zone, and 18 locations in the fen. Manual head measurements were conducted weekly at all monitoring locations from May to August of each year.

Groundwater samples were collected between 3 and 5 times per year throughout the summer season at a subset of monitoring wells and piezometers. Samples were analyzed for major anions (Cl^-, $SO4^{2-}$) and cations (Na^+, Ca^{2+}, Mg^{2+}) using ion chromatography. A detailed description of the sampling and analysis methodology can be found in Kessel et al. (2018).

5.3.2 Numerical modelling

The three-dimensional groundwater flow and solute transport model of the Nikanotee Fen Watershed was developed using the finite-difference numerical code MODFLOW-SURFACT (Panday and Huyakorn, 2008). MODFLOW-SURFACT was selected as the simulator because it can accurately and robustly delineate the position of the water table in an unconfined aquifer without requiring the implementation of variably-saturated groundwater flow equations, through the use of the gravity-segregated vertical equilibrium method (Huyakorn et al., 1994). The model domain extended from ground surface to the lateral and vertical limits of the geosynthetic clay liner, which fully encompassed the fen and upland, and included

the toe of the hillslopes (Figure 5-1). The model was spatially discretized into 63 unconfined planar layers with lateral dimensions of 4 m by 4 m, with a vertical cell thickness of 0.2 m, resulting in 110,784 active cells. The simulation period was temporally discretized into daily stress-periods, however, the duration of each annual simulation commenced with the thawing of ground-frost in the spring and concluded with the onset of freezing in autumn, as estimated using the Stefan's equation (Jumikis, 1977; Appendix A). The average length of the unfrozen period at the site was 183 days (Chapter 3).

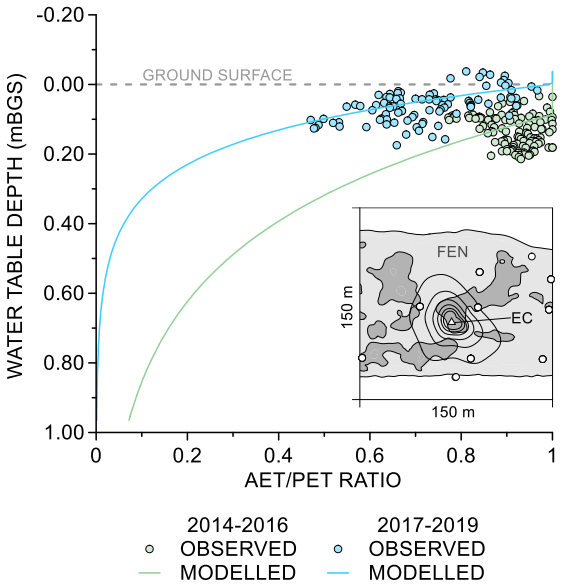

Figure 5-2. Relationship between the daily measurements of the spatially-averaged water table depth within the EC flux footprint and the ratio of actual to potential evapotranspiration. The modelled curves represent the minimum least squares fit to the data, which reaches an AET:PET ratio of 0 at the extinction depth. The inset map shows the location of the EC tower, extent of the EC flux footprint in the fen, and areas susceptible to ponding (dark grey).

5.3.2.1 Boundary conditions

The bottom and lateral boundaries coincide with the position of the geosynthetic clay liner, which due to the extremely low permeability, allow it to be adequately represented by a no-flow boundary condition. The upper model boundary is a head-dependent flux condition that allows water to enter the domain through prescribed recharge provided the water table is below a specified maximum ponding elevation, and leave the domain as evapotranspiration and saturation excess overland flow. Actual evapotranspiration was calculated as a function of water table depth scaled by potential evapotranspiration, and only explicitly simulated in the fen, the rationale for which is explained below. The actual evaporative flux in the fen is equal to the potential level when the water table is coincident with or above the surface and decreases in a

quasi-exponential manner with increasing water table depth – up to the extinction depth (below which ET losses are vanishingly small). The relationship between water table depth and the ratio of actual to potential evapotranspiration in the fen was derived from measured daily AET data at the fen EC tower, estimated daily PET from the fen meteorological station, and the daily spatially-averaged water table depth within the flux footprint (Figure 5-2). The seepage component of outflow was represented as a head-dependent flux boundary; when the water table was located at or below ground surface, water (and any solutes) were removed at a transmissivity-controlled rate of approximately 11 m^3 d^{-1}, as measured in a downgradient flume. Episodic surface water discharge events from the fen were represented with a combination of boundary conditions. A separate head-dependent flux boundary condition removed water above ground surface at a theoretically unlimited conductance, however this flux was restricted by the rate of lateral water movement to the boundary. Additionally, the model would also reject recharge if the hydraulic head was above a maximum ponding elevation, this rejected flux would be immediately partitioned towards surface water discharge.

5.3.2.2 Recharge parameterization

The differing soil moisture dynamics of the fen, upland, and recharge basins necessitated separate approaches for quantifying groundwater recharge. Specifically, spatial variations in recharge arose due to proximity to hillslopes (and thus additional water supply), depth of the water table, thickness of the LFH cover soil, and connectivity between the water table and the surface. In the fen, the water table fluctuated close to ground surface, and remained hydraulically connected to the surface. Since simulated evapotranspiration in the fen was a function of water table depth, and calculated explicitly by the model, the recharge flux prescribed to the fen was equal to direct precipitation. In contrast, the upland water table fluctuates below the evapotranspiration extinction depth, and therefore was disconnected from surface processes of soil evaporation, interception, and root water uptake. Accurate delineation of groundwater recharge across the upland required accounting for these processes. Consequently, upland recharge was parameterized using HYDRUS 1D (Šimůnek et al., 2008), which simulated the near-surface soil moisture dynamics with a range of cover soil thicknesses. The water flux across the bottom boundary of the HYDRUS 1D model was assumed to reach the water table, and therefore was used to specify groundwater recharge. As such the HYDRUS 1D model was not explicitly coupled to MODFLOW, but rather acted as a preprocessing step to determine the upland recharge boundary flux. Details of these models can be found in Chapters 2 and 3. Basins adjacent to hillslopes received and detained large volumes of surface runoff, notably the East recharge basin, and Southeast Corner. To account for this surface runoff, separate

HYDRUS 1D models were used to estimate groundwater recharge under the basins based on ponded water depth (measured by a surface water gauge) instead of precipitation, with a range of maximum ponding elevations (determined by basin bathymetry). A summary of average annual groundwater recharge between

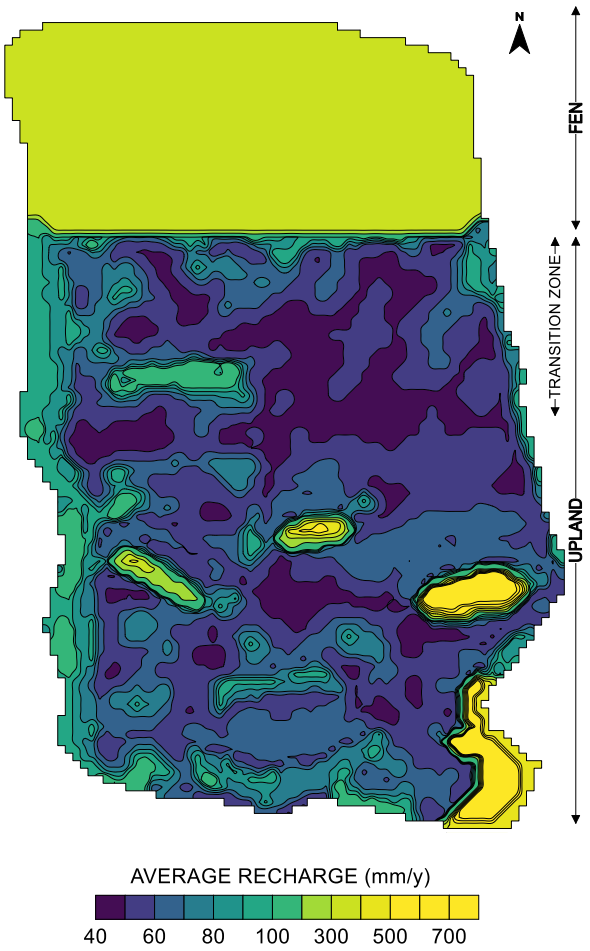

Figure 5-3. Average annual recharge of the calibration and validation period. Due to the tight coupling between water table and the surface processes of evapotranspiration and surface runoff, the recharge across the entire fen is equal to precipitation. Spatial variation in upland groundwater recharge was a consequence of differences in LFH thickness, which varied between 0 and 0.65 m.

2014 and 2019, is shown in Figure 5-3.

5.3.2.3 Stratigraphic representation

Detailed surveys taken during construction allowed for the delineation of the subsurface topography of all construction materials, reducing geological uncertainty to a level uncommon in groundwater flow models of this scale. These measurements were conducted with approximately 4 m spacing, coinciding with the

lateral spatial discretization of the finite difference grid, for the layers of LFH, peat, tailings sand, petroleum coke, and the geosynthetic clay liner. Within the model, most materials were represented with a single set of homogeneous soil properties, however, the peat was subdivided into surficial peat and deep peat (0-0.4 m below ground surface), which field and laboratory measurements indicated differed modestly in their hydraulic and geochemical properties (Nwaishi et al., 2015). Details of the material discretization can be found in Figure C-1.

5.3.2.4 Initial conditions

The main simulation period began on April 30, 2014, and although the site was operational in 2013, the first year was characterized by a wetting-up of the aquifer and an initially sparse monitoring network. To generate a head and sodium distribution that closely resembled the conditions in early 2014, the model was run in a quasi-steady-state manner for 160 days. Initial sodium concentrations for this spin-up period were specified homogeneously in the tailings sand, petroleum coke, and peat at 350, 100, and 50 mg L^{-1}, respectively. These concentrations represent the average of water samples taken in each material during the first sampling event in May 2013. The total initial sodium mass was 30,180 kg, close to the estimate of leachable sodium mass in the system conducted by Simhayov et al. (2017).

5.3.2.5 Parameterization and calibration

Initial parameterization of hydraulic and transport properties of the aquifer materials was largely informed by the extensive field and laboratory measurements conducted between 2013-2019. As such, the majority of hydraulic and transport properties were directly based on previous work conducted at the Nikanotee Fen Watershed. The measured and calibrated values for saturated hydraulic conductivity, porosity, specific yield, dispersivity, and sodium adsorption distribution coefficients are summarized in Table 5-1, along with their respective sources. In addition, the calculation of effective diffusion used a free water diffusion coefficient of 1.33×10^{-9} m^2 s^{-1} (Li and Gregory, 1974), and a tortuosity estimated using the method of Pisani (2011).

Calibration was conducted with the support of the parameter estimation and uncertainty analysis code PEST (Doherty, 2015). The objective function minimized the residual sum of squares (RSS) between 13,000 daily manual and transducer hydraulic head measurements. PEST performed optimization of horizontal and vertical hydraulic conductivity of tailings sand, petroleum coke, surficial peat, and deep peat; specific yield of tailings sand, and surficial peat. Due to the range of water table fluctuations at the site, certain materials never became saturated or unsaturated, therefore there were no data to inform optimization

of specific yield. Consequently, deep peat and petroleum coke were assumed to have the same specific yield as surficial peat and tailings sand, respectively. The calibration period was conducted between 2014-2016, and the model was validated from 2017-2019 using an additional 13,000 hydraulic head measurements. Although not included in the objective function, the model was further validated against measurements of cumulative actual evapotranspiration, and 130 Na^+ groundwater samples taken between 2013-2019.

5.3.3 Monte Carlo simulations

The large inter- and intra-annual variability in climate that is characteristic of the AOSR was anticipated to influence the flushing of sodium through the system, peak solute concentrations at the surface, and position of the fen water table. Therefore, assessing the probable future evolution and trajectory of the fen required the explicit consideration of climatic variability. A combination of long-term hydrometric data (1953-2017) from a nearby Environment Canada weather station and previous modelling (Chapter 2; 3), the latter of which derived statistical characteristics of groundwater recharge, was used to perform Monte Carlo simulations with 50 climate realizations. Each realization consisted of 30 years, starting in 2020 (7 years post-construction), and each annual simulation consisted of 183 days – equal to the average duration of the hydrologically active period.

5.3.3.1 Climate realizations

For each annual simulation, potential evapotranspiration was parameterized by randomly selecting one of 65 years of historical data (see Appendix B for details). Weak temporal autocorrelation in cumulative annual precipitation, which was identified for lag periods of one year, was accounted for using the method of Willemain and Desautels (1993), whereby the uniform random numbers that were generated had the same level of serial correlation as the historical precipitation data (0.32). These correlated random numbers were used to select one of 65 years of historical precipitation data, which directly parameterized the fen recharge boundary. The random numbers were also used in conjunction with the cumulative probability density functions of groundwater recharge identified in Chapter 3 to parameterize upland groundwater recharge (Figure B-2). This previous work defined the statistical characteristics of cumulative annual groundwater recharge in the upland, as a function of cover soil thickness, and derived an exponential relationship to describe the partitioning of recharge on a daily basis throughout the hydrologically active period. Following reclamation, the hillslopes surrounding the upland underwent soil and vegetation development that reduced the quantity of surface overland flow generated during the early post-construction period (Ketcheson and Price, 2016). A relationship was derived using multiple non-linear regression

between site age and cumulative annual precipitation, to estimate cumulative annual runoff (Figure B-3). This relationship was implemented in the Monte Carlo simulations to parameterize recharge at the East Basin and Southeast Corner.

5.4 Results

5.4.1 Model calibration and validation

Calibration of the model resulted in modest changes from the initial parameter values for the majority of hydraulic parameters (Table 5-1). While the optimized hydraulic conductivity of tailings sand deviated negligibly from the initial parameter, surficial peat was decreased by over an order of magnitude. The optimized value of peat specific yield (0.06) was relatively low compared to undisturbed acrotelmic fen peat (Goetz and Price, 2015); however, it was within the range measured at the Nikanotee Fen (Nwaishi et al., 2015; Scarlett and Price, 2019), and a regional saline fen (Wells and Price, 2015). Although the horizontal (K_h) and vertical hydraulic conductivity (K_v) of surficial and deep peat were allowed to vary independently during calibration, a value of 0.1 m d^{-1} for K_h and K_v of both surficial and deep peat was selected by the optimization scheme, meaning that the peat was represented as isotropic and homogeneous within the model. During calibration, PEST identified the high sensitivity of peat and tailings sand specific yield and horizontal hydraulic conductivity, while the least sensitive parameters were the horizontal and vertical hydraulic conductivity of the petroleum coke layer.

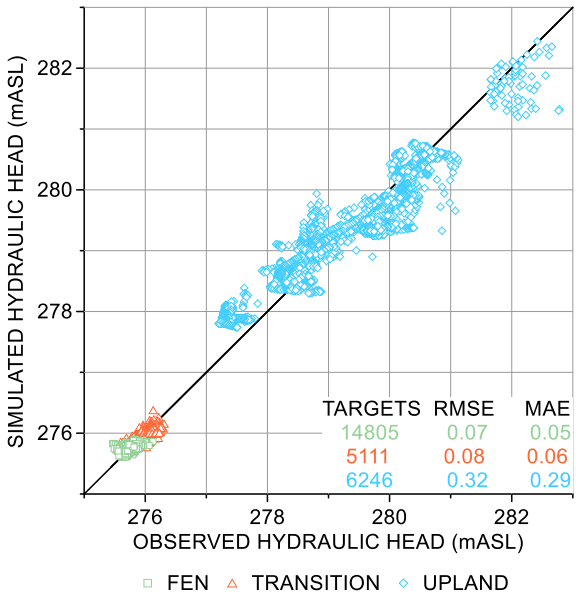

Figure 5-4. Daily simulated vs. observed hydraulic head plot for calibration and validation periods. Head plotting above the 1:1 line indicates model overprediction.

The water table dynamics of the upland, transition zone and fen were adequately represented by the model in the calibration and validation periods. During the calibration period, the mean absolute error (MAE) between simulated and observed hydraulic head was 0.23 m in the upland, 0.06 m in the transition zone, and 0.04 m in the fen. During the validation period, the average error between simulated and observed head was 0.24 in the upland, 0.06 m in the transition zone, and 0.06 m in the fen. By design, the fen and transition zone maintained relatively stable water tables throughout the study period. In contrast, the upland experienced large fluctuations in water table, varying by up to 3 m in close proximity to recharge basins. The magnitude of these fluctuations across the site was generally captured appropriately by the model (Figure 5-4). The calibration and validation period included years that were substantially wetter (2016) and drier (2015) than the long-term average. Distinct seasonal patterns of water table were apparent in the fen, with the lowest water tables occurring in June, and July, corresponding to the period of highest evaporative demand. Between the 2014-2019 study period the eddy covariance system measured a total of 3.27 m of potential evapotranspiration and 2.22 m of actual evapotranspiration from the fen. The cumulative simulated actual evapotranspiration in the fen from the same time period was 2.25 m, a deviation of less than 2% (Figure 5-5). The global mass-balance error over the calibration and validation period was less than 0.1%, demonstrating that the closure criteria of the solver were suitable.

Table 5-1. Model parameters and citations

Parameter	Symbol	Final / calibrated value (initial value)					Unit
		Tailings Sand	LFH	Petroleum Coke	Surficial Peat	Deep Peat	
Hydraulic properties							
Specific yield	Sy	0.33 (0.33)[a]	0.05[a]	0.33[b]	0.06 (0.10)[c,d]	0.06	$m^3\ m^{-3}$
Porosity	n	0.40[a]	0.41[a]	0.45[e]	0.90[f]	0.90[f]	$m^3\ m^{-3}$
Horizontal saturated hydraulic conductivity	K_x	2.84 (3.40)[g]	0.10[a]	177 (82)[h]	0.10 (6.9)[h]	0.10 (0.26)[h]	$m\ d^{-1}$
Vertical saturated hydraulic conductivity	K_z	1.63 (3.40)[g]	0.10[a]	10 (82)[h]	0.10 (6.9)[h]	0.10 (0.26)[h]	$m\ d^{-1}$
Geochemical parameters							
Initial sodium concentration	C_0	350[e]	0[i]	100[e]	50[e]	50[e]	$mg\ L^{-1}$
Longitudinal dispersivity	α_L	0.49[g]	0.49[b]	0.49[b]	0.25[j]	0.25[j]	m
Transverse dispersivity	α_T	0.1[g]	0.1[b]	0.1[b]	0.25[j]	0.25[j]	m
Distribution coefficient	Kd	0[i]	0[i]	0[i]	9×10^{-4} [j]	5×10^{-3} [j]	$m^3\ kg^{-1}$

[a] Chapter 3, [b] assumed to equal tailings sand, [c] Scarlett and Price (2019), [d] Nwaishi et al. (2015), [e] measured site data, [f] Simhayov et al. (2018), [g] Chapter 4, [h] Ketcheson et al. (2017), [i] assumed to equal zero, [j] Kessel et al. (unpublished)

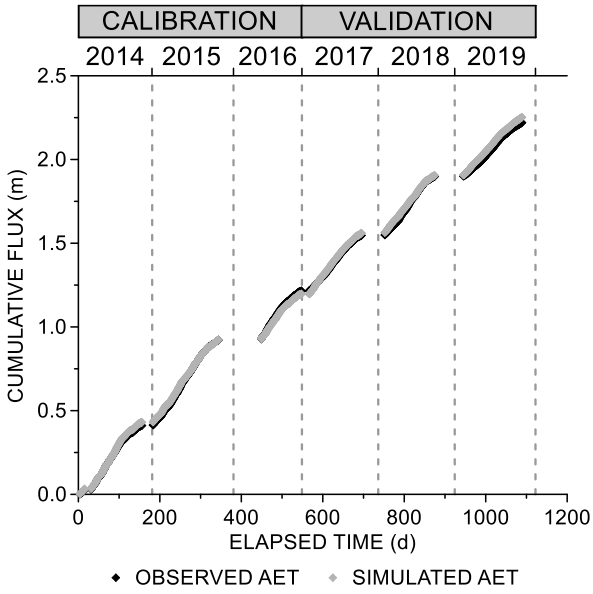

Figure 5-5. Plot of cumulative simulated and observed actual evapotranspiration. The observed AET was measured at the fen eddy covariance tower, and the simulated AET was extracted from the model only within the bounds of the flux footprint - not the entire fen surface. Although this comparison is shown for both the calibration and validation periods, the observed data was never used in the optimization procedure.

Water samples taken between 2013-2018 illustrated the transport of sodium in groundwater from the upland tailings sand aquifer, along the petroleum coke, and through the fen peat (Figure 5-6). In the early post-construction period the highest sodium concentrations were observed in the upland aquifer. However, due to dilution from relatively fresh recharge, the downgradient migration of salts, and evapoconcentration in the fen, by 2017 the highest salinity was at the surface along the interface between fen and transition zone. Beginning in 2014, a distinct pulse of sodium moving from upland to fen was apparent in both observed and simulated sodium data. This pulse of high sodium was followed by relatively fresh groundwater from distal areas of the upland that flushed quickly. Although a steep geochemical gradient existed across the surface of the fen, by 2017 the majority of the fen had higher sodium concentrations than the background concentrations of the tailings sand aquifer (350 mg L^{-1}). The model was generally capable of reproducing these spatial patterns of sodium, as indicated by the MAE between observed and simulated sodium concentrations, which was 43 mg L^{-1}. Error between simulated and observed sodium concentration was highest at the interface between fen and transition zone, which had abrupt changes in surface concentration.

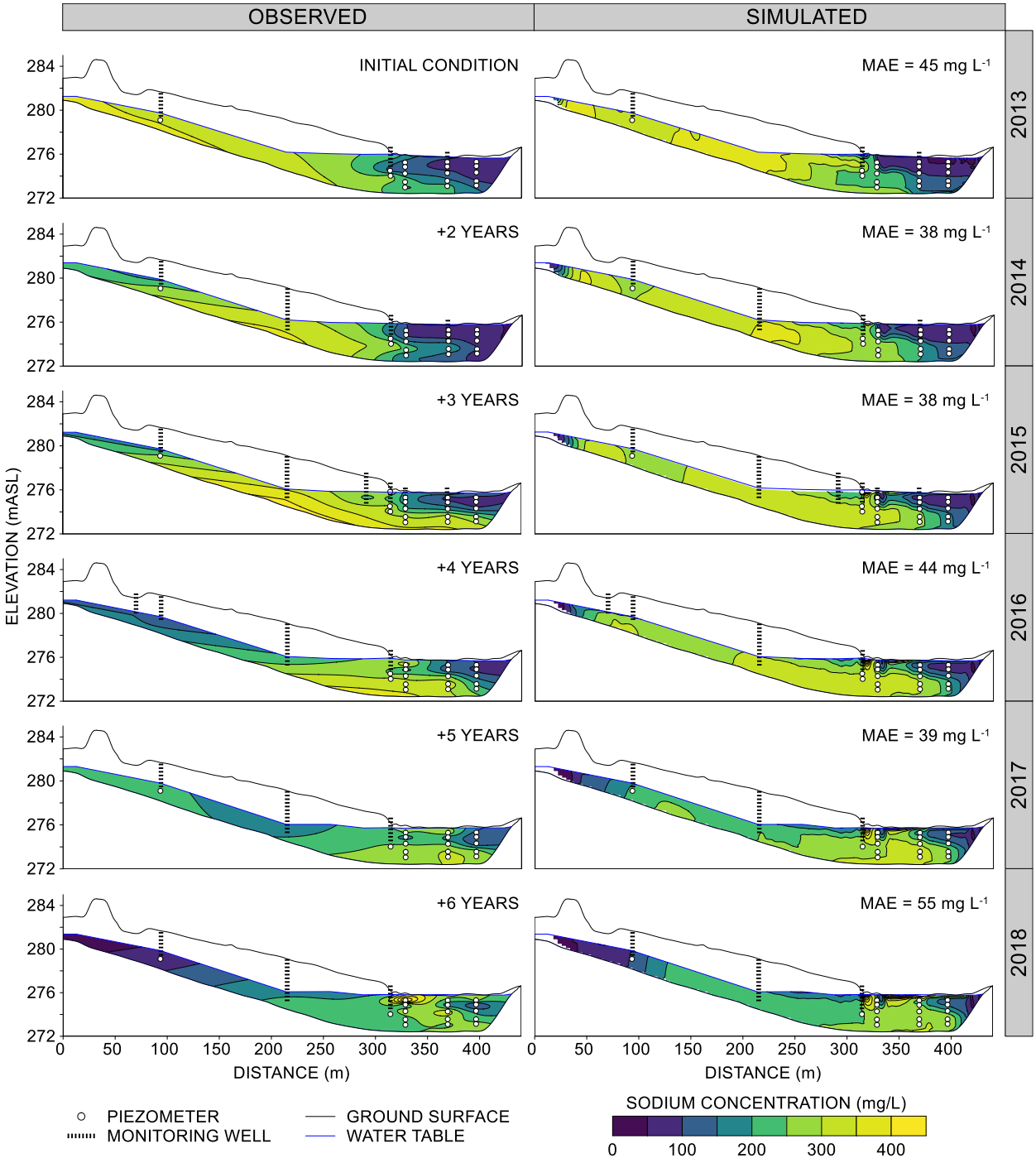

Figure 5-6. Cross-sections of observed and simulated average annual sodium concentrations down the central transect of the watershed. The mean absolute error (MAE) reflects the difference between measured and modelled sodium at the midscreen of wells and piezometers. Each monitoring location was sampled 3-5 times per year, between May-September.

5.4.2 Projected hydrologic function

Across all climate realizations, cumulative annual groundwater recharge to the watershed (upland and fen) varied by an order of magnitude, with a minimum of 6,000 m^3 to a maximum of 54,000 m^3. Average annual groundwater recharge (including fen precipitation) was 18,500 m^3 or 183 mm when standardized to the area of the fen and upland. Among all climate realizations, the longest consecutive period of below-average recharge was 11 years out of a total Monte Carlo simulation period of 30 years. This resulted in a cumulative recharge deficit of 44%, compared to what would be expected under average climatic conditions. However, the relatively weak temporal autocorrelation meant that it was unusual for climate realizations to deviate in such a sustained manner from the long-term average, or accrue such a large water deficit. Declining recharge contributions from hillslope runoff caused a decrease in upland water table, resulting in a reduction in effective upland storage, defined as the quantity of groundwater above the water table of the fen. At the start of the Monte Carlo simulation period, 7 years post-construction, the effective upland water storage in the saturated zone amounted to 23,000 m^3. By the end of the simulation period, 37 years-post-construction, the ensemble mean storage had declined to 17,000 m^3. Actual evapotranspiration was typically of similar magnitude to surface water discharge, and during atypically dry years could supplant discharge as the dominant water loss from the fen (Figure 5-7). The ensemble mean of these fluxes – the average of all Monte Carlo realizations – was 10,600 m^3 y^{-1} and 8,300 m^3 y^{-1} for surface water discharge and actual evapotranspiration, respectively. The ratio of cumulative annual actual evapotranspiration to potential evapotranspiration in the fen varied between 0.5 to 1.0, however on average was 0.79.

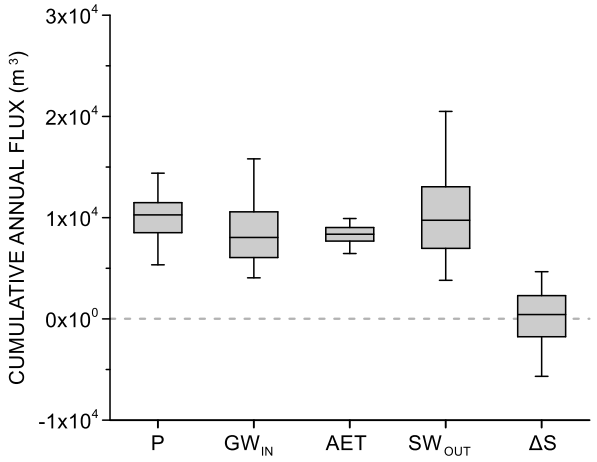

Figure 5-7. Projections of annual fen water balance components: fen recharge (equal to precipitation; P), lateral groundwater inflow from upland to fen (GW_{IN}), actual evapotranspiration (AET), and surface water discharge (SW_{OUT}). For comparison purposes the annual change in upland aquifer storage (ΔS) is shown.

Water balance fluxes and water table depth exhibited distinct seasonality, with the lowest (deepest) annual water tables consistently coinciding with peak annual evaporative demand, and consequently evaporative flux. Surface water discharge was highly variable between and within individual realizations, depending on the specific timing of precipitation events. However, the ensemble mean revealed that discharge peaked during the spring freshet, tended to decrease to a minimum during the summer, and increased throughout the autumn. Groundwater inflow to the fen averaged 8,700 $m^3 y^{-1}$, and although it was distributed relatively evenly throughout the growing season, it varied across an order of magnitude between years depending on the prevailing and preceding meteorological conditions.

The ensemble mean spatially-averaged water table depth in the fen varied between 0.04 and 0.14 m below ground surface, with an average depth of 0.08 m (Figure 5-8). However, within individual realizations the water table depth fluctuated between 0.03 and 0.21 m. Water table depth varied across the fen due to peat microtopography, resulting in a spatial standard deviation of 0.08 m, which was consistent across all climate realizations (i.e. the fen water table was always planar). Due to the diminishing contributions of hillslope runoff to upland groundwater recharge (Figure B-3), there was a general tendency for a slight decline (0.01 m) in average annual fen water table depth over the 30-year simulation period.

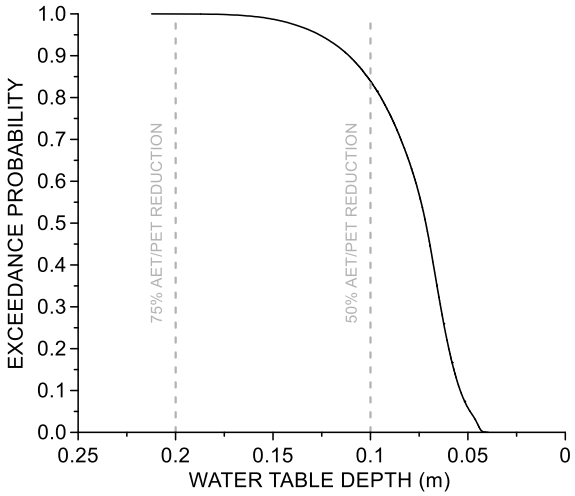

Figure 5-8. Exceedance probability of daily spatially-averaged water tables (across the entire fen) based on the Monte Carlo simulations. This water table variability is placed in the context of the reduction in AET/PET ratio with increased water table depth (as described in Figure 5-2).

5.4.3 Projected solute transport

Although the ensemble mean solute export indicated that 50% of the total sodium mass would be eluted within 15 years post-construction, the timeline associated with solute export varied greatly between realizations (Figure 5-9). The discrepancy between the 5th and 95th percentile associated with the export of 50% of total sodium mass spanned 12 years. For any given time period, the difference between the 5th and 95th percentile was, on average, 26% of total sodium mass (7,900 kg), however, these realizations appeared to be slowly converging over time. Based on the ensemble mean, by the end of the Monte Carlo simulation period, 37 years post-construction, 78% of the total sodium mass had been removed from the system. Extrapolating the export trajectory of the remaining sodium mass would suggest that the system will continue to elute appreciable, albeit diminishing, quantities of salt for several further decades.

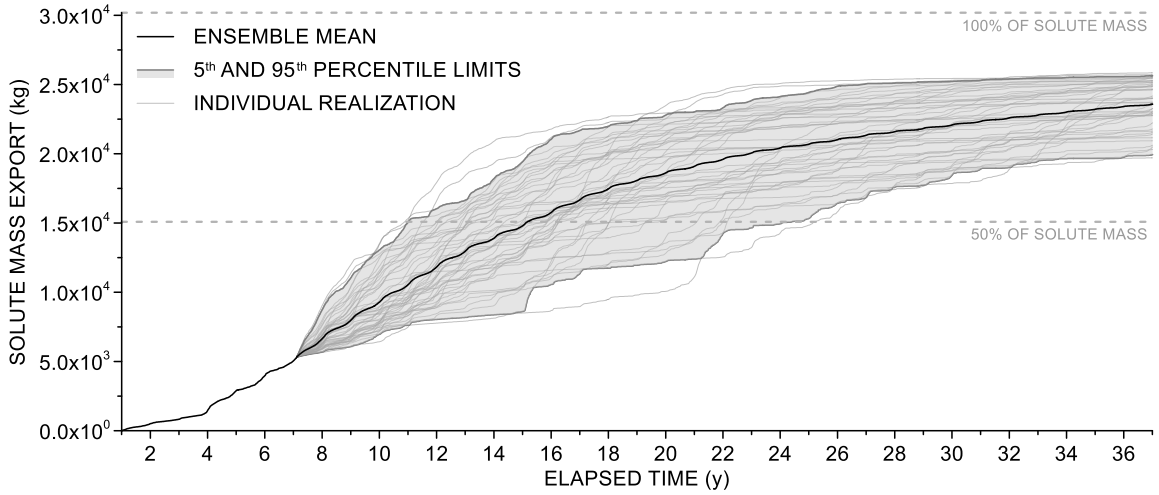

Figure 5-9. Projections of sodium mass export from the watershed. Between 1 and 6 years post-construction represents the calibration and validation period of the model. Monte Carlo simulations begin 7 years post-construction (2020), and indicate that 50% of solute mass will be removed by 15 years post-construction.

The ensemble mean fen surface concentration continued to rise until 12 years post-construction, stabilized for 4-years at approximately 600 mg L^{-1}, and subsequently began to noticeably, albeit slowly, decline (Figure 5-10). The time to reach peak surface concentration varied between realizations, with the 5th and 95th percentile occurring at 8 and 20 years, respectively. Realizations that had a prolonged rise in solute surface concentration also had higher surface concentrations. The 5th and 95th percentile simulations corresponded to peak surface concentration of 450 and 900 mg L^{-1}. Within individual years, there was a cyclical trend in fen surface concentration that coincided with the seasonal patterns of evapotranspiration, resulting in a maximum seasonal concentration in the middle of the summer. By the end of the Monte Carlo

simulation period (year 37) the ensemble mean surface concentration had decreased to 240 mg L^{-1}. However, among all realizations there was substantial spatial variability in surface concentration across the fen (Figure 5-11). Initially, concentrations across the surface of the fen were uniformly low (<100 mg L^{-1}), however over the following 5 years salinity began to increase, particularly in localized areas along the interface between fen and transition zone, and in the southeastern corner. The propagation of this pulse of sodium from southeast to northwest is expected to continue until 12 years post-construction, at which point, the entire fen surface would have sodium levels greater than the initial pore-water concentrations of the tailings sand. Subsequently, the fen experienced surface flushing, commencing at the transition zone and southeast corner, and continuing in a northwesterly direction for an additional 26 years. However, despite the fact that areas of the fen adjacent to the upland were beginning to flush by 12 years post-construction, the peak sodium concentration would continue to climb for a further decade, by which point (on average) 20% of the fen had surface concentrations greater than 1000 mg L^{-1}. The final year in the Monte Carlo simulation period saw high concentrations persist in the northwestern corner; approximately 40% of the fen had surface concentrations greater than 300 mg L^{-1}. However, the proportion of the fen surface with concentrations in excess of 1000 mg L^{-1} had decreased markedly and could only be found in isolated areas along the periphery of the fen. High salinity at the surface of the fen occurred as an increasingly thin veneer, which caused a steep geochemical gradient with depth (data not shown).

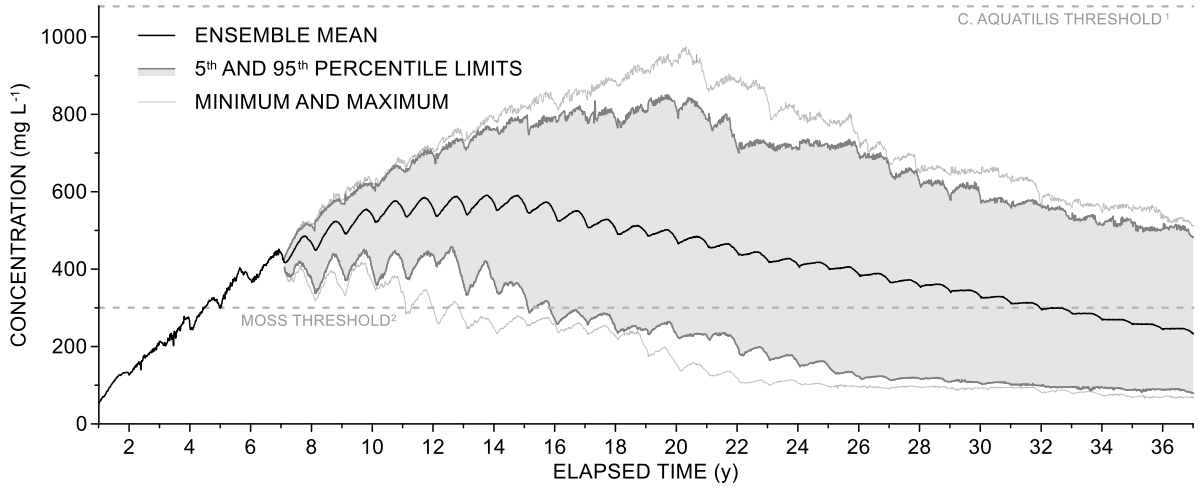

Figure 5-10. Spatially-averaged surface concentration across the fen. The average surface concentration is contextualized by the salinity-stress thresholds identified by Vitt et al (2020)[1], and Pouliot et al (2013)[2] for *C. aquatilis* and mosses (*B. pseudotriquetrum*, *T. nitens*), respectively.

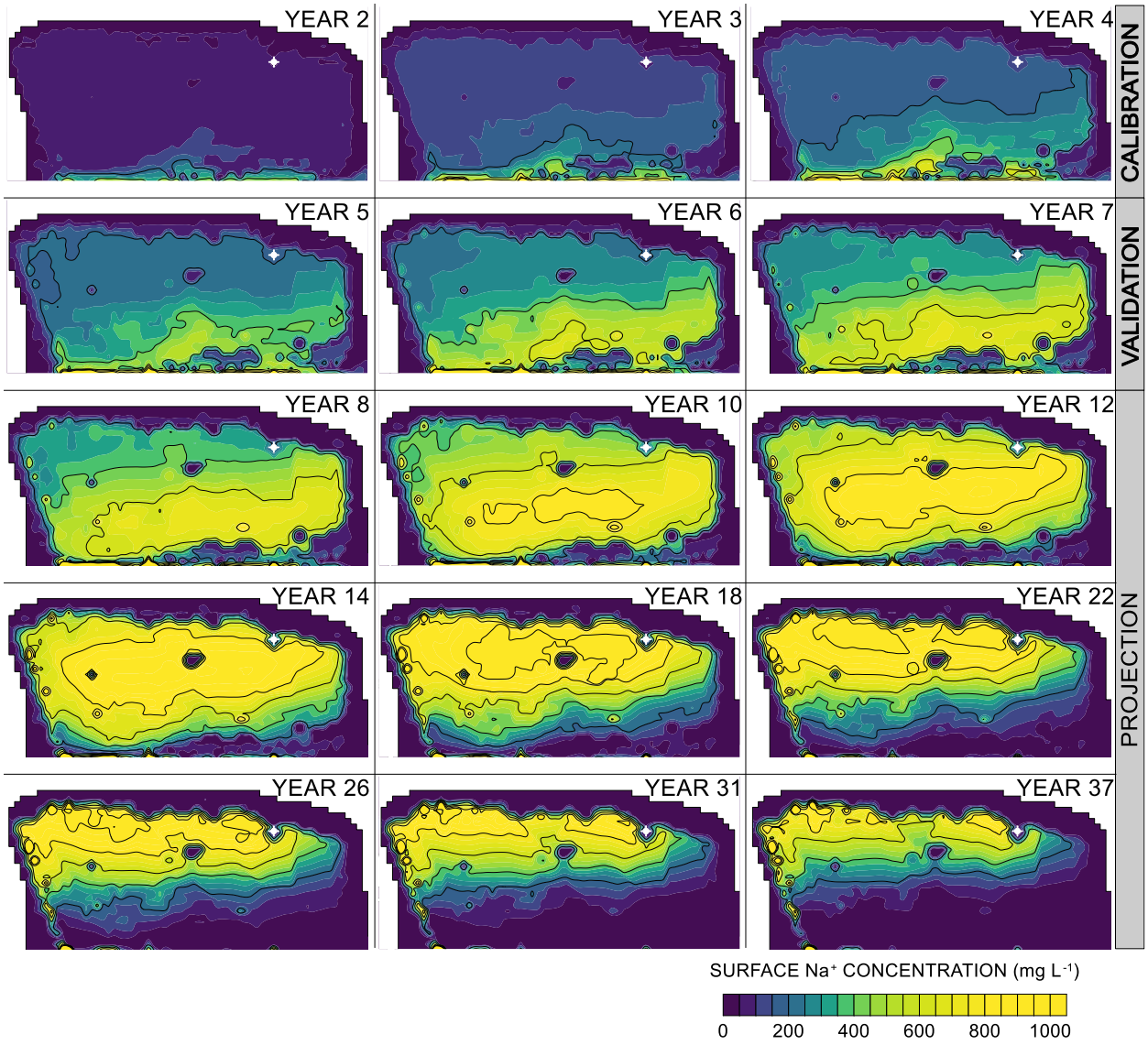

Figure 5-11. Maps illustrating the rise and fall of ensemble mean surface sodium concentration (0 - 0.2 m bgs) across the fen. Site discharge is identified with a white cross symbol.

Surface water discharge concentrations, which integrated the salinity of both seepage and episodic outflow water, exhibited similar inter-annual patterns as average fen surface concentration (Figure 5-12). However, the peak concentration in discharge occurred earlier, after only 7-years post-construction. Intra-annual variability was typically much greater and exhibited the opposite seasonal trends in concentration relative to surface concentration, whereby the discharge concentration was highest during spring freshet, and lowest in the middle of the summer. During atypically dry realizations, the outflow sodium concentration could exceed the initial source concentration in the tailings sand by a factor of 2. The

ensemble mean indicated that by 25-years post-construction, the sodium concentration of the discharge water would generally decrease below the background levels found in the donor peat deposit immediately following construction. (50 mg L^{-1}), although this could be exceeded during snowmelt.

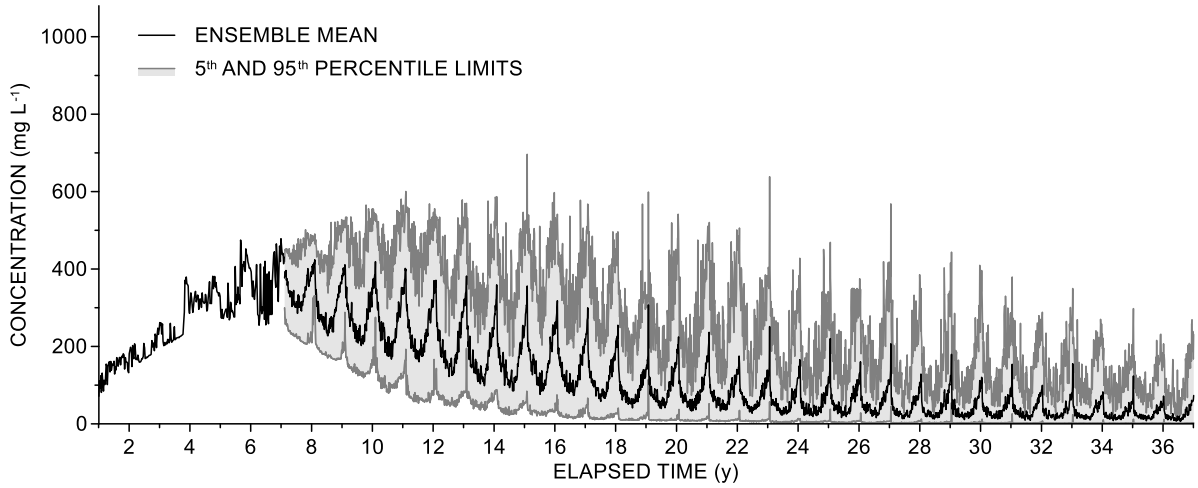

Figure 5-12. Sodium concentration of the discharge water from the fen. Surface water discharge concentrations peak in the spring and fall, and are lowest in the summer due to dilution from relatively fresh seepage. The initial Na^+ concentration of the tailings sand aquifer was 350 mg L^{-1}, in rare circumstances this concentration can be exceeded by a factor of 2 in the outflow water.

The projected timeline associated with sodium flushing (<10 mg L^{-1}) from the upland varied depending on location (Figure 5-13). Distal areas of the upland – adjacent to the interface between hillslopes and upland – flushed within the first two years post-construction, while the centre of the upland and transition zone took between 10-18 years to flush. Flushing times were reduced in close proximity to recharge basins, particularly the east and southeast basins, which received additional infiltration from hillslope runoff. Portions of the fen that were topographically elevated maintained consistently low sodium surface concentrations compared to the surrounding area. In the most extreme cases, these topographically elevated locations had sodium flushing times that preceded the adjacent fen by over a decade. As was indicated by the solute export data, by the end of the Monte Carlo simulation period high salinity endured across large areas of the fen and would likely take further decades to flush.

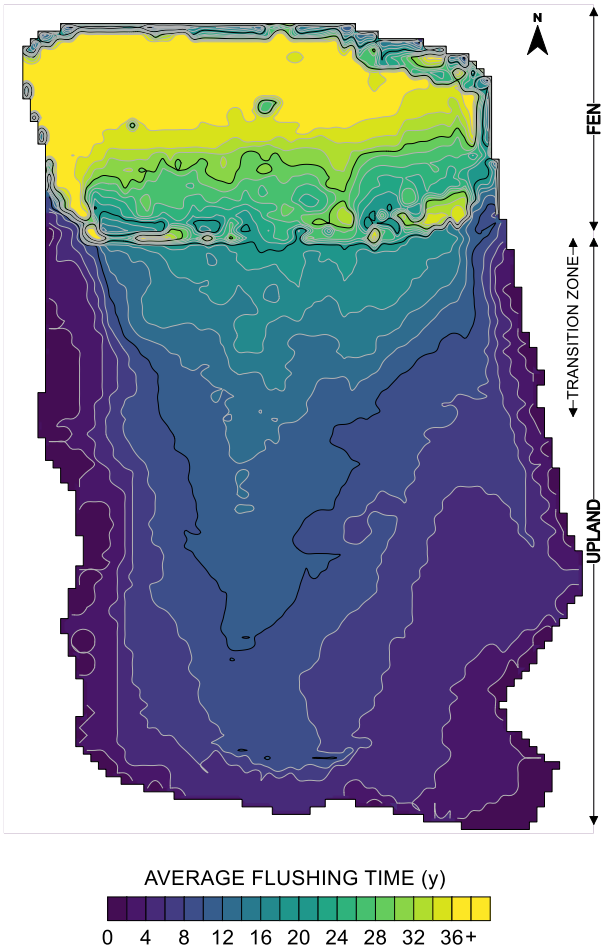

Figure 5-13. Ensemble mean elapsed time for the vertically-integrated simulated sodium concentrations to decrease below 10 mg L^{-1} (which, for the purposes of this discussion is interpreted as "flushed").

5.5 Discussion

5.5.1 Model adequacy

Validation of the model between 2017-2019 demonstrate the suitability of the conceptual model, its implementation within the modelling environment, and the parameterization of the model; this suggests it is appropriate to apply the model to projections of solute fate and transport (Figures 5-4, 5-5, and 5-6). The purpose-built nature of the site as a research watershed greatly reduced many of the sources of uncertainty that typically afflict field-scale groundwater flow models. In particular, the delineation of subsurface topography during construction all but eliminated stratigraphic uncertainty, and the incorporation of a low-permeability geosynthetic clay liner greatly simplified the model boundary conditions. Furthermore, the

long history of monitoring and site investigations conducted by other researchers into the hydrometeorological function of the Nikanotee Fen Watershed (Ketcheson and Price, 2016a; Ketcheson and Price, 2016b; Ketcheson et al., 2017; Scarlett et al., 2017; Kessel et al., 2018; Chapter 3), and hydraulic and geochemical properties of construction materials (Nwaishi et al., 2015; Simhayov et al., 2017; Simhayov et al., 2018; Scarlett and Price, 2019; Chapter 2) substantially reduced parameter uncertainty. However, in spite of these supporting studies, a variety of simplifications and abstractions in the modelling environment introduced parameter and model structure uncertainty (see below), and likely contributed to model error (Appendix B). Furthermore, it should be noted that uncertainty in these supporting studies is propagated through the work discussed presently. Perhaps of greatest consequence is the uncertainty associated with the spatiotemporal patterns and statistical properties of upland groundwater recharge, which was informed by previous modelling (Chapter 2; 3).

5.5.2 Sensitivity to recharge

Parameter optimization gave an indication of model sensitivity to hydraulic conductivity and specific yield. However, groundwater flow and transport at the site is driven exclusively by recharge, and therefore it was necessary to quantify the impact of uncertainty and potential error associated with recharge on the hydrology and salinity of the fen. The sensitivity analysis demonstrated varying groundwater recharge resulted in a commensurate deviation in surface water discharge (Figure 5-14a). In contrast, both actual evapotranspiration and groundwater inflow to the fen (Figure 5-14b,c) had a muted response to deviations in groundwater recharge. This response illustrates the value of the upland aquifer, which ameliorates the impact of atypically wet or dry periods on the fen. The moderating influence of the upland aquifer on groundwater inflow to the fen is apparent in the sensitivity of water table depth to groundwater recharge (Figure 5-14d), which was more stable as a consequence. The least sensitive environmental variable to groundwater recharge was the average surface concentration of the fen (Figure 5-14e), due to the relationship between recharge, actual evapotranspiration, and groundwater inflow to the fen. Specifically, higher actual evapotranspiration diminished the impact of dilution by enhancing evapoconcentration of solutes at the surface, and higher groundwater inflow replenished sodium mass lost by surface water discharge. In contrast, cumulative annual solute export (Figure 5-14f) was the sole variable for which changes in recharge amplified variability. This was a result of both higher surface water discharge proportionally increasing sodium mass export and higher water tables mobilizing salts from isolated areas of the fen that produced discharge infrequently.

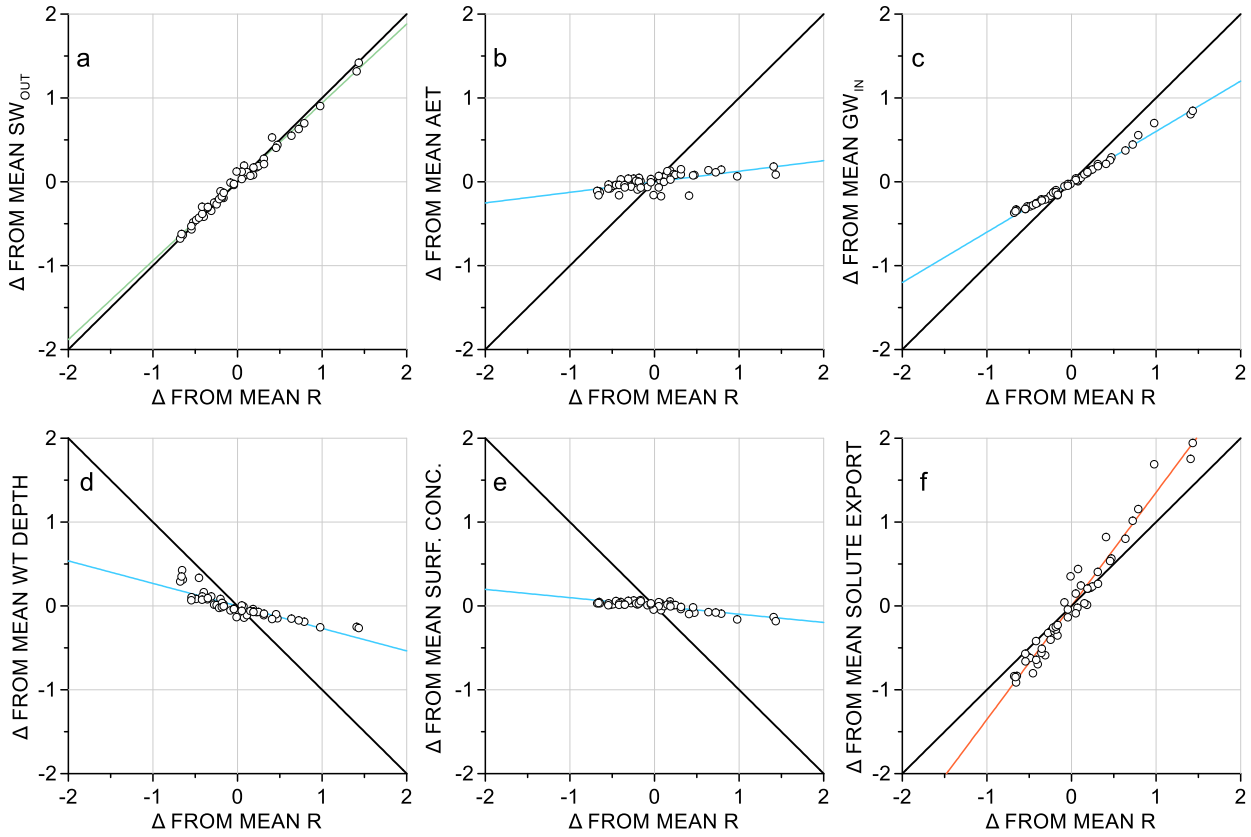

Figure 5-14. Sensitivity analysis of the impact of varying groundwater recharge (R) on (a) modelled surface water discharge, (b) actual evapotranspiration, (c) groundwater inflow to the fen, (d) average fen water table depth, (e) average fen surface concentration, (f) and solute export. All values are shown as fractional deviation from the mean. Relationships with a slope >1 indicate variables with amplified sensitivity to recharge, slope <1 indicate variables with dampened sensitivity to recharge. Variability about the line of best-fit was due to differing potential evapotranspiration and temporal patterns of recharge delivery.

5.5.3 Sources of uncertainty

Given that the model simulations are on a timescale of decades, the assumption of temporal stationarity of model boundaries and parameters should be critically evaluated. Over the coming decades climate change is projected to increase air temperature and rainfall in the AOSR, resulting in increases to both actual evapotranspiration and the net percolation released from near-surface soils (Alam et al., 2018). Increased groundwater recharge would accelerate salt flushing from the upland into the fen. However, additionally, warmer winter temperatures (Alam et al., 2018) would likely delay the onset of ground frost in the fall and advance the spring thaw earlier in the year, resulting in a longer period that groundwater flow and solute

transport could occur. Ultimately, these changes to the Nikanotee Fen Watershed would result in more rapid flushing of salts from the upland to the fen, and therefore a steeper rise in surface concentrations.

A high degree of geochemical heterogeneity was assumed to exist in the tailings sand, and to a lesser degree, petroleum coke, and peat. However, it was expected that this spatial concentration variability manifest at scales smaller than the sampling network could resolve. Therefore, due to inadequacies of the sampling network, and the absence of knowledge on the covariance structure of sodium concentrations in the tailings sand, the specified initial sodium distribution was assumed to be homogeneous within each construction material. This unrepresented initial geochemical heterogeneity was partly responsible for the error between observed and simulated sodium concentrations. Nonetheless, the spatial and temporal patterns of sodium transport appear to be well represented by the model (Figure 5-6). Furthermore, high-resolution temporal sampling of surface water discharge sodium concentrations in 2019 allowed for an estimate in sodium mass export from the system. The estimated mass export between June 3 and August 13, 2019 was 261 kg (S. Yang, personal communication), while the simulated mass export during the same time period was 284 kg, a difference of less than 10%. Since the discharge concentration integrates spatial variability of surface and pore-water salinity, the close agreement between field-estimated and simulated mass export is a favourable indication that the model faithfully reproduces the dominant transport processes.

Although water loss from the fen was typically dominated by surface water discharge (Figure 5-7), any changes to the structure of the peat that alter the relationship between water table depth and evapotranspiration could have a substantial impact on the projected hydrology and geochemistry of the site. Physical changes to the peat structure due to decomposition (Scarlett et al., 2019), or litter accumulation at the surface (Scarlett et al., 2017) could enhance, or further limit evapotranspiration. In particular, *C. aquatilis*, the dominant vascular plant in the Nikanotee Fen, tends to produce dense litter (Borkenhagen and Cooper, 2019), which suppresses evapotranspiration by decreasing surface temperature and the near-surface vapour-pressure deficit (Scarlett et al., 2017). Over the relatively short monitoring period since reclamation, the fen has undergone shifts in the composition of the vegetation community, resulting in the proliferation of *C. aquatilis*, likely instigated by the onset of rising near-surface salinity (Borkenhagen and Cooper, 2019). This shift, and the consequent suppression of evapotranspiration by plant mulch, could be responsible for the apparent change in the evapotranspiration extinction depth that occurred following the first three years post-construction (Figure 5-2). Should the relationship between water table depth and evapotranspiration continue to change in the future, the water balance of the fen would subsequently be altered, as would the timeline associated with solute export and the projected peak surface concentrations.

This interaction is difficult to predict, and constitutes a meaningful source of uncertainty. It is also important to note that the relationship derived between water table depth and evapotranspiration (Figure 5-2) would be inappropriate to apply to a site or scenario that experiences a greater range of water table fluctuation, or substantially deeper average position of the water table. It is speculated that the steep reduction in actual evapotranspiration disproportionately impacted the soil evaporation component of the total AET flux, with the transpiration component remaining relatively unaffected. Since the water table remained close to the surface throughout the monitoring period, there were no data to inform the relationship between water table and evapotranspiration at depths that might limit root water uptake. Therefore, at projected water table depths below approximately 0.20 m the simulated evapotranspiration flux should be viewed with reservation. However, the projected spatially-averaged water table had less than a 1% probability to fall below this threshold (Figure 5-8).

5.5.4 Projected hydrology

Considering the wide range in meteorological forcing applied in the Monte Carlo simulations, it can be stated with confidence that the fen water table will remain stable and within close proximity to the surface over the coming decades. The position of the water table close to the surface, and small range of fluctuation, was maintained by the threshold-like behaviour of the surface water discharge control structure and the negative feedback between water table depth and evapotranspiration. Microtopography, and the near-planar water table, caused persistent inundation of low-lying areas of the fen. These areas of ponding typically extended across 10% of the fen surface area and acted as evaporative windows, consistent with the findings of Scarlett et al. (2017). Given the range of water table positions (Figure 5-8) and the ratio of actual to potential evapotranspiration, drought stress in vascular vegetation would be exceedingly rare. While this is partly due to the apparent water conservation mechanisms operating in the fen (Figure 5-2), the supply of groundwater from the upland was also crucial to maintaining evapotranspiration, particularly during dry years. This challenges the assertion that the conceptual model of groundwater flow from forested uplands to wetlands is inappropriate to apply to landscape reclamation in the AOSR (Hokanson et al., 2020). Whether this conceptual model can be applied ubiquitously to upland-wetland connectivity in the AOSR, is not clear. Nor is it confirmed that this conceptual model is the most suitable to accomplish reclamation objectives. However, observed hydrological data (Ketcheson et al., 2017), geochemical data (Kessel et al., 2018), and modelling unequivocally upholds that the Nikanotee Fen Watershed functions in a manner consistent with this theory. Moreover, the system appears to possess the necessary hydrologic characteristics to promote and sustain peatland function.

5.5.5 Patterns of salinity and flushing

Spatial patterns of surface salinity were predominantly influenced by proximity to the upland and transition zone (Figure 5-11). Although the petroleum coke was largely successful in channeling groundwater flow underneath the fen and upwards through the peat profile, some flow did occur from the tailings sand directly to the surface of the fen. This was apparent in both observed and simulated data, whereby the emergence of above-background sodium first occurred at the interface between fen and transition zone. Originally illustrated in Ketcheson et al. (2017), groundwater flow from upland to fen occurred in a nested pattern reminiscent of the systems described by Tóth (1963). Groundwater that converged into the petroleum coke from the transition zone had far shorter flow paths, and therefore arrived at the fen surface earlier. In contrast, groundwater from the distal areas of the upland travelled along the entire length of both the upland aquifer and the petroleum coke underdrain, before emerging closer to the northern boundary of the fen. Although this delayed the arrival of process-affected water from the tailings sand, evapoconcentration of salts already present in the peat caused a four-fold increase in surface concentration across the northern portion of the fen after only 5 years post-construction.

Crucially, even under atypically dry climate realizations, the peak projected surface concentration will remain far below the level found in naturally occurring saline fens in the region, which can be in excess of 13,000 mg L^{-1} (Wells and Price, 2015). Therefore, these natural saline systems may not be the most appropriate analogues for the relatively short period in the evolution of the constructed fen characterized by rising surface salinity. Yet, spanning many decades, sodium concentrations of the constructed system will remain markedly higher than that of regionally-characteristic moderate-rich fens (e.g. Elmes and Price, 2019).

The timing of sodium flushing across the upland was determined by the magnitude of groundwater recharge and the total vertically-integrated sodium mass, which was directly related to the thickness of the tailings sand aquifer. The unsaturated zone of the upland was largely flushed by the end of 7 years post-construction. This was a consequence of the magnitude of early-time groundwater recharge and the low specific retention of the tailings sand. While the geometry of the aquifer is generally symmetric about the north-south axis of the system, the influence of the east and southeast hillslopes and the adjacent recharge basins, resulted in a large discrepancy in groundwater recharge between the east and west upland. In the early post-construction period, large volumes of infiltrated surface water runoff from the hillslopes caused faster flushing of sodium and higher hydraulic gradients. This pattern was also identified in the first few years post-construction by Kessel et al. (2018). The increased groundwater flux along the eastern boundary

of the upland was also responsible for the earlier arrival of sodium at the surface of the fen, and consequently partially caused the more rapid elution of sodium from the southeast corner. Proximity to the fen outflow also appeared to be an important determinant of flushing time in the fen. Seepage through the discharge control structure induced a lateral head gradient that resulted in groundwater flow converging towards the discharge location. Areas of the fen in close proximity to the site discharge location experienced a greater lateral flux of groundwater, and therefore earlier flushing.

5.5.6 Implications for vegetation development

Recent research has investigated the impact of salinity in oil sands process-affected water (OSPW) on several regionally abundant boreal wetland vascular plants and mosses, including species targeted in the Nikanotee Fen. While generally averse to high salinity, some moss species, including *Bryum pseudotriquetrum*, and *Tomenthypnum nitens*, exhibit tolerance to the sodium concentrations typically found in OSPW (Pouliot et al., 2013). However, a threshold of 300 mg L^{-1} of sodium was found to impede the growth of *B. pseudotriquetrum*, and *T. nitens* (Pouliot et al., 2013). Similarly, a sodium stress threshold for *C. aquatilis* was identified between 1079 mg L^{-1} and 2354 mg L^{-1} by Vitt et al. (2020). This work demonstrated that *C. aquatilis* exhibited tolerance to a wide range in salinity, seemingly through regulatory mechanisms that limit the movement of sodium within the plant from roots upwards to the stems and leaves (Vitt et al., 2020). Although not experimentally confirmed in the same manner as *C. aquatilis*, *J. balticus* is anticipated to exhibit similar tolerance to high sodium concentrations, as it can be found in saline wetlands across the boreal region (Purdy et al., 2005).

Assuming the most conservative threshold of 1079 mg L^{-1}, the average fen surface concentration was never projected to exceed the level that would instigate the onset of salinity stress in *C. aquatilis*, even when subject to the Monte Carlo realizations with the driest conditions and therefore highest surface concentrations (Figure 5-10). Yet, as a consequence of spatial variability in surface salinity, projections indicate that the conservative threshold for *C. aquatilis* stress would be exceeded in limited areas of the fen (Figure 5-11), and under particularly dry climate realizations, across most of the fen surface. Due to a combination of evapoconcentration and the strong upward hydraulic gradients, high salinity would occur directly at the surface, but pore-water salinity at depths of 0.2 m and greater would be considerably lower (data not shown). Given that the rooting depths of *C. aquatilis* extended to 0.6 m below ground surface (Murray et al., 2017), water absorption by the roots would integrate pore-water concentrations, thus decreasing the concentration of the uptake water. Ultimately, due to both the projected salinization and typical range of water table fluctuation, which rarely varied greater than the optimal condition of 0.2 m

from ground surface (Koropchak, et al. 2012), the fen will likely remain amenable to the growth of *C. aquatilis* throughout the coming decades.

In contrast, the average fen surface concentration increased beyond the threshold associated with moss salinity stress (Pouliot et al., 2013) after only 4 years post-construction (Figure 5-10). Vegetation surveys at the Nikanotee Fen showed that moss cover declined after 3-4 years post-construction (Borkenhagen and Cooper, 2019), providing corroboration of the simulated surface concentration and its implications on moss stress. The ensemble mean fen surface concentration strongly suggests that water chemistry will be inhospitable to moss growth across the majority of the fen for approximately three decades post-construction. However, spatial variability in surface concentration due to microtopography may allow for isolated areas of the fen to act as refugia for mosses. Furthermore, given the gradient of flushing times across the fen, some areas of the fen will have prevailing sodium concentrations amenable to moss growth far earlier than others (Figure 5-13). However, it is unknown whether the advent of lower pore-water concentrations will allow mosses to compete with vascular species subsequent to their assumed long period of proliferation and establishment. Following the elution of sodium from the system, and the associated decreases in surface salinity, the high water tables maintained in the fen may be a persistent barrier to wide-spread moss establishment (Borkenhagen and Cooper, 2019). Consequently, the growth of mosses could be restricted to topographically elevated areas of the fen, or the vegetation community could be steered towards moss species tolerant of frequent inundation.

While this work has solely focused on sodium contamination, which is anticipated to be of principal concern to the development of fen vegetation, other solutes were present at elevated concentrations in the process-affected construction materials. These solutes include calcium, magnesium, sulfate, and chloride (Kessel et al., 2018). In some cases, the presence of calcium could be advantageous to plants, as there is research to suggest high calcium concentrations can reduce plant stress in soils with high sodium concentrations; conversely, calcium may have a detrimental impact on some mosses (Clymo, 1973). Patterns of groundwater transport from upland to fen of other major ions would generally be consistent with the spatial patterns of sodium, however sulfate, in particular, experiences more complex biogeochemical cycling in peatlands (Wieder et al., 1990). Regardless, rising sodium concentration in the fen will be accompanied by increases in concentration of other ions abundant in tailings sand.

5.5.7 Landscape reclamation and reclamation design

Exclusively from a water quantity perspective, the modelling suggests that the area of upland relative to the fen could be substantially reduced without adverse consequences to the hydrology of the system. This

would allow future watersheds to more closely reflect the proportions of the undisturbed landscape of the AOSR. While the water table would undoubtedly experience a greater range of fluctuation and average annual depth, this would not place it outside the normal range of conditions for natural systems. Studies conducted at several nearby reference fens, including a poor fen (Wells et al., 2017), moderate-rich fen (Elmes and Price, 2019), and saline fen (Wells and Price, 2015), had water tables that varied 0.70 m, 0.77 m, and 0.65 m, respectively. However, any alterations to the design of the system that have consequences for surface water discharge need to be assessed within the context of solute export and surface salinization. Since surface water discharge is the only pathway for solute removal from the watershed, reductions in outflow would decrease sodium mass export and increase near-surface salinity (Figure 5-14e,f). However, given that elevated salinity will be a temporary concern this may be a compromise worthy of consideration.

Conversely, the large water surplus from the system which manifest as surface water discharge, could be regarded as water available for downgradient ecosystems. Linking constructed watersheds hydrologically in a cascading manner could offer more flexibility in the proportions and morphology of future systems. However, the timing of construction and the techniques employed to connect these watersheds would need to be employed carefully to avoid amplifying salinity down the topographic (and hydraulic) gradient. Furthermore, while it may be possible for sodium transport in the reclaimed landscape to be choreographed to minimize the potential for stress-inducing salinization, ultimately a downgradient receptor must receive and manage the sodium discharged from process-affected materials. For a time, the salinity of this surface water discharge (Figure 5-12) will likely be greater than the initial concentration of the tailings sand (350 mg L^{-1}).

Peat is anticipated to be a limiting resource in landscape-scale reclamation, and as such must be used parsimoniously. The Nikanotee Fen incorporated a peat thickness greater than both many undisturbed reference systems and what could realistically be expected for constructed peatlands in the post-mined landscape (Daly et al., 2012). Including a relatively thick layer of peat was intended to delay the arrival of solutes at the surface by increasing the adsorptive capacity, thereby lengthening the period for vegetation to establish (Daly et al., 2012). Furthermore, the petroleum coke was designed to direct groundwater upwards through the peat profile, which would fully exploit the capability of peat to retard solute transport. Although care was taken during construction to ensure materials were placed in accordance with the design, the reality of using heavy earth-moving equipment introduced deviations in the surface and subsurface topography of peat and petroleum coke in the fen. These deviations conspired to cause a range of peat thicknesses from 1.2 to 2.2 m. Since there was no apparent correlation between peat thickness and the

timing or magnitude of salinization at the surface of the fen, this suggests that future systems could reduce peat thickness without dramatically altering the patterns of surface salinity. In contrast, the introduction of microtopography appeared to have a pronounced impact on surface salinity, which could be adopted in reclamation design to increase the diversity of vegetation habitats and accelerate the mobilization of salts from remote or stagnant areas of the peatland. Forthcoming research on the Nikanotee Fen following the placement of a raised peat plateau in the northwestern corner of the fen will provide valuable insight into the use of microtopography to modify the hydrochemistry of reclaimed systems.

5.6 Conclusion

Hydrochemical numerical modelling at the Nikanotee Fen Watershed strongly suggest that the system will continue to support a stable water table in the peatland that would fluctuate close to the surface, and be capable of meeting the majority of evaporative demand. Due to consistent groundwater flow from the upland aquifer and internal water conservation mechanisms, the fen will be exceptionally resilient to climatic stress. However, sodium mass export and surface concentrations in the fen can be expected to vary widely as a consequence of the prevailing and preceding climatic conditions. The most probable scenario would suggest sodium concentrations in the near-surface of the fen would continue to rise for approximately 15 years post-construction. However, as a result of considerable climatic variability of the region, average surface concentrations could rise for as few as 9 years, or as many as 20 years if the post-construction period climate is atypically wet or dry, respectively. This climatic variability also influenced the peak spatially-averaged sodium concentration of the fen, which varied between 450 and 850 mg L^{-1}, with an ensemble mean of 600 mg L^{-1}. Sodium elution from the upland, is projected to occur comparatively rapidly, with the more distal and peripheral areas of the upland flushing in the first 4-6 years, the central upland flushing in 8-12 years, and the fen flushing over much longer time periods (>40 years). Spatial variability in groundwater recharge in the upland, and proximity to the discharge point in the fen, resulted in clear east-west differences at the site. Large volumes of surface overland flow contributed by the hillslopes to the southeast corner of the upland resulted in considerably faster salt flushing. Similarly, the location of the spillbox in the eastern portion of the fen caused a salinity gradient, with the northwest corner maintaining much higher salinity for a longer period of time.

The Nikanotee Fen Watershed was designed and built for the express purpose of developing research and operational knowledge on fen construction, however the underlying ambition of this project was for the system to be self-sustaining, have the requisite conditions for carbon accumulation, and support a variety of ecological habitats for regionally abundant fen vegetation species. This modelling suggests that

the Nikanotee Fen will continue to be self-supporting and maintain the hydrological and geochemical conditions that encourage carbon accumulation and vegetation growth. While the projected salinity in the near-surface of the fen would likely limit the proliferation of mosses for decades post-construction, this would be a temporary circumstance. Following the elution of sodium from the system, water chemistry is expected to return to a condition favourable for moss growth. In the intervening time period, *C. aquatilis*, *J. balticus*, and other saline tolerant vegetation species could be expected to become well-established across most areas of the fen. While the presence of elevated sodium concentrations in the watershed is indeed temporary, fens of similar design may experience periods of decades, and perhaps longer, where many targeted vegetation species will experience rooting zone salinity that could negatively impact growth and productivity. Whether these systems will return to functional equivalence following the elution of sodium from the system, or if novel functionality will persist, is a matter that requires further investigation.

Ultimately, these projections suggest an optimistic future for the Nikanotee Fen Watershed, and represent a validation of the original design principles and philosophy that guided the creation of the watershed by Price et al. (2010). Nonetheless, this work indicates that design alterations could improve upon aspects of this design. The results suggests that even large increases in the area of the fen relative to the upland would not have a detrimental impact on the hydrology of the fen, specifically the ability of the system to maintain a high water table. This could allow for the proportion of peatlands on the reclamation landscape to more faithfully reflect the pre-disturbance environment. However, such a design alteration could have consequences for surface sodium concentrations due to reductions in surface water discharge. Furthermore, the thickness of peat used in the fen could likely be reduced without dramatic changes to the timing or peak of near-surface salinity. However, modifications to the morphology and layering of the system design should be explored explicitly with further modelling. Testing the sensitivity of the system to altered morphology, dimensions, layering, and deviations in material hydraulic properties will aid in the revision and advancement of future constructed peatland watershed design.

5.7 Acknowledgements

The authors would like to thank B. Gharedaghloo, A. Green, E. Kessel, and J. Sherwood for general advice, data processing, and project management. Funding from the following sources is gratefully acknowledged: the Natural Sciences and Engineering Research Council (NSERC) Canadian Graduate Scholarship (NSERC-CGS) and Collaborative Research and Development Grant (NSERC-CRD; 418557-2011) titled “Evaluating the success of fen creation in the post oil sands landscape” with field support and direct funding from Suncor Energy Inc., Imperial Oil Resources Ltd., Shell Canada Ltd., and Teck Resources Ltd.

Chapter 6: Conclusion

This study was motivated by the pressing need to generate information on the likely trajectory of constructed fen watersheds in order to integrate these systems into the regulatory framework that will shape the configuration of the mine closure landscape. As a novel endeavour, the first experimental designs of these watersheds were based on a simplified conceptual understanding of hydrologic connectivity between uplands and wetlands. In ideal circumstances, all design should be refined in an iterative process of conceptualization, implementation, analysis, and evaluation. However, adopting this process in the context of peatland reclamation is challenging due to the considerable investment in resources required to perform such trial and error, and the length of time necessary to obtain compelling evidence regarding the efficacy of the design. The initial conceptualization of the Nikanotee Fen Watershed was aided by a simplified numerical model, which tested a variety of morphological attributes and material properties to identify a design that could plausibly create and sustain the hydrological conditions that would promote fen ecohydrological function. The implementation of this design on a portion of the post-mined landscape closely adhered to the previously identified specifications associated with system morphology and material hydraulic properties. Although limitations on available resources with appropriate hydraulic characteristics necessitated the inclusion of waste materials that were impacted by the oil sands extraction process, this was ultimately beneficial as it offered insight into the conditions that could be expected if peatland reclamation is realized on an industrial-scale. Beginning in the first-year post-construction and continuing to present, monitoring of the hydrology, geochemistry, ecology, and micrometeorology at the Nikanotee Fen Watershed witnessed it transition from a dry and barren landscape into a burgeoning ecosystem. Early assessments concluded that the system was operating as intended, and successfully replicating many of the ecohydrological functions of the undisturbed peatlands that inspired its design. Yet the relatively short monitoring period offered a limited perspective on the impact of climatic variability, and is only beginning to illustrate the repercussions of rising surface salinity introduced as a consequence of using process-affected materials. This study represents the first attempt to project the hydrochemical trajectory of a constructed fen watershed into the future, thus completing the first cycle in the development of peatland reclamation design. Informed by the hydrological, geochemical, and meteorological data collected in the field and laboratory, a series of models that represented the processes associated with soil moisture dynamics, groundwater flow, and solute transport were used to elucidate the evolving hydrologic response of the system as the site matures.

In the early post-construction period, the LFH cover soil across the upland experienced rapid and marked change in hydraulic properties, including increased saturated hydraulic conductivity, decreased air-entry pressure, and a broadening of the pore-size distribution. These changes weakened the capillary barrier established between the LFH and tailings sand. This weakening altered the partitioning of soil moisture between evaporation and groundwater recharge, and ultimately allowed a greater proportion of soil moisture to percolate across the interface between the two materials. Over longer timescales, vegetation growth in the upland can be expected to markedly reduce groundwater recharge, predominantly as a consequence of root water uptake exploiting previously inaccessible soil moisture above the capillary barrier. However, prior to the wide-spread establishment of vegetation, the dynamic evolution of soil hydraulic properties will enhance groundwater recharge and expedite the saturation of the aquifer. Spatial patterns of forest growth across the upland will be intrinsically linked to the arrangement and properties of the cover soil; simulations suggest that thicker covers had greater available water holding capacity, and thus would be capable of supporting the development of denser vegetation. Given the anticipated balance between productivity and water stress, the upland is expected to reach a somewhat lower vegetation density than many boreal forest stands. Following the development of a climax vegetation community, snowmelt will be the primary contributor to upland groundwater recharge. As a consequence of the specific soil moisture dynamics of the cover system, simulations indicate that snowmelt has a particularly short residence time in the rooting zone of upland vegetation, and was commonly lost by soil evaporation and deeper percolation prior to the onset of the peak growing season. Since the rooting zone is also entirely disconnected from the local water table, this means that uplands of similar design to the Nikanotee Fen Watershed have no mechanism to enhance resilience to interannual water deficits – in contrast to uplands in the undisturbed landscape. Groundwater recharge will progressively flush salt from the tailings sand aquifer, however the timeline associated with this elution will depend on location. This variability in flushing will predominantly arise due to proximity to boundaries and basins, thickness of the aquifer, and spatial patterns of recharge, as opposed to heterogeneity in the hydraulic conductivity field of the upland aquifer. Solute transport modelling shows that the following decades will manifest rising near-surface salinity in the fen. Although the specific temporal patterns and magnitude of sodium concentrations will be intimately tied to the prevailing climatic conditions, evapoconcentration can be expected to increase salinity above the tolerance of many mosses. However, the processes of surface water discharge and freshwater dilution will counteract this, thereby mitigating rooting zone salinity, and maintaining conditions amenable to vascular vegetation with moderate salt-tolerance.

The emerging knowledge on the function of fen watersheds gained from the pilot projects in the AOSR has already generated some clear recommendations to improve the performance during the initial post-construction period. Although this research fundamentally upholds much of the original design, and its specific implementation at the Nikanotee Fen Watershed, a variety of design alterations and operational procedures could enhance the efficiency with which certain reclamation goals are attained. The results of this study strongly suggest future watersheds could accommodate a higher proportion of peatland relative to upland, thereby achieving a ratio that is more representative of the undisturbed landscape, without undue consequences to the hydrology of the fen. Furthermore, by altering the design of the upland, specifically the spatial arrangement and thickness of cover soil, the same recharge could be supplied while also allowing for a higher average vegetation density. The soils salvaged from areas of mine expansion are precious resources that must be used strategically, as such, reducing the thickness of the peat deposit would allow for a proportional increase in the maximum possible extent of peatlands on the closure landscape. While this would reduce the adsorptive capacity of the peatland, thereby causing a higher peak and more rapid rise in surface salinity, this appears to be a compromise worth making.

It is important to acknowledge that the outcome from any modelling exercise is subject to considerable uncertainty and error, which can be compounded during the many stages of model development. Deviations from the actual system behaviour can arise from an unsuitable conceptual framework; error and bias in data collection, aggregation, and interpretation; and abstraction to the numerical environment. These sources of error can have profound repercussions on the conclusions and recommendations drawn from a model, and in this case, could introduce error in the evaluation of fen trajectory. However, this research attempted to contend with these challenges by rigorous verification of model results through comparisons with mutually-supporting observations and measurements from a variety of sources. Fortunately, the extensively instrumented and intensively monitored Nikanotee Fen Watershed provided many opportunities to perform such a validation. Furthermore, many of the conclusions drawn from the modelling were not based on marginal quantities that would be easily swayed by alternative parameterizations. Yet any effort that attempts to project behaviour of a complex system into an uncertain future must confront the fact that a genuine validation cannot be performed, and thus should be viewed critically and within the context of the assumptions and simplifications concomitant with the modelling process.

Ultimately, only patience and diligent monitoring will illuminate the true development of the Nikanotee Fen. Although arguably the most dynamic period of the Nikanotee Fen has concluded – a period

characterized by rapidly evolving soils, the initial establishment of vegetation, and the progressive elution of salts from the aquifer – it has only begun to undergo the slower, but no less consequential, period of rising surface salinity. The interrelated ecological, geochemical, and hydrological processes that will dictate the long-term evolution of the fen cannot be definitively predicted. However, it can be stated with some confidence that the upland will be capable of supporting a forest of similar density to undisturbed reference sites, despite the limited moisture availability, and the fen will remain hospitable to a variety of regionally-abundant vegetation species, despite the elevated salinity. Near-surface sodium concentrations are likely to exceed the stress-thresholds of mosses, limiting establishment across the majority of the fen. Yet, this salinity will abate over the course of several decades as it is steadily removed by surface water discharge, returning the fen to a condition that is amenable to moss growth.

Undoubtedly, the Nikanotee Fen Watershed has provided a remarkable opportunity to study environmental processes at a depth and breadth that has few equals. As a tool to generate research and operational knowledge on fen construction, it has been a resounding success. Moreover, observational and modelling studies conducted at the Nikanotee Fen Watershed suggest it is on a trajectory to accomplish many of the goals associated with system performance identified prior to construction. In particular, maintaining hydrologic conditions in the fen that promote carbon accumulation. However, more can be gleaned from further study of the Nikanotee Fen, and more knowledge will be needed for the science of peatland reclamation to mature from a wholly exploratory to an applied discipline. There remain gaps in our understanding of system design and long-term hydrologic behaviour. The multitude of impacts associated with projected climate change, the complex feedbacks associated with ecology, atmospheric fluxes, and biogeochemical cycling, and the anticipated increase in permeability of the geosynthetic clay liner are all uncertain and have the potential to alter the trajectory of the Nikanotee Fen Watershed. Furthermore, adapting the watershed design to different morphological configurations, and at a scale necessary for industrial implementation needs to be explored in detail.

This research represents a resolution to many of the questions posed regarding the initial tentative experiment into peatland reclamation on the post-mined landscape of the Athabasca Oil Sands Region. Yet, it also heralds the opportunity to update our conceptualization of water movement, assimilate recommendations, and refine the design to augment resilience and improve the efficiency with which these systems can be built on the closure landscape. The insights provided by this study demonstrate that peatland reclamation can succeed, and will aid reclamation practitioners, regulatory decision-makers, and mine operators in their pursuit to return functional wetland attributes to the post-mined landscape.

References

Alam, M. S., Barbour, S. L., Elshorbagy, A., & Huang, M. (2018). The impact of climate change on the water balance of oil sands reclamation covers and natural soil profiles. *Journal of Hydrometeorology*, *19*(11), 1731-1752.

Alberta Environment. 2010. Guidelines for Reclamation to Forest Vegetation in the Athabasca Oil Sands Region, 2nd Edition. Prepared by the Terrestrial Subgroup of the Reclamation Working Group of the Cumulative Environmental Management Association, Fort McMurray, Alberta.

Angers, D. A., & Caron, J. (1998). Plant-induced changes in soil structure: processes and feedbacks. *Biogeochemistry*, 42(1-2), 55-72.

Archer, G. E. B., Saltelli, A., & Sobol, I. M. (1997). Sensitivity measures, ANOVA-like techniques and the use of bootstrap. *Journal of Statistical Computation and Simulation*, 58(2), 99-120.

Aris, R. (1956). On the dispersion of a solute in a fluid flowing through a tube. *Proceedings of the Royal Society of London. Series A. Mathematical and Physical Sciences*, *235*(1200), 67-77.

Baker, R. S., & Hillel, D. (1990). Laboratory tests of a theory of fingering during infiltration into layered soils. *Soil Science Society of America Journal*, 54(1), 20-30.

Barr, A. G., Black, T. A., Hogg, E. H., Kljun, N., Morgenstern, K., & Nesic, Z. (2004). Inter-annual variability in the leaf area index of a boreal aspen-hazelnut forest in relation to net ecosystem production. *Agricultural and forest meteorology*, 126(3-4), 237-255.

Benson, C. H., Abichou, T. H., Olson, M. A., & Bosscher, P. J. (1995). Winter effects on hydraulic conductivity of compacted clay. *Journal of Geotechnical Engineering*, 121(1), 69-79.

Benson, C. H., Sawangsuriya, A., Trzebiatowski, B., & Albright, W. H. (2007). Postconstruction changes in the hydraulic properties of water balance cover soils. *Journal of geotechnical and geoenvironmental engineering*, 133(4), 349-359.

Biagi, K. M., Oswald, C. J., Nicholls, E. M., & Carey, S. K. (2019). Increases in salinity following a shift in hydrologic regime in a constructed wetland watershed in a post-mining oil sands landscape. *Science of the Total Environment*, 653, 1445-1457.

Boerner, R. E., & Forman, R. T. (1975). Salt spray and coastal dune mosses. *Bryologist*, 57-63.

Borkenhagen, A. K., & Cooper, D. J. (2019). Establishing vegetation on a constructed fen in a post-mined landscape in Alberta's oil sands region: A four-year evaluation after species introduction. *Ecological Engineering*, *130*, 11-22.

Bouwer, H., & Rice, R. C. (1976). A slug test for determining hydraulic conductivity of unconfined aquifers with completely or partially penetrating wells. *Water resources research*, *12*(3), 423-428.

Braden, H. (1985). Ein energiehaushalts-und verdunstungsmodell für wasser-und stoffhaushaltsuntersuchungen landwirtschaftlich genutzer einzugsgebiete. Mittelungen Deutsche Bodenkundliche Geselschaft, 42(S), 294-299.

Bradford, K. J., & Hsiao, T. C. (1982). Physiological responses to moderate water stress. In O. L. Lange, P. S. Nobel, C. B. Osmond, & H. Ziegler (Eds.), *Physiologica plant ecology II water relations and carbon assimilation* (pp. 263–324). Berlin, Germany: Springer-Verlag.

Brunetti, G., Šimůnek, J., Turco, M., & Piro, P. (2017). On the use of surrogate-based modeling for the numerical analysis of Low Impact Development techniques. *Journal of Hydrology*, 548, 263-277.

Canadian Association of Petroleum Producers (CAPP). (2018). Canada's oil sands factbook. Calgary, Alberta.

Carey, S. K. (2008). Growing season energy and water exchange from an oil sands overburden reclamation soil cover, Fort McMurray, Alberta, Canada. *Hydrological Processes,* 22(15), 2847-2857.

Caylor, K. K., Scanlon, T. M., & Rodriguez-Iturbe, I. (2009). Ecohydrological optimization of pattern and processes in water-limited ecosystems: A trade-off-based hypothesis. *Water Resources Research*, 45(8).

Chasmer, L., McCaughey, H., Barr, A., Black, A., Shashkov, A., Treitz, P., & Zha, T. (2008). Investigating light-use efficiency across a jack pine chronosequence during dry and wet years. *Tree physiology*, 28(9), 1395-1406.

Chee, W. L., & Vitt, D. H. (1989). The vegetation, surface water chemistry and peat chemistry of moderate-rich fens in central Alberta, Canada. *Wetlands*, *9*(2), 227-261.

Clymo, R. S. (1973). The growth of Sphagnum: some effects of environment. *The Journal of Ecology*, 849-869.

Cumulative Environmental Management Association (CEMA). (2006). Land capability classification system for forest ecosystems in the oil sands. CEMA, Fort McMurray, AB, Canada.

Dagan, G. (1978). A note on packer, slug, and recovery tests in unconfined aquifers. *Water Resources Research*, *14*(5), 929-934.

Dagan, G. (1984). Solute transport in heterogeneous porous formations. *Journal of fluid mechanics*, *145*, 151-177.

Daly, C., Price, J. S., Rezanezhad, F., Pouliot, R., Rochefort, L., Graf, M. D. (2012). Initiatives in oil sand reclamation: considerations for building a fen peatland in postmined oil sands landscape. In D.H. Vitt & J.S. Bhatti (Eds.), *Restoration and Reclamation of Boreal Ecosystems: Attaining Sustainable Development* (179-201). Cambridge: Cambridge University Press.

Devito, K., Creed, I., Gan, T., Mendoza, C., Petrone, R., Silins, U., & Smerdon, B. (2005). A framework for broad-scale classification of hydrologic response units on the Boreal Plain: is topography the last thing to consider?. *Hydrological Processes*, 19(8), 1705-1714.

Devito, K., Mendoza, C., & Qualizza, C. (2012). *Conceptualizing water movement in the Boreal Plains. Implications for watershed reconstruction*. Synthesis report prepared for the Canadian Oil Sands Network for Research and Development, Environmental and Reclamation Research Group.

Doherty, J. (2015). Calibration and uncertainty analysis for complex environmental models. Brisbane, Australia: Watermark Numerical Computing.

Eliassi, M., & Glass, R. J. (2001). On the continuum-scale modeling of gravity-driven fingers in unsaturated porous media: The inadequacy of the Richards equation with standard monotonic constitutive relations and hysteretic equations of state. *Water Resources Research*, 37(8), 2019-2035.

Elmes, M. C., & Price, J. S. (2019). Hydrologic function of a moderate-rich fen watershed in the Athabasca Oil Sands Region of the Western Boreal Plain, northern Alberta. *Journal of Hydrology*, *570*, 692-704.

Elshorbagy, A., Jutla, A., Barbour, L., & Kells, J. (2005). System dynamics approach to assess the sustainability of reclamation of disturbed watersheds. *Canadian Journal of Civil Engineering*, 32(1), 144-158.

Feddes, R. A., Bresler, E., & Neuman, S. P. (1974). Field test of a modified numerical model for water uptake by root systems. *Water Resources Research*, 10(6), 1199-1206.

Freyberg, D. L. (1986). A natural gradient experiment on solute transport in a sand aquifer: 2. Spatial moments and the advection and dispersion of nonreactive tracers. *Water Resources Research*, *22*(13), 2031-2046.

Fung, M. Y., & Macyk, T. M. (2000). Reclamation of oil sands mining areas. In R.I. Barnhisel, R.G. Darmody, & W.L. Daniels (Eds.), *Reclamation of drastically disturbed lands, 2nd ed*. (755–774). Madison, WI: American Society of Agronomy

Gelfan, A. N., Pomeroy, J. W., & Kuchment, L. S. (2004). Modeling forest cover influences on snow accumulation, sublimation, and melt. *Journal of Hydrometeorology*, 5(5), 785-803.

Gelhar, L. W., Welty, C., & Rehfeldt, K. R. (1992). A critical review of data on field-scale dispersion in aquifers. *Water resources research*, *28*(7), 1955-1974.

Glaeser, L. C., Vitt, D. H., & Ebbs, S. (2016). Responses of the wetland grass, Beckmannia syzigachne, to salinity and soil wetness: Consequences for wetland reclamation in the oil sands area of Alberta, Canada. *Ecological Engineering*, *86*, 24-30.

Goetz, J. D., & Price, J. S. (2015). Role of morphological structure and layering of Sphagnum and Tomenthypnum mosses on moss productivity and evaporation rates. *Canadian Journal of Soil Science*, *95*(2), 109-124.

Gosselin, P., Hrudey, S. E., Naeth, M. A., Plourde, A., Therrien, R., Van Der Kraak, G., & Xu, Z. (2010). Environmental and health impacts of Canada's oil sands industry. *Royal Society of Canada, Ottawa, ON*, *10*.

Government of Alberta. (1993). Conservation and reclamation regulation. Alberta regulation: 115/1993. Alberta Queen's Printer, Edmonton, Alberta.

Graf, M., & Rochefort, L. (2009). Examining the peat-accumulating potential of fen vegetation in the context of fen restoration of harvested peatlands. *Ecoscience*, *16*(2), 158-166.

Güven, O., Molz, F. J., & Melville, J. G. (1984). An analysis of dispersion in a stratified aquifer. *Water Resources Research*, *20*(10), 1337-1354.

Havranek, W. M., & Benecke, U. (1978). The influence of soil moisture on water potential, transpiration and photosynthesis of conifer seedlings. *Plant and Soil*, 49(1), 91-103.

Hedstrom, N. R., & Pomeroy, J. W. (1998). Measurements and modelling of snow interception in the boreal forest. *Hydrological Processes*, *12*(10-11), 1611-1625.

Hepler, L. G., & Smith, R. G. (1994). The Alberta oil sands: industrial procedures for extraction and some recent fundamental research, AOSTRA technical publication series 14. Alberta Oil Sands Technology and Research Authority, Edmonton, Alberta.

Hillel, D., & Baker, R. S. (1988). A descriptive theory of fingering during infiltration into layered soils. *Soil Science*, 146(1), 51-56.

Howard, E. A., Gower, S. T., Foley, J. A., & Kucharik, C. J. (2004). Effects of logging on carbon dynamics of a jack pine forest in Saskatchewan, Canada. *Global Change Biology*, 10(8), 1267-1284.

Hokanson, K. J., Peterson, E. S., Devito, K. J., & Mendoza, C. A. (2020). Forestland-peatland hydrologic connectivity in water-limited environments: hydraulic gradients often oppose topography. *Environmental Research Letters*, *15*(3), 034021.

Huyakorn, P. S., Wu, Y. S., & Park, N. S. (1994). An improved sharp-interface model for assessing NAPL contamination and remediation of groundwater systems. *Journal of contaminant hydrology*, *16*(3), 203-234.

Huang, M., Lee Barbour, S., Elshorbagy, A., Zettl, J., & Cheng Si, B. (2011). Water availability and forest growth in coarse-textured soils. *Canadian Journal of Soil Science*, 91(2), 199-210.

Huang, M., Zettl, J. D., Barbour, S. L., Elshorbagy, A., & Si, B. C. (2013). The impact of soil moisture availability on forest growth indices for variably layered coarse-textured soils. *Ecohydrology*, 6(2), 214-227.

Huang, M., Barbour, S. L., & Carey, S. K. (2015). The impact of reclamation cover depth on the performance of reclaimed shale overburden at an oil sands mine in Northern Alberta, Canada. *Hydrological Processes*, 29(12), 2840-2854.

Huang, M., Ireson, A., Barbour, S. L., DeMars, S., & Appels, W. M. (2018). Fully coupled heat and water dynamics modelling of a reclamation cover for oil sands shale overburden. *Journal of Hydrology*, 566, 250-263.

Jarvis, P. G., & Jarvis, M. S. (1963). The water relations of tree seedlings.: IV. Some aspects of the tissue water relations and drought resistance. *Physiologia plantarum*, 16(3), 501-516.

Jarvis, N. J. (2011). Simple physics-based models of compensatory plant water uptake: Concepts and eco-hydrological consequences. *Hydrology and Earth System Sciences*, 15(11), 3431-3446.

Johnson, E. A., & Miyanishi, K. (2008). Creating new landscapes and ecosystems: the Alberta oil sands. *Annals of the New York Academy of Sciences*, 1134(1), 120-145.

Jumikis, A. R. (1977). Thermal Geotechnics, Rutgers University Press, New Brunswick, New Jersey.

Jury, W. A., Wang, Z., & Tuli, A. (2003). A conceptual model of unstable flow in unsaturated soil during redistribution. *Vadose Zone Journal*, 2(1), 61-67.

Kasperski, K. L., & Mikula, R. J. (2011). Waste streams of mined oil sands: characteristics and remediation. *Elements*, *7*(6), 387-392.

Kelln, C., Barbour, L., & Qualizza, C. (2007). Preferential flow in a reclamation cover: hydrological and geochemical response. *Journal of Geotechnical and Geoenvironmental Engineering*, 133(10), 1277-1289.

Kelln, C., Barbour, S. L., & Qualizza, C. (2008). Controls on the spatial distribution of soil moisture and solute transport in a sloping reclamation cover. *Canadian Geotechnical Journal*, 45(3), 351-366.

Kessel, E. D., Ketcheson, S. J., & Price, J. S. (2018). The distribution and migration of sodium from a reclaimed upland to a constructed fen peatland in a post-mined oil sands landscape. *Science of the Total Environment*, 630, 1553-1564.

Kessel, E. D., Sutton, O.F., & Price, J. S. (2019). The use of recharge basins to modify the hydrology of a constructed tailings sand aquifer for oil sands reclamation and its implications on solute flushing. Manuscript submitted for publication.

Ketcheson, S. (2015). Hydrology of a constructed fen watershed in a post-mined landscape in the Athabasca oil sands region, Alberta, Canada (Doctoral Dissertation). University of Waterloo, Ontario, Canada. UW Space http://hdl.handle.net/10012/10175.

Ketcheson, S. J., & Price, J. S. (2016a). Comparison of the hydrological role of two reclaimed slopes of different ages in the Athabasca oil sands region, Alberta, Canada. *Canadian Geotechnical Journal*, *53*(9), 1533-1546.

Ketcheson, S. J., & Price, J. S. (2016b). Snow hydrology of a constructed watershed in the Athabasca oil sands region, Alberta, Canada. *Hydrological Processes*, *30*(14), 2546-2561.

Ketcheson, S. J., Price, J. S., Carey, S. K., Petrone, R. M., Mendoza, C. A., & Devito, K. J. (2016). Constructing fen peatlands in post-mining oil sands landscapes: challenges and opportunities from a hydrological perspective. *Earth-science reviews*, 161, 130-139.

Ketcheson, S. J., Price, J. S., Sutton, O., Sutherland, G., Kessel, E., & Petrone, R. M. (2017). The hydrological functioning of a constructed fen wetland watershed. *Science of the Total Environment*, 603, 593-605.

Khire, M. V., Benson, C. H., & Bosscher, P. J. (2000). Capillary barriers: Design variables and water balance. *Journal of Geotechnical and Geoenvironmental Engineering*, 126(8), 695-708.

Kling, H., Fuchs, M., & Paulin, M. (2012). Runoff conditions in the upper Danube basin under an ensemble of climate change scenarios. *Journal of Hydrology*, 424, 264-277.

Koropchak, S., Vitt, D. H., Bloise, R., & Wieder, R. K. (2012). Fundamental paradigms, foundation species selection, and early plant responses to peatland initiation on mineral soils. In D.H. Vitt & J.S. Bhatti (Eds.), *Restoration and Reclamation of Boreal Ecosystems: Attaining Sustainable Development* (76-100). Cambridge: Cambridge University Press.

Kurylyk, B. L., & Watanabe, K. (2013). The mathematical representation of freezing and thawing processes in variably-saturated, non-deformable soils. *Advances in Water Resources*, 60, 160-177.

Lewis, J., & Sjöstrom, J. (2010). Optimizing the experimental design of soil columns in saturated and unsaturated transport experiments. *Journal of contaminant hydrology*, *115*(1-4), 1-13.

Li, Y. H., Gregory, S. (1974) Diffusion of ions in seawater and in deep-sea sediments. *Geochim. Cosmochim. Acta*, *38*, 703-714.

Loch, R. J., & Orange, D. N. (1997). Changes in some properties of topsoil at Tarong Coal–Meandu Mine coalmine with time since rehabilitation. *Soil Research*, 35(4), 777-784.

MacKenzie, D. D., & Naeth, M. A. (2007). Assisted natural recovery using a forest soil propagule bank in the Athabasca oil sands. *Seeds Biology, Development and Ecology*, 374-382.

Majid, A., Kotlyar, L., & Sparks, B. D. (1996, January). Potential applications of oil sands industry wastes. In *Annual Technical Meeting*. Petroleum Society of Canada.

Masliyah, J., Zhou, Z. J., Xu, Z., Czarnecki, J., & Hamza, H. (2004). Understanding water-based bitumen extraction from Athabasca oil sands. *The Canadian Journal of Chemical Engineering*, *82*(4), 628-654.

McKenna, G. T. (2002). Sustainable mine reclamation and landscape engineering (Doctoral Dissertation). University of Alberta, Edmonton, Canada. Education and Research Archive https://doi.org/10.7939/R3H70882S.

Meiers, G. P., Barbour, S. L., Qualizza, C. V., & Dobchuk, B. S. (2011). Evolution of the hydraulic conductivity of reclamation covers over sodic/saline mining overburden. *Journal of Geotechnical and Geoenvironmental Engineering*, 137(10), 968-976.

Mikula, R. (2012). Advances in oil sands tailings handling: building the base for reclamation. In D.H. Vitt & J.S. Bhatti (Eds.), *Restoration and Reclamation of Boreal Ecosystems: Attaining Sustainable Development* (103-122). Cambridge: Cambridge University Press.

Mitsch, W. J., & Wilson, R. F. (1996). Improving the success of wetland creation and restoration with know-how, time, and self-design. *Ecological applications*, *6*(1), 77-83.

Monteith, J. L. (1965). Evaporation and environment, in the state and movement of water in living organisms. In Symp. Soc. Exp. Biol. (205-234). Academic Press.

Moreno-de Las Heras, M., Merino-Martín, L., & Nicolau, J. M. (2009). Effect of vegetation cover on the hydrology of reclaimed mining soils under Mediterranean-Continental climate. *Catena*, 77(1), 39-47.

Murray, K. R., Barlow, N., & Strack, M. (2017). Methane emissions dynamics from a constructed fen and reference sites in the Athabasca Oil Sands Region, Alberta. *Science of the Total Environment*, *583*, 369-381.

Naeth, M. A., Chanasyk, D. S., & Burgers, T. D. (2011). Vegetation and soil water interactions on a tailings sand storage facility in the Athabasca oil sands region of Alberta Canada. *Physics and Chemistry of the Earth, Parts A/B/C*, 36(1-4), 19-30.

Naeth, M. A., Wilkinson, S. R., Powter, C. B., Archibald, H. A., & Mackenzie, D. D. (2013). Potential of LFH mineral soil mixes for land reclamation in Alberta. Oil Sands Research and Information Network Report No. TR-35. University of Alberta, School of Energy and the Environment, Edmonton, Alberta.

Neuman, S. P., Winter, C. L., & Newman, C. M. (1987). Stochastic theory of field-scale Fickian dispersion in anisotropic porous media. *Water Resources Research*, *23*(3), 453-466.

Nicholls, E. M., Carey, S. K., Humphreys, E. R., Clark, M. G., & Drewitt, G. B. (2016). Multi-year water balance assessment of a newly constructed wetland, Fort McMurray, Alberta. *Hydrological Processes*, 30(16), 2739-2753.

Nwaishi, F., Petrone, R. M., Price, J. S., & Andersen, R. (2015). Towards developing a functional-based approach for constructed peatlands evaluation in the Alberta oil sands region, Canada. *Wetlands*, 35(2), 211-225.

Nwaishi, F., Petrone, R. M., Price, J. S., Ketcheson, S. J., Slawson, R., & Andersen, R. (2015). Impacts of donor-peat management practices on the functional characteristics of a constructed fen. *Ecological Engineering*, *81*, 471-480.

Ogata, A., & Banks, R. B. (1961). A solution of the differential equation of longitudinal dispersion in porous media: fluid movement in earth materials. US Government Printing Office.

Panday, S., & Huyakorn, P. S. (2008). MODFLOW SURFACT: A state-of-the-art use of vadose zone flow and transport equations and numerical techniques for environmental evaluations. *Vadose Zone Journal*, *7*(2), 610-631.

Penman, H. L. (1948). Natural evaporation from open water, bare soil and grass. *Proceedings of the Royal Society of London. Series A. Mathematical and Physical Sciences*, *193*(1032), 120-145.

Peters, A., Durner, W., & Wessolek, G. (2011). Consistent parameter constraints for soil hydraulic functions. *Advances in water resources*, 34(10), 1352-1365.

Petrone, R. M., Silins, U., & Devito, K. J. (2007). Dynamics of evapotranspiration from a riparian pond complex in the Western Boreal Forest, Alberta, Canada. *Hydrological Processes: An International Journal*, 21(11), 1391-1401.

Pisani, L. (2011). Simple expression for the tortuosity of porous media. *Transport in Porous Media*, *88*(2), 193-203.

Pollard, J., McKenna, G. T., Fair, J., Daly, C., Wytrykush, C., & Clark, J. (2012). Design aspects of two fen wetlands constructed for reclamation research in the Athabasca oil sands. *Mine Closure 2012*, 815-829.

Pouliot, R., Rochefort, L., & Graf, M. D. (2013). Fen mosses can tolerate some saline conditions found in oil sands process water. *Environmental and Experimental Botany*, *89*, 44-50.

Price, J. S., McLaren, R. G., & Rudolph, D. L. (2010). Landscape restoration after oil sands mining: conceptual design and hydrological modelling for fen reconstruction. *International Journal of Mining, Reclamation and Environment*, 24(2), 109-123.

Purdy, B. G., Ellen Macdonald, S., & Lieffers, V. J. (2005). Naturally saline boreal communities as models for reclamation of saline oil sand tailings. *Restoration Ecology*, *13*(4), 667-677.

R Core Team. (2013). R: A language and environment for statistical computing.

Rezanezhad, F., Andersen, R., Pouliot, R., Price, J. S., Rochefort, L., & Graf, M. D. (2012). How fen vegetation structure affects the transport of oil sands process-affected waters. *Wetlands*, *32*(3), 557-570.

Ritchie, J. T. (1974). Atmospheric and soil water influences on the plant water balance. *Agricultural meteorology*, 14(1-2), 183-198.

Rodriguez-Iturbe, I., D'odorico, P., Porporato, A., & Ridolfi, L. (1999). On the spatial and temporal links between vegetation, climate, and soil moisture. *Water Resources Research*, 35(12), 3709-3722.

Rooney, R. C., Bayley, S. E., & Schindler, D. W. (2012). Oil sands mining and reclamation cause massive loss of peatland and stored carbon. *Proceedings of the National Academy of Sciences*, *109*(13), 4933-4937.

Scarlett, S. J., Petrone, R. M., & Price, J. S. (2017). Controls on plot-scale evapotranspiration from a constructed fen in the Athabasca Oil Sands Region, Alberta. *Ecological engineering*, 100, 199-210.

Scarlett, S. J., & Price, J. S. (2019). The influences of vegetation and peat properties on the hydrodynamic variability of a constructed fen, Fort McMurray, Alberta. *Ecological Engineering*, *139*, 105575.

Schlüter, S., Vogel, H. J., Ippisch, O., & Vanderborght, J. (2013). Combined impact of soil heterogeneity and vegetation type on the annual water balance at the field scale. *Vadose Zone Journal*, 12(4).

Schröder, N., Lazarovitch, N., Vanderborght, J., Vereecken, H., & Javaux, M. (2014). Linking transpiration reduction to rhizosphere salinity using a 3D coupled soil-plant model. *Plant and Soil*, 377(1-2), 277-293.

Scott, R. L. (2010). Using watershed water balance to evaluate the accuracy of eddy covariance evaporation measurements for three semiarid ecosystems. *Agricultural and Forest Meteorology*, 150(2), 219-225.

Seyfried, M. S., Grant, L. E., Du, E., & Humes, K. (2005). Dielectric loss and calibration of the Hydra Probe soil water sensor. *Vadose Zone Journal*, 4(4), 1070-1079.

Simhayov, R. B., Price, J. S., Smeaton, C. M., Parsons, C., Rezanezhad, F., & Van Cappellen, P. (2017). Solute pools in Nikanotee Fen watershed in the Athabasca oil sands region. *Environmental pollution*, 225, 150-162.

Simhayov, R. B., Weber, T. K., & Price, J. S. (2018). Saturated and unsaturated salt transport in peat from a constructed fen. *Soil*, 4(1), 63-81.

Šimůnek, J., Šejna, M., Saito, H., Sakai, M., & Van Genuchten, M. T. (2008). The HYDRUS-1D Software Package for Simulating the One-Dimensional Movement of Water, Heat, and Multiple Solutes in Variably-Saturated Media, Version, 4, 281.

Šimůnek, J., Van Genuchten, M. T., & Šejna, M. (2012A). HYDRUS: Model use, calibration, and validation. *Transactions of the ASABE*, 55(4), 1263-1274.

Skaggs, T. H., van Genuchten, M. T., Shouse, P. J., & Poss, J. A. (2006). Macroscopic approaches to root water uptake as a function of water and salinity stress. *Agricultural Water Management*, 86(1-2), 140-149.

Sudicky, E. A. (1986). A natural gradient experiment on solute transport in a sand aquifer: Spatial variability of hydraulic conductivity and its role in the dispersion process. *Water Resources Research*, *22*(13), 2069-2082.

Sutton, O. F., & Price, J. S. (2020). Soil moisture dynamics modelling of a reclaimed upland in the early post-construction period. *Science of the Total Environment*, 718, 134628.

Sutton, O. F., & Price, J. S. (2020). Modelling the hydrologic effects of vegetation growth on the long-term trajectory of a reclamation watershed. *Science of the Total Environment*, 734, 139323.

Toth, J. (1963). A theoretical analysis of groundwater flow in small drainage basins. *Journal of geophysical research*, *68*(16), 4795-4812.

Turetsky, M. R. (2003). The role of bryophytes in carbon and nitrogen cycling. *The bryologist*, *106*(3), 395-409.

Van Genuchten, M. T. (1980). A closed-form equation for predicting the hydraulic conductivity of unsaturated soils 1. *Soil science society of America journal*, 44(5), 892-898.

van Genuchten, M. T. (1987). A numerical model for water and solute movement in and below the root zone. Agricultural Research Service U.S. Salinity Laboratory, U.S. Department of Agriculture, Riverside, California.

Vaz, C. M., Jones, S., Meding, M., & Tuller, M. (2013). Evaluation of standard calibration functions for eight electromagnetic soil moisture sensors. *Vadose Zone Journal*, 12(2).

Vitt, D. H., House, M., & Hartsock, J. A. (2016). Sandhill Fen, an initial trial for wetland species assembly on in-pit substrates: lessons after three years. *Botany*, *94*(11), 1015-1025.

Vitt, D. H., Glaeser, L. C., House, M., & Kitchen, S. P. (2020). Structural and functional responses of *Carex aquatilis* to increasing sodium concentrations. *Wetlands Ecology and Management*, *28*(5), 753-763.

Vogel, J. G., & Gower, S. T. (1998). Carbon and nitrogen dynamics of boreal jack pine stands with and without a green alder understory. *Ecosystems*, 1(4), 386-400.

Weber, T. K., Durner, W., Streck, T., & Diamantopoulos, E. (2019). A modular framework for modeling unsaturated soil hydraulic properties over the full moisture range. *Water Resources Research*, *55*(6), 4994-5011.

Wells, C. M., & Price, J. S. (2015). A hydrologic assessment of a saline-spring fen in the Athabasca oil sands region, Alberta, Canada–a potential analogue for oil sands reclamation. *Hydrological Processes*, *29*(20), 4533-4548.

Wells, C., Ketcheson, S., & Price, J. (2017). Hydrology of a wetland-dominated headwater basin in the Boreal Plain, Alberta, Canada. *Journal of Hydrology*, *547*, 168-183.

Wieder, R. K., Yavitt, J. B., & Lang, G. E. (1990). Methane production and sulfate reduction in two Appalachian peatlands. *Biogeochemistry*, *10*(2), 81-104.

Willemain, R. T., & Desautels, A. P. (1993). A method to generate autocorrelated uniform random numbers. *Journal of statistical computation and simulation*, *45*(1-2), 23-31.

Woo, M. K., & Xia, Z. (1996). Effects of Hydrology on the Thermal Conditions of the Active Layer: Paper presented at the 10th Northern Res. Basin Symposium (Svalbard, Norway—28 Aug./3 Sept. 1994). *Hydrology Research*, *27*(1-2), 129-142.

Zech, A., Attinger, S., Cvetkovic, V., Dagan, G., Dietrich, P., Fiori, A., ... & Teutsch, G. (2015). Is unique scaling of aquifer macrodispersivity supported by field data?. *Water resources research*, *51*(9), 7662-7679.

Zech, A., Attinger, S., Bellin, A., Cvetkovic, V., Dietrich, P., Fiori, A., ... & Dagan, G. (2019). A critical analysis of transverse dispersivity field data. *Groundwater*, *57*(4), 632-639.

Zoltai, S. C., Taylor, S., Jeglum, J. K., Mills, G. F., & Johnson, J. D. (1988). Wetlands of boreal Canada. Wetlands of Canada, Ecological Land Classification Series, 24, 97-154.

Appendix A:
Estimating the duration of the ice-free period

The numerical models used in Chapters 2, 3, and 5 did not simulate the winter period or the processes of snow accumulation, sublimation, and snowmelt. Therefore, the model required the dates associated with the thawing of seasonal ground ice in the spring and onset of ground frost in the fall, to define the "hydrologically active period". Furthermore, given the importance of precipitation delivered during the winter to the annual water budget, it was necessary to account for snow accumulation that occurred over this period, as well as losses from the snowpack due to sublimation. Freezing and thawing of the upland was estimated using the Stefan equation (Jumikis, 1977):

$$X = \sqrt{\frac{2k_u I(t) n}{\omega \rho_b L}} \quad (1)$$

where X is depth of the freezing or thawing front (m), k_u is the thermal conductivity (W m^{-1} $°C^{-1}$), I(t) is the negative or positive air temperature integrated since the initiation of freezing or thawing, respectively (°C s), *n* is an empirical correction factor accounting for the differences between air and surface temperature, ω is the mass of pore water or ice initially present in the soil divided by the mass of dry soil, ρ_b is the dry bulk density of the soil (kg m^{-3}), and L is the latent heat of fusion of water (334,000 J kg^{-1}). For the sake of simplicity, a single thermal conductivity (1.61 W m^{-1} $°C^{-1}$) was used to represent the entire soil profile, and did not vary in time (due to differing soil moisture), or with the phase change of water. However, this thermal conductivity value did integrate the differences in mineral and organic matter content, and the typical volumetric water content along the depth profile. In the upland, this profile consisted of LFH and tailings sand, for which the dry bulk density, mineral and organic matter content can be found in Ketcheson (2015). The thermal conductivity of the individual constituents of the soil were obtained from Woo and Xia (1996). Typical distribution of volumetric water content with depth was informed by soil moisture data collected at several soil moisture stations across the upland.

The algorithm was used to estimate the freezing and thawing dates of the upper 35 cm of the upland soil profile, which coincides with the average depth of the LFH cover soil. The fine-grained LFH had persistently higher volumetric water content than the underlying tailings sand, thus it was presumed that infiltration and percolation past the interface between LFH and tailings sand would be limited by the presence of pore-ice. However, once this upper layer of LFH thawed, the high hydraulic conductivity of

the tailings sand and the near-residual pore-ice content would not be a barrier to deeper percolation towards the water table. Historical air temperature data (1953-2017) was obtained from a nearby Environment Canada monitoring station located at the Fort McMurray airport. Soil temperature data at the SAF 220U soil moisture station was used to validate the adequacy of the Stefan equation to model the descent of the freezing and thawing front (Figure A1). Due to battery failure in early Spring, ground thaw was only observed in 2014. The value of the *n* factor was adjusted to obtain a better match between the observed and simulated descent of the freezing front. This calibration procedure identified an *n* factor of 0.85, which is consistent with expectations when using air temperature to drive the algorithm, as opposed to ground surface temperature. The *n*-factor had a proportional impact on the maximum depth of the freezing front, however timing of the ice-free period was insensitive to this parameter. Although the algorithm cannot capture the patterns of deep thaw in the tailings sand, due to the unidirectional implementation of the Stefan equation, the freezing and thawing of the near-surface LFH is represented adequately, and thus was appropriate to use for the purpose of defining the hydrologically active period. Additionally, by allowing for multiple freezing and thawing fronts, this implementation of the Stefan equation allowed for brief temperature fluctuations above zero to be explicitly represented (Figure A1), which currently has not been published on. This data also illustrated that the near-surface of the soil profile would typically experience more than one freeze-thaw cycle each year – thus contributing to the gradation of weathering noted in Chapter 2. The average thaw and freezing date occurred on April 23 and October 23, respectively.

Following spring thaw, the remaining snow water equivalent (SWE) that had accumulated over the winter was partitioned to snowmelt. The SWE of the freshly fallen snow was modified from the constant assumed by Environment Canada (100 kg m^{-3}) based on the relationship of Hedstrom and Pomeroy (1998):

$$\rho_s = 67.92 + 51.25e^{(T_a/2.59)} \quad (2)$$

where ρ_s is the density of snow (kg m^{-3}), and T_a is the measured air temperature (°C). Sublimation was calculated using the Kuz'min equation (Gelfan et al., 2004):

$$E_s = (0.18 + 0.098u_{10})(e_s - e_a) \quad (3)$$

where E_s is the snow sublimation from the snowpack (mm d^{-1}), u_{10} is the wind velocity at 10 m above ground surface (m s^{-1}), e_s is the saturated vapour pressure over ice (mb), and e_a is the air vapour pressure (mb) at 2 m height above ground surface. Meteorological data collected on an hourly basis by Environment Canada between 1953-2017 was used to calculate hourly sublimation, which was summed and subtracted from the existing snowpack on a daily basis. On average, sublimation removed 30% of total annual SWE.

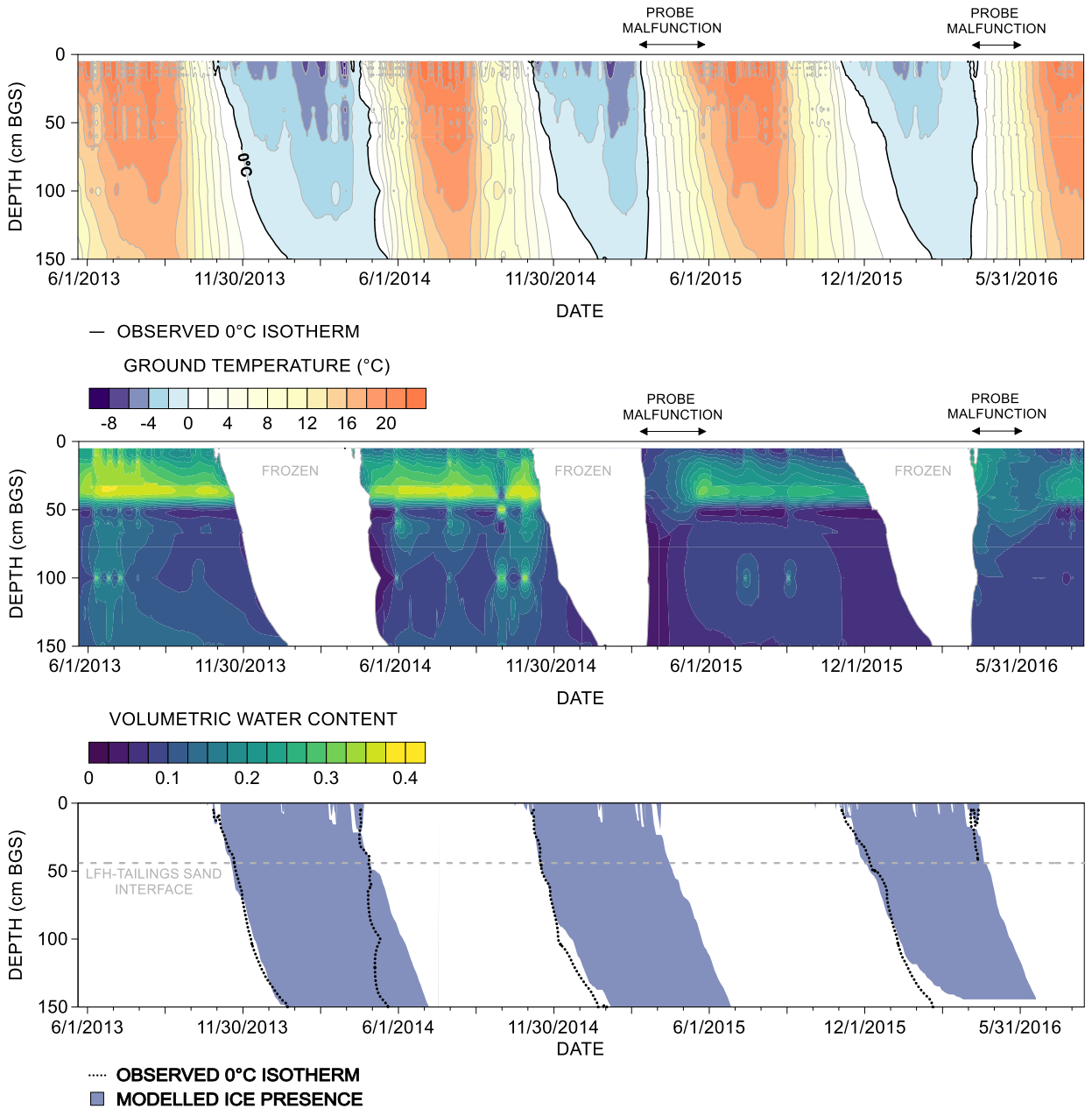

Figure A-1. Implementation of the Stefan equation in the upland. Upper panel depicts the ground temperature over time at the SAF 220U soil moisture station; the interface between LFH and tailings sand is apparent in the soil moisture data (middle panel); the bottom panel illustrates the observed 0°C isotherm and the modelled ice presence using the Stefan equation.

Appendix B:
Details on the Monte Carlo simulation methodology

Projections of groundwater flow and solute transport required the specification of recharge and evapotranspiration boundary conditions that explicitly accounted for the considerable climatic variability characteristic of the region. This was accomplished through an automated implementation of the Monte Carlo method coded in R (R Core Team, 2013), which parameterized recharge and potential evapotranspiration; summarized simulated head, fluxes, and concentration; parsed out the three-dimensional head and sodium concentration arrays from the final timestep of each annual simulation; and wrote the MODFLOW SURFACT input files (.rch, .ets, .bas, .btn). Given the different hydrologic processes operating across the fen, upland, and recharge basins, and in consideration of the capabilities of the numerical simulator to represent these phenomena, a variety of approaches were used to parameterize recharge. The general workflow of the automation procedure is shown in a process diagram (Figure B-1).

Parameterization of recharge and potential evapotranspiration were conducted independently, as no statistically significant correlation between the two variables on a cumulative annual basis was identified from the 65-year meteorological record. However, in both cases, the daily record of precipitation and potential evapotranspiration were preprocessed to coincide with a 183-day simulation period. Specifically, the meteorological data from the growing season was temporally interpolated to either compress or elongate the record if it was longer or shorter than the simulation period, respectively. This modestly altered the intensity of the fluxes on a daily basis, however, it ensured that the total cumulative quantity of water gained (or potentially lost) was respected. Time series of both precipitation and potential evapotranspiration data was ranked based on the cumulative annual flux, and an individual sample was selected for each annual simulation. In the case of potential evapotranspiration this was entirely random, and uncorrelated with the PET from the previous year. However, the precipitation and recharge data demonstrated weak temporal autocorrelation. This was accounted for with the method of Willemain and Desautels (1993), which generated random uniformly distributed numbers (x_n) with the desired serial correlation (0.32). These uniform numbers ($0 \leq x_n \leq 1$) represented the cumulative probabilities of precipitation and recharge. With respect to an individual year within a single Monte Carlo realization, x_n was used to: (1) select one of 65 years of precipitation data to parameterize recharge in the fen, (2) calculate the corresponding cumulative annual groundwater recharge across the upland for each LFH cover soil thickness based on the gamma probability distributions (Figure B-2) identified in Chapter 3, and (3) calculate the cumulative annual

recharge associated with the east basin and southeast corner based on cumulative annual precipitation and the age of the site (Figure B-3). Despite the variety of methods to parameterize recharge, by using a single probability as the basis for all methods, the magnitude of groundwater recharge across the site from year-to-year would be internally consistent.

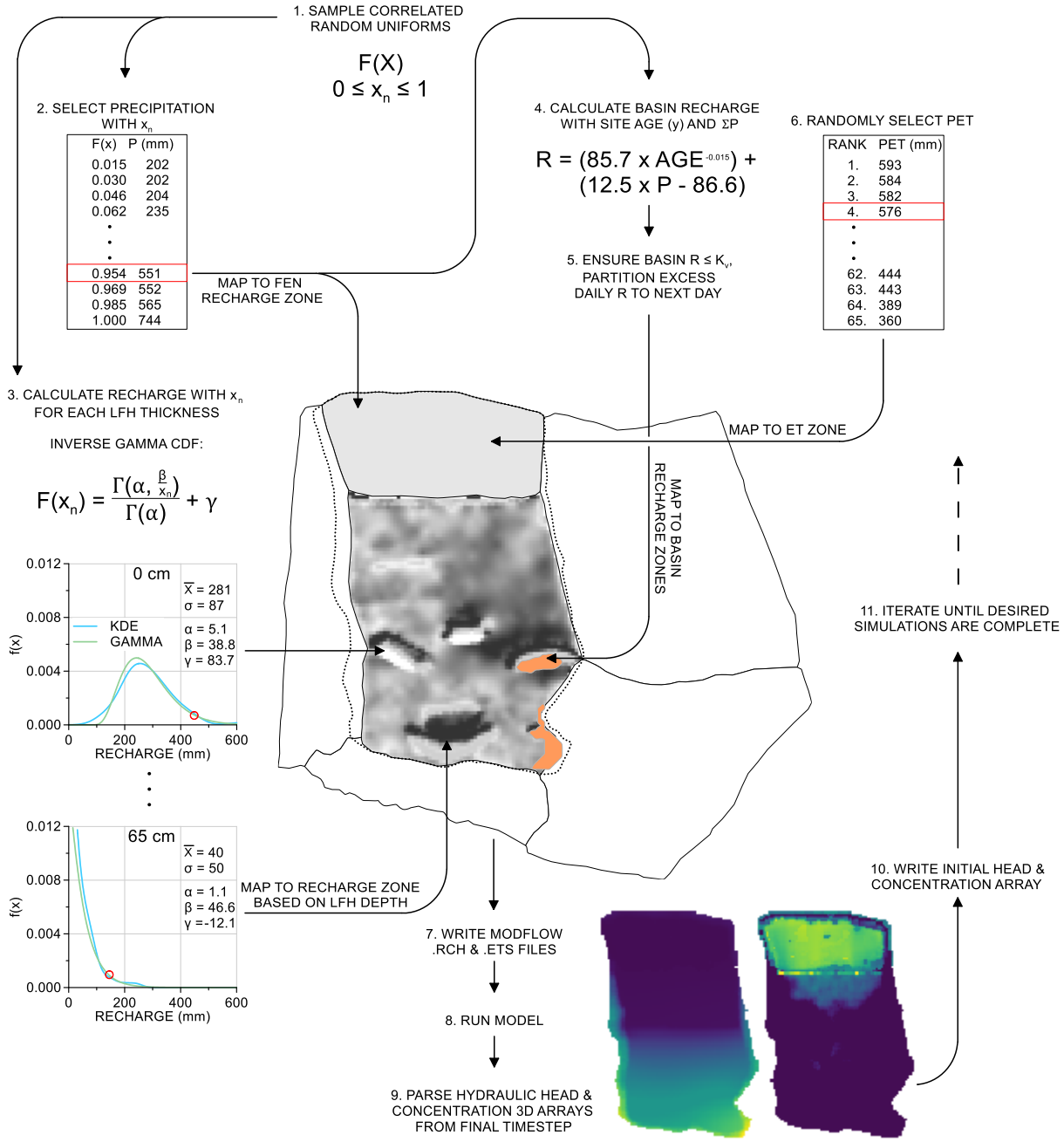

Figure B-1. Monte Carlo simulation process diagram.

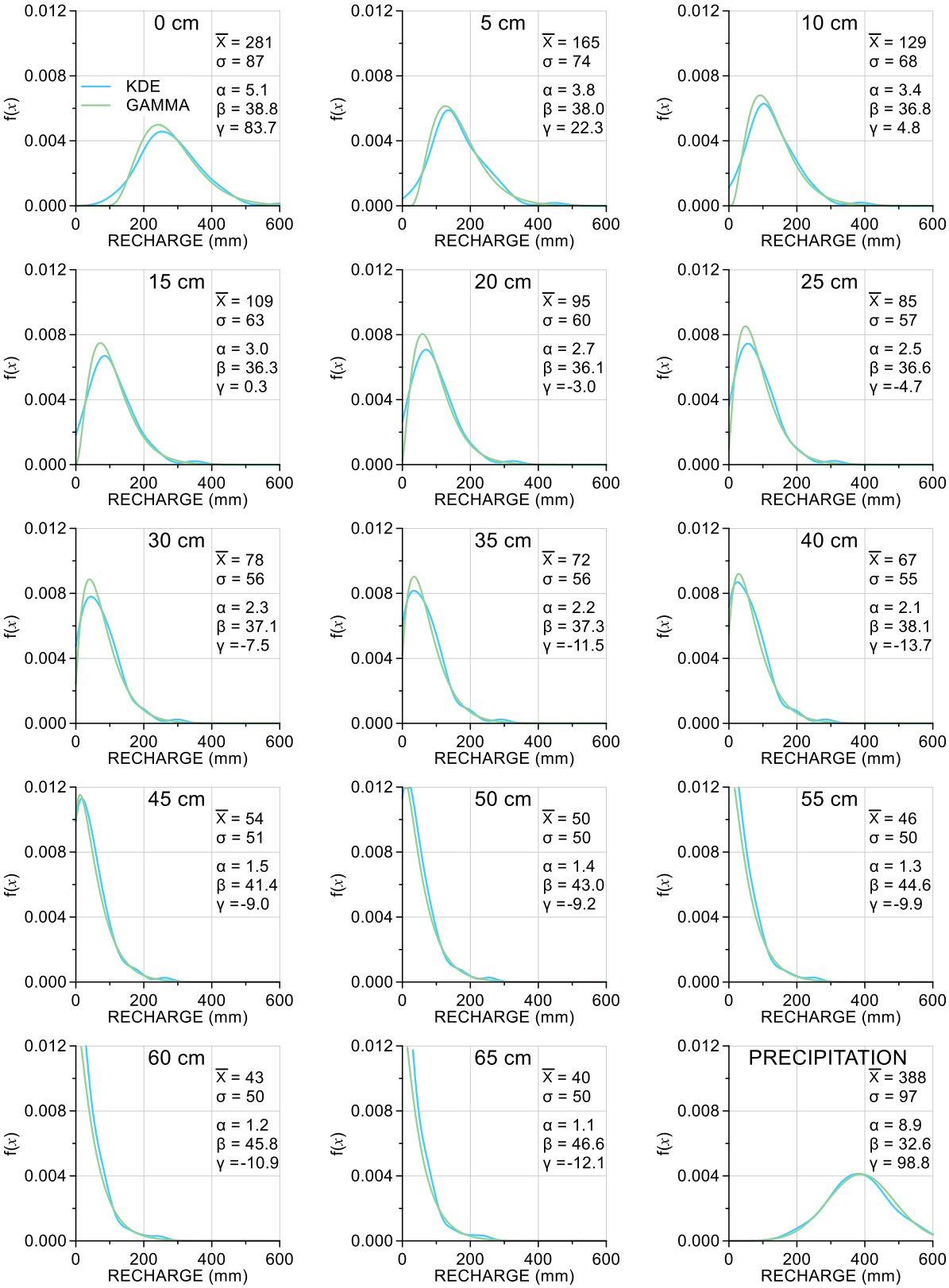
0 cm
X̄ = 281
σ = 87
KDE
GAMMA
α = 5.1
β = 38.8
γ = 83.7
5 cm
X̄ = 165
σ = 74
α = 3.8
β = 38.0
γ = 22.3
10 cm
X̄ = 129
σ = 68
α = 3.4
β = 36.8
γ = 4.8
15 cm
X̄ = 109
σ = 63
α = 3.0
β = 36.3
γ = 0.3
20 cm
X̄ = 95
σ = 60
α = 2.7
β = 36.1
γ = -3.0
25 cm
X̄ = 85
σ = 57
α = 2.5
β = 36.6
γ = -4.7
30 cm
X̄ = 78
σ = 56
α = 2.3
β = 37.1
γ = -7.5
35 cm
X̄ = 72
σ = 56
α = 2.2
β = 37.3
γ = -11.5
40 cm
X̄ = 67
σ = 55
α = 2.1
β = 38.1
γ = -13.7
45 cm
X̄ = 54
σ = 51
α = 1.5
β = 41.4
γ = -9.0
50 cm
X̄ = 50
σ = 50
α = 1.4
β = 43.0
γ = -9.2
55 cm
X̄ = 46
σ = 50
α = 1.3
β = 44.6
γ = -9.9
60 cm
X̄ = 43
σ = 50
α = 1.2
β = 45.8
γ = -10.9
65 cm
X̄ = 40
σ = 50
α = 1.1
β = 46.6
γ = -12.1
PRECIPITATION
X̄ = 388
σ = 97
α = 8.9
β = 32.6
γ = 98.8
f(x)
RECHARGE (mm)
0.000
0.004
0.008
0.012
0
200
400
600

Figure B-2. Kernel density estimates (KDE) and three-parameter gamma probability distribution fits to modelled cumulative annual recharge derived in Chapter 3. The gamma distributions in the cumulative form were sampled with correlated random uniform numbers to generate each realization of upland groundwater recharge in the Monte Carlo simulations.

In the case of fen recharge, which was equal to precipitation, no further processing was required, and daily values were mapped to the appropriate recharge zones in the model. However, upland and basin recharge required an additional processing step to partition the cumulative annual flux to daily values. Cumulative annual recharge in the upland was partitioned using a power function identified in Chapter 3, which took the form:

$$y = t^{0.371} \tag{1}$$

where y is normalized groundwater recharge, and t is normalized elapsed time following spring thaw (see Figure 3-10 in Chapter 3). To obtain daily recharge, the relationship was multiplied by the cumulative annual value and differentiated.

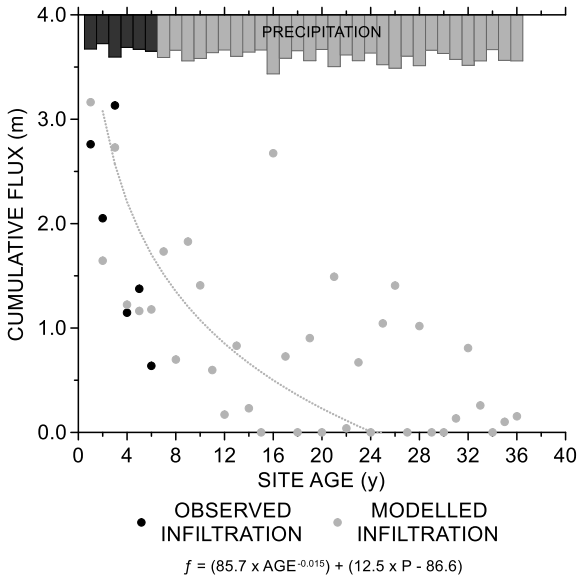

Figure B-3. Relationship between site age, precipitation, and cumulative annual infiltration at the east basin. The observed and simulated infiltration is shown for the first 7 years post-construction ($r^2 = 0.82$). Following that period is an example of a synthetic time series of stochastically generated (hypothetical) precipitation data and the resulting modelled infiltration. The dashed line represents the cumulative annual infiltration resulting from invariant average precipitation.

Recharge at the east basin and southeast corner were dominated by runoff events from the hillslopes, and as such, the temporal patterns of daily recharge were closely correlated to the timing and

magnitude of rainfall events. Therefore, the time series of daily rainfall was normalized such that it summed to unity, and then multiplied by the cumulative annual recharge previously identified for basins. Under certain circumstances this method could lead to a daily recharge flux that exceeded the saturated hydraulic conductivity of the surficial soil. As a means of rectifying this physically (and numerically) untenable condition, the daily recharge time series was processed and filtered, such that any water in excess of the daily infiltration capacity would be carried over to the subsequent day. This was conducted in an iterative manner, until the recharge flux was distributed throughout the year without exceeding the daily infiltration capacity.

The model was run for a period of 30 years (with the first simulation representing the year 2020), however, due to the quantity of data produced, each simulation was run for a single year and the final head and concentration distribution was applied as the initial condition for the subsequent year. Prior to the output files being overwritten, mass balance, hydraulic head, and sodium concentration data were processed, summarized and printed.

Appendix C:
Discussion on model error

As a consequence of deliberate design choices and detailed surveys conducted during construction, the system could be characterized by a relatively simple hydrogeologic conceptual model. Discussed in detail within Ketcheson et al. (2017), the conceptual model of water flow illustrated that the system is driven by groundwater recharge, which due to the hydraulic gradient established by the sloping low-permeability liner, directs groundwater flow towards the fen. Water loss from the fen occurred as surface or open-water evaporation, transpiration, and surface water discharge. This conceptual model was adapted for implementation in the numerical modelling environment of MODFLOW SURFACT with few compromises. In particular, the low permeability geosynthetic clay liner (maximum initial hydraulic conductivity of 5×10^{-10} cm s^{-1}) allowed for a natural physical boundary to be delineated in the numerical model, and adequately represented with a no-flow boundary condition. However, the numerical model did not explicitly simulate processes of surface water movement or the subsurface thermal regime. Furthermore, the model did not incorporate heterogeneity in the hydraulic conductivity field, nor was it capable of capturing the subtle variations in fen surface topography. These compromises in the numerical model likely introduced error into the simulated water balance fluxes, hydraulic head distribution, and transport of solutes. The implications of these choices are discussed below.

Surface overland flow was an important mechanism of water gain and loss from the system (Ketcheson et al., 2017). In the early post-construction period, hillslope runoff into recharge basins provided up to one-third of total upland groundwater recharge (Kessel et al., submitted). This was concentrated in the east recharge basin and southeast corner, which were adjacent to hillslopes with a propensity for runoff generation (Kessel et al., submitted). While site data indicated a diminishing contribution from hillslopes to the east recharge basin (Figure B-3), only limited data was available for the southeast corner. The impact of this uncertainty was apparent during the calibration and validation period, whereby the highest error between simulated and observed head was associated with monitoring locations downgradient of the southeast corner and east basin. In the most extreme case, hydraulic head was underpredicted by 1.7 m. Since this occurred at the most distal location of the upland, with no upgradient area to contribute lateral groundwater flow, this error can be predominantly attributed to error in estimated surface overland flow. Although the peaks in hydraulic head, which corresponded to specific events, were generally well-represented, these distal locations often exhibited a more rapid

decline in simulated head than what was observed. This could be indicative of interflow contributions from the hillslopes, although this has been shown to be a comparatively small water flux at similar reclaimed hillslopes in the region (Kelln et al., 2007). Perhaps a more probable explanation would be a localized area of lower tailings sand hydraulic conductivity, resulting in a slower dissipation of the groundwater mound. Although the tailings sand (and the other materials) was generally well-represented by a single homogeneous hydraulic conductivity, a decision which was supported by the data (see Chapter 4), the presence of heterogeneity is inevitable. This unrepresented heterogeneity has the potential to impact the projected timeline associated with solute elution from the upland. The presence of localized areas of high hydraulic conductivity could result in preferential movement of water and therefore faster solute flushing. Conversely, zones of comparatively lower hydraulic conductivity would lengthen the elution of sodium from the system. The relatively sparse monitoring network (see Figures 5-1 and 5-6 in Chapter 5) in the upland provides little information on this matter. However, in spite of the paucity of water chemistry data in the upland, the simulated transport of sodium from the aquifer to the fen appeared to closely resemble the observed data.

During the calibration and validation period, simulated surface water discharge constituted 45% of the total water lost from the system. The design of the discharge control structure allowed groundwater to seep out of the system at a slow, but consistent rate, when the water table was below the elevation of the spillway (approximately equal to ground surface). However, surface water could be rapidly shuttled out of the system when the water table was above this threshold. Although a v-notch weir was located immediately upstream of the discharge control structure to measure surface water outflow, quantification of discharge had several uncertainties associated with it. Most crucially, the nature of its construction allowed surface water to bypass the weir during high flow events. In addition, the manual stage-discharge relationship for the weir was only informed by relatively low-flows. Furthermore, snowmelt, which represented the largest annual surface water discharge event, was never captured by the monitoring equipment. This led to a judgement that discharge data had relatively low reliability and information value. A direct comparison between cumulative observed and simulated discharge over the calibration and validation period resulted in a 27% overprediction. Furthermore, the timing and relative magnitude of simulated discharge events compared poorly with the observed temporal patterns of discharge. While the aforementioned methodological approach to quantifying discharge in the field could impact the apparent observed temporal patterns, the internal representation of discharge within the model was considered a more likely culprit.

Episodic discharge was represented in the model with two head-dependent flux boundary conditions. In the terminology of MODFLOW SURFACT, a seepage-face boundary condition located at the same coordinates as the discharge control structure allowed water above the surface to be removed at a theoretically unlimited conductance. However, in reality, the rate of water movement out of this boundary condition was controlled by the lateral and vertical rate of water transfer to this location, which was itself a function of the hydraulic conductivity and hydraulic gradient. In addition, a maximum ponding elevation was specified across the fen, which would reduce or completely eliminate the prescribed recharge depending on the storage capacity of the surface, such that the maximum ponding elevation would be maintained. Conceptually, this "rejected" flux is considered as surface runoff out of the model domain, however this occurs instantaneously. This causes a much more pronounced peak in the simulated discharge data compared to the observed discharge, which exhibits a more conventional discharge recession. Although the rejected flux can carry solutes out of the model domain, the absence of surface water physics does preclude the redistribution of solutes across the surface of the fen.

To an extent, hydraulic conductivity and groundwater recharge have a compensatory relationship in the model. The implication of this relationship is that error in the specified recharge flux can be obscured during calibration by erroneous modification of saturated hydraulic conductivity. In this context, hydraulic head targets could be adequately matched with a variety of combinations of recharge and permeability. Therefore, this places greater importance on matching observed data that characterizes fluxes of water, including actual evapotranspiration, surface water discharge, and the spatial patterns of sodium. Although the sole priority of the objective function was fitting hydraulic head, an excellent match between simulated and observed actual evapotranspiration was achieved (Figure 5-5). Moreover, sodium concentration data also illustrated that the combination of recharge and hydraulic conductivity implemented in the model could adequately represent the rate of sodium transport from upland to fen (Figure 5-6). Confidence in the optimized hydraulic conductivity was further bolstered by supporting studies that were specifically intended to reduce uncertainty in recharge (Chapter 2; 3), and tailings sand hydraulic conductivity (Chapter 4). These investigations appear to have been worthwhile, as the initial tailings sand hydraulic conductivity (3.3 m d^{-1}), derived during analysis of a large-scale tracer test, was decreased during the optimization procedure by only 0.5 m d^{-1}. This optimized value of horizontal hydraulic conductivity was almost identical to the average of single-well response tests conducted in the tailings sand aquifer (2.9 m d^{-1}). Ultimately, despite the apparent poor model performance associated with the timing and magnitude of surface water discharge, the

parameterization of recharge and hydraulic conductivity are supported by the results, which are consistent with much of the hydrologic, hydrometric, and geochemical data available at the site.

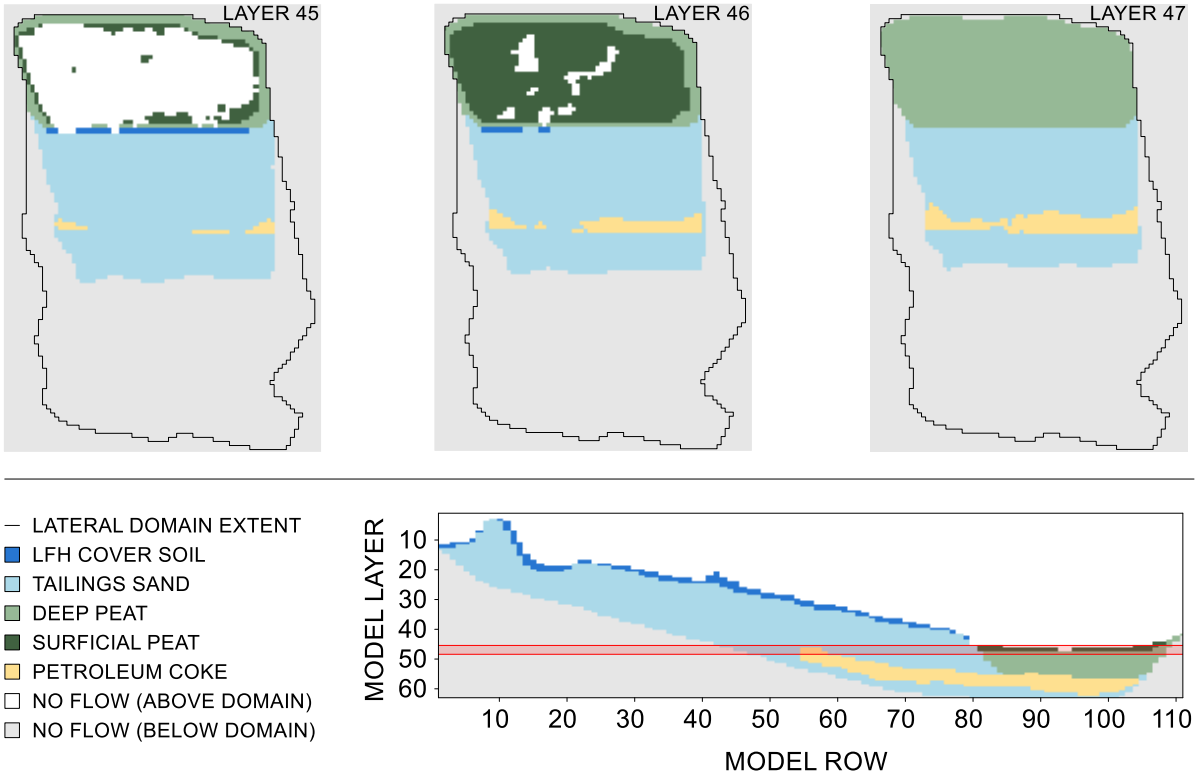

Figure C-1. Selection of model layers (45-47) that intersect the near-surface of the fen, illustrating the specific spatial discretization scheme employed for the groundwater flow and solute transport model in Chapter 5. The position of this model cross-section corresponds to the stratigraphic cross-section in Figure 5-1.

Both the upland and fen, as shallow groundwater flow systems, were impacted by ground frost. While ground temperature data in the upland demonstrated that ground frost would not penetrate to the depth of the water table (Appendix A), it severely limited the percolation of water across the interface between LFH and tailings sand (Chapter 2). In contrast, the fen would form a thick, cohesive layer of seasonal ground ice below the surface, which would propagate downwards through the saturated zone. This continuous layer of seasonal ground ice prevented groundwater flow from upland to fen. However, redistribution of groundwater water within the upland could still occur. This was observed in hydraulic head data, whereby over the winter period the upland groundwater mound would slightly dissipate and move downgradient towards the transition zone. Typically, this resulted in overprediction of hydraulic head in the distal areas of the upland, and underprediction in the central upland. MODFLOW

SURFACT has the capability to simulate materials with time-varying hydraulic properties, which would allow for the vast reduction in hydraulic conductivity due to pore-occlusion by ice to be represented. However, this was seen as an unnecessary complication that would likely present numerical difficulties and contribute to parameter uncertainty. Instead, Stefan's equation (Jumikis, 1977) was used to estimate the timing and duration of the unfrozen period (Appendix A), and assumed that the fen and upland would become "hydrologically active" concurrently. The calibration and validation period estimated the presence of seasonal ground ice based on measured air temperature data at the site, while the Monte Carlo simulations used the average duration of the ice-free period based on 65 years of regional meteorological data (Chapter 2). Since it was assumed that sodium transport would be able to occur only 183 days of the year (in the Monte Carlo simulations), any error in that estimate (or uncertainty due to climate change, for example) would have an inverse proportional impact on the estimated number of years for the site to flush.

The granularity of vertical discretization and specific implementation of the discretization scheme likely had an influence on the simulated patterns of sodium at the surface of the fen (see Figure C-1). Steep geochemical gradients related to surface topography were apparent with depth and laterally across the fen. The approximation of surface topography within the numerical modelling environment was limited by the vertical thickness of the finite difference grid (0.2 m). Furthermore, given that these layers were planar, the upper model boundary could not conform more closely to the true surface topography of the site. Consequently, the elevation of the discretized fen surface could deviate from the true elevation by up to 0.1 m, which is not a trivial discrepancy considering the profound changes in salinity (Figure 5-6) and hydrologic behaviour (Figure 5-2) that occurred with depth. A variety of strategies were implemented in the model to limit the impact of this imperfect representation. Firstly, the planar discretization scheme was capable of including deviations in the fen surface greater than 0.1 m, allowing for the delineation of larger depressions and mounds. Secondly, the "true" surface topography was used as the evapotranspiration surface, which is the elevation that defines the upper boundary of the relationship between water table and AET:PET (see "Ground Surface" in Figure 5.2). Simply put, it represents the minimum water table elevation where actual evapotranspiration is occurring at the potential (maximum) level. Finally, multiple zones of maximum ponding depth were specified across the fen, allowing depressions in the peat surface to form persistent areas of ponding above ground surface. This is in contrast to the majority of the fen, which did not allow surface water to accumulate above ground surface, instead removing it instantaneously from the domain as surface water discharge. The Monte Carlo simulations demonstrated that surface topography had a pronounced

impact on surface salinity in the fen. In particular, elevated areas of the fen experienced periodic downward hydraulic gradients, which greatly limited the potential for surface salinization. The crude depiction of surface topography within the model does not invalidate this finding. However, a more refined representation of microtopography would likely illustrate more subtle lateral and vertical variations in fen sodium concentration than what was identified in this current model (see Figure 5-11). An additional consideration associated with the granularity of vertical discretization, is the impact of dilution and evapoconcentration. Within the model, the impact of dilution or evapoconcentration is distributed over the entire thickness of the finite difference cell, thereby ameliorating the magnitude of the fluctuation in surface concentration. However, in reality, these processes will have a considerably more pronounced effect directly at the surface than at even modest depths of 0.1 m below ground surface (S. Yang, personal communication).

Although not considered germane to the overall goal of this research, the Nikanotee Fen Watershed will experience another time-dependent process, which will have profound consequences to the hydrology of the system; the reduced efficacy of the low-permeability liner. The geosynthetic clay liner used to isolate the system from deep percolation losses, and to direct groundwater from upland to fen, is composed of sodium bentonite laminated between a flexible geotextile membrane. The as-built hydraulic conductivity of the liner is exceptionally low (5×10^{-10} cm s^{-1}), however, due to the processes of ion exchange between Na^{+} cations in the bentonite of the liner and abundant Ca^{2+} from the pore-water of the tailings sand and differential settlement of the underlying fill, the hydraulic conductivity can be expected to increase several orders of magnitude. The underlying fill material is composed of mechanically-compacted saline-sodic shale and lean oil sands, which are both of relatively low hydraulic conductivity. Yet, as the geosynthetic liner degrades, zones of poor-compaction could allow for substantial deep percolation losses from the upland and the fen. Since the upland vegetation will be unaffected by this degradation, and the fen generally exists in a state of water surplus, the trajectory of the system may not be drastically altered - although this is contingent on the magnitude of the permeability increase. Considering that the timeline of this reduced efficacy is on the order of decades to centuries (BGC Engineering, 2012), it is likely that the majority of sodium will have been flushed from the system (Chapter 5). The brunt of the increased water loss to deep percolation will be borne by surface water discharge from the fen, which can be expected to decrease. However, following the removal of sodium from the watershed, the “utility” of high surface water discharge is greatly reduced. Therefore, this anticipated reduction in surface discharge will not be as detrimental to the performance of the system as it would be earlier in the post-construction period.